Hall A Status Report - 2007

Edited by Bryan Moffit and Kees de Jager

January 2008

Contents

1 Introduction **6**

2 Standard Hall A Facilities **7**

2.1 Polarized ^{3}He Target . . . 7
2.2 BigBite Spectrometer . . . 9
2.3 New Amplifier/Discriminator Cards for Multi-Wire Drift Chambers . . . 13

3 General Hall Developments **16**

3.1 The Compton Polarimeter Upgrade . . . 16
3.2 Data Analysis . . . 24
3.3 A New Concept for an Adiabatic Light Guide for Scintillator Counters . . . 28
3.4 RICH upgrade . . . 31
3.5 12 GeV DAQ / Trigger Upgrade Plans . . . 33

4 Summaries of Experimental Activities **34**

4.1 Experiment E94-107 . . . 34
4.2 Experiment E97-110 . . . 36
4.3 Experiment E00-102 . . . 38
4.4 Experiment E01-015 . . . 44
4.5 Experiment E02-013 . . . 46
4.6 Experiment E03-101 . . . 55
4.7 Experiment E03-104 . . . 58
4.8 Experiment E03-106 . . . 61
4.9 Experiment E04-018 . . . 66
4.10 Experiments E05-103 & E05-004 . . . 72
4.10.1 E05-103 . . . 72
4.10.2 E05-004 . . . 73
4.11 Experiment E05-110 . . . 76
4.12 Experiment E06-002 . . . 83
4.13 Experiment E06-007 . . . 85

5 Hall A Collaboration Member List **92**

6 Publications **98**

7 Theses **99**

List of Figures

1 Photo of repairing a plane of a BigBite wire-chamber. . . . 10
2 Summer student Emily Sykes (Phebus High School) 12
3 The new A/D card based on MAD ASIC. . . . 14
4 The LVDS to ECL converter panel. . . . 14
5 Rate *vs.* high-voltage curves for the old and the new cards 15
6 Schematic layout of the Hall A Compton polarimeter. . . . 16
7 The new electron detector housing and vacuum chamber 18
8 The new electron detector silicon micro-strip assembly. . . . 19
9 Optics table of the green Compton polarimeter. . . . 20
10 Optics table setup showing the assembled Fabry-Perot cavity 20
11 40-minute strip-chart recorded with EPICS during cavity-laser lock acquisition . . . 21
12 Temperature scan of the PPLN crystal 22
13 Power scan of the PPLN crystal 22
14 MC simulation of light propagation in the three-strip design 28
15 S-shape light guide construction and laser light through the light guide 29
16 3D expanded view of the upgraded RICH detector 31
17 Monte Carlo simulation of the upgraded RICH 32
18 E94-107: Preliminary data for the ${}^{16}_{\Lambda}$N missing-energy spectrum. . . . 35
19 E97-110: Preliminary results for Γ_1^n. . . . 37
20 E00-102: Projected A_{LT} data 39
21 E00-102: Kinematics 39
22 E00-102: Waterfall target 40
23 E00-102: Coincidence time spectra from the ROOT/C++ analyzer 41
24 E00-102: Extraction of the elastic peak from the ΔE spectrum 41
25 E00-102: Selected results from the Lund/Madrid MCEEP simulations. . . . 42
26 E00-102: $1p_{1/2}$ cross section relative to the $\mathrm{H}(e,e')$ cross section 42
27 E01-015: The measured and extrapolated yield ratios 45
28 E02-013: Conceptual lay-out of the experiment 47
29 E02-013: ^{3}He target polarization 48
30 E02-013: The angle between the beam direction and the holding field direction . . . 49
31 E02-013: The beam-helicity asymmetry of T2(T3) trigger rates 50
32 E02-013: Calibration of the momentum reconstruction 50
33 E02-013: Calibration of the time off-sets for BigHAND 51
34 E02-013: The amplitude spectrum in the front neutron detector 52
35 E02-013: The electric form factor of the neutron 53
36 E03-101: The cross section as a function of energy for ^{3}He photodisintegration . . . 56
37 E03-104: Recoil-polarization data as a function of Q^2 59
38 E03-106: The n-DVCS results and the contributions J_u and J_d to the proton spin . . 64
39 E03-106: Expected results for n-DVCS (left) and d-DVCS (right) 65
40 E04-018: ^{3}He F_C data compared to four different calculations 67
41 E04-018: ^{3}He F_M data compared to four different calculations 67
42 E04-018: ^{4}He F_C data compared to two IA calculations 68
43 E04-018: Raw time-of-flight (TOF) spectrum 69
44 E04-018: Raw "elastic stripe" with radiation tail 70
45 E05-103: The proton form-factor ratio as a function of Q^2 shown with world data . . 73
46 E05-103: Angular distributions for recoil-proton polarizations 74

47 E05-110: Energy resolution of the pion rejector 76
48 E05-110: Schematic of one individual box holding 90 crystals. 77
49 E05-110: Schematics of the optical coupling 78
50 E05-110: The CSR NaI(Tl) calorimeter mounted in its final position 79
51 E05-110: The CSR NaI(Tl) calorimeter mounted inside the FPP doors. 80
52 E05-110: Preliminary results for the calorimeter resolution 81
53 E05-110: Calorimeter resolution at 420 MeV/c 82
54 E05-110: Calorimeter resolution at 121 MeV/c 82
55 E06-007: Electron scattering, online. 87
56 E06-007: Electron scattering, improved 87
57 E06-007: Sieve slit, HRS-L 88
58 E06-007: Tl states, 0 to 200 MeV/c 89
59 E06-007: Tl at 300 MeV/c, data 89
60 E06-007: Tl at 300 MeV/c, simulation 90
61 E06-007: Carbon unrastered 90

List of Tables

1 Main design parameters of the green Compton polarimeter upgrade 17
2 E94-107: Levels and cross sections for $^{16}\mathrm{O}(e, e'\mathrm{K}^+)^{16}_{\Lambda}\mathrm{N}$ 34
3 E94-107: Comparison of B_Λ values 35
4 E02-013: The four kinematics of G_E^n measurements 47
5 E05-110: Resolution of the NaI(Tl) calorimeter 81
6 E06-007: Coulombs collected. 91

1 Introduction

Contributed by Kees de Jager

At the start of 2007 experiment E04-018, a measurement of the elastic form factors of ^{3,4}He up to large Q^2-values (Alexandre Camsonne, Javier Gomez, Mina Katramatou, Makis Petratos) was interrupted for three months. The accelerator was tuned to 325 MeV per pass for the first extension of the low-energy backward-angle G0 running. In February a two-week run (Doug Higinbotham, Ron Gilman) was carried out in parallel in Hall A to measure the elastic scattering cross section on ^{7}Li and ^{10}B. In early March the accelerator was retuned to 653 MeV per pass for the second and final extension of the low-energy backward-angle G0 running. E06-007, Impulse Approximation limitations to the $(e,'p)$ reaction on ^{208}Pb (K. Aniol, A. Saha, J. Udias, G. Urciuoli), was successfully completed during March. In April E04-018 resumed running but before this experiment could be fully completed, we first ran E03-101, hard pp photodisintegration using the $\gamma^3\mathrm{He} \rightarrow pp + n$ (R. Gilman, E. Piasetzky), ran for three weeks in June. E04-018 then was completed in a two-week run in July.

In the second half of 2007 we started with a 15 week long down to absorb the budget shortfall. In this period we succeeded thanks to very hard work by Alexandre Camsonne and Sasha Lukhenin, helped by many others, to assemble a NaI(Tl) calorimeter necessary for the Coulomb Sum Rule experiment. This experiment, E05-110 (J.-P. Chen, S. Choi, Z.E. Meziani) started running on October 23, taking data at 13 different energies, four scattering angles and targets and countless spectrometer momentum settings until the Christmas break.

The efforts to initiate two programs of parity-violating electron scattering in Hall A to be carried out with the 12 GeV Upgrade, one to study Møller scattering, the other Deep Inelastic Scattering, made significant progress in 2007, with strong explicit endorsement by the NSAC Long Range Plan.

Although last year Hall A published a respectful number of ten publications, the average publication output remains quite modest. We have completed 44 experiments, but published only 52 scientific papers, approximately 1.5 publication per experiment that has reached the publication stage. Although the mean time between the completion of an experiment and the submission of a first publication is 24 months, there are presently six experiments that have not submitted a publication three years after its completion. The impact of the Hall A publications is impressive, we have 2 publications with a citation index of over 250 and another 12 with over 50 citations. I want to strongly encourage all of you to dedicate more energy into timely publications, especially the completion of a number of long overdue archival papers. For major experiments it is essential that the details of the data taking, the analysis and the interpretation are widely accessible through publications in refereed journals.

It is with a very sad heart that I acknowledge the loss of two long-time friends and collaboration members, Jim Kelly and Kim Egiyan. Jim Kelly passed away in April after battling courageously a long illness. Jim's contributions to Hall A, have been many and valued over the past couple of decades. His archival paper on the "N-Delta experiment" (E91-011) will remain as a testament to Jim's amazing attention to detail and thoroughness. Kim Egiyan passed away in August. Kim Egiyan devoted a large fraction of his scientific life to a detailed and successful study of short-range correlations.

2 Standard Hall A Facilities

2.1 Polarized ^{3}He Target

Contributed by J. P. Chen

The Hall A polarized ^{3}He target[1] was successfully used in it's standard configuration for the experiments E94-010[2] and E95-001[3], E99-117[4], E97-103[5], E01-012[6] and E97-110[7]. It was also successfully used for E02-013[8] with a different configuration, which was reported in the Status Report in 2005.

The polarized ^{3}He target initially used optically pumped Rubidium vapor to polarize ^{3}He nuclei via spin exchange. Two sets of Helmholtz coils provided a 2.5 mT holding field for any direction in the scattering (horizontal) plane. Target cells were up to 40 cm long with a density of about 10 amg (10 atm at 0°C). The beam current on target ranged from 10 to 15 μA to keep the beam depolarization effects small and the cell survival time reasonably long (3 weeks). The luminosity was about 10^{36} nuclei/s/cm^2. The in-beam average target polarization achieved was typically over 40%. Two kinds of polarimetry, NMR and EPR (Electron-Paramagnetic- Resonance), were used to measure the polarization of the target. The uncertainty achieved for each method is 3% relative and the methods agreed well within errors. A new hybrid technique for spin-exchange by using a K-Rb mixture[9] was used for E02-013. Due to the much higher K-^{3}He spin exchange efficiency, the new hybrid cells achieved significantly shorter spin-up times (5-8 hours) and improved polarization ($\sim 50\%$).

A number of experiments, Transversity[10], d_2^n[11], A_y^n[12], $(e, e'd)$[13] which have been scheduled to run next year, will use the polarized ^{3}He target. Some of them will need vertical polarization. A new set of Helmholtz coils providing vertical field were procured. They were set up in the new target lab. Tests and a field mapping were performed. The field and field gradients satisfy the specifications. Fast target-spin reversals are needed for the Transversity and the A_y^n experiments (every 10-20 minutes). The fast spin reversal was achieved with the Adiabatic Fast Passage (AFP) technique. The polarizing laser spin direction reversal was accomplished with rotating 1/4-wave plates. The test results are consistent with expectations. The polarization loss due to fast spin reversal is at the order of $5-10\%$ depending on the AFP loss, which is typically $0.3-0.5\%$, and the spin-up time. The improvement of spin-up time with the hybrid cell has significantly reduced the polarization loss due to the fast spin reversal.

The new hybrid cell requires a higher temperature (230−250°C) than the rubidium cell (170°C). A test oven was designed, and constructed. It was able to achieve the required temperature, but its heavy weight caused problems. Reinforcements in the support had to be added to allow cell testing to start. The new oven has been tested to the operating temperature. With this oven, tests have been performed with a hybrid cell and new set-up for NMR and EPR. Initial tests showed that both polarimeter systems work well. Some improvements on the EPR system will be added. Additional pick-up coils were added to allow NMR to be performed in the pumping chamber. An improved oven with lighter material has been designed in the mean time together with an improved support structure.

To accommodate all four experiments with minimum change-over, a number of modifications and upgrades were implemented in the new design, including six optics line (two for each polarizing directions) and a compact layout in the pivot area. Ten new long optical fibers were procured along with three 5-to-1 combiners. All have been tested and satisfy our requirements. To have enough laser power to last for the duration of the experiments, three new 30 W lasers were ordered. A new access platform is being designed to allow work in the target area.

A new design of glass cells with pull-off on the side was developed.

About 18 cells have been manufactured by William and Mary (Todd Averett's group) and UVa (Gordon Cates' group) with glass cells supplied by a glass blower from Princeton University. Initial tests showed that most of the cells have polarizations around 50%.

A compass system to measure the vertical polarization is being developed at the University of Kentucky. A prototype system has been built and tested. An improved version is being designed and manufactured.

A new system to measure the Rb and K polarization and density using a Faraday Rotation technique has been successfully developed by the UVa group[14]. This will significantly improve the diagnostic ability.

References

[1] http://hallaweb.jlab.org/targets/polhe3/polhe3_tgt.html; and tech notes in http://www.jlab.org/e94010/.

[2] M. Amarian *et al.*, Phys. Rev. Lett. **89**, 242301 (2002); **92**, 022301 (2004); **93**, 152301 (2004); Z.-E. Meziani *et al.*, Phys. Lett. B **613**, 148 (2005).

[3] W. Xu *et al.*, Phys. Rev. Lett. **85**, 2900 (2000); F. Xiong *et al.*, Phys. Rev. Lett. **87**, 242501 (2001).

[4] X. Zheng *et al.*, Phys. Rev. Lett. **92**, 012004 (2004); Phys. Rev. C **70**, 065207 (2004).

[5] K. Kramer *et al.*, Phys. Rev. Lett. **95**, 142002 (2005).

[6] J.P. Chen, S. Choi and N. Liyanage, spokespersons, JLab Experiment E01-012.

[7] J.P. Chen, A. Deur and F. Garibaldi, spokespersons, JLab Experiment E97-110.

[8] G. Cates, N. Liyanaga and B. Wojtsekhowski, spokespersons, JLab Experiment E02-013.

[9] E. Babcock *et al.*, Phys. Rev. Lett. **91**, 123003 (2003).

[10] J.P. Chen, E. Cisbani, H. Gao, X. Jiang and J.C. Peng, spokespersons, JLab Experiment E06-010.

[11] S. Choi, X. Jiang, Z.-E. Meziani and B. Sawatzky, spokespersons, JLab Experiment E06-014.

[12] T. Averett, J.P. Chen and X. Jiang, spokespersons, JLab Experiment E05-015.

[13] S. Gilad, D. Higinbotham, W. Korsch, B. Norum and S. Širca, spokespersons, JLab Experiment E05-102.

[14] G. Cates, private communication.

2.2 BigBite Spectrometer

Contributed by Douglas W. Higinbotham
for the BigFamily of Experiments

With the first two BigBite spectrometer experiments completed, SRC[1] and G_E^n[2], the year 2006 has been spent preparing for the upcoming BigFamily[3] of BigBite experiments[4, 5, 6, 7, 8, 9]. This has meant that the Hall A area of the test lab has been overflowing with equipment as both an electron detection package and a hadron detection package are being assembled and tested simultaneously.

As a major upgrade from the G_E^n experiment, the middle wire-chamber, which was a three-plane chamber, has been upgraded to a full six-plane chamber under the direction of Nilanga Liyanage (UVa). Thanks to Xiaodong Jiang (LANL) and Evaristo Cisbani (INFN), we have secured the MAD chips needed for the front-end of all wire-chambers. These boards are being assembled off-site and should arrive for installation in December 2007. For reading out the chambers, we have gathered nearly complete VME and Fastbus systems. The plan is to start with the VME system with 767 and 1190 cards; but if a problem occurs with this system, to switch to the older Fastbus system with 1877 and 1879 cards.

Xin Qian (Duke) has lead the effort to test the wire-chambers and is presently organizing the effort to label and test the ribbon cables for the BigFamily of experiments. When the chambers were first tested in the test lab, all wires worked, but during their stay in the test lab, two wires broke, one wire in chamber one and one wire in chamber three. While it is impossible to prove what happened, there was a correlation between the breaking of a wire and nearby drilling. Thus, from now on drilling is forbidden on the frames while the chambers are attached.

To repair the chambers, we have moved the UVa wire-chamber repair equipment to Jefferson Lab. Under the direction of Brad Sawatzky (Temple), with the steady hands of Mitra Hashemi Shabestari (UVa), and the help of many others, we have already repaired the broken wire in chamber one and, as of the writing of this report, are repairing the second chamber. Figure 1 shows a wire-plane being repaired at Jefferson Lab. The broken wire in chamber one had clearly been damaged during installation. For chamber three, along with the broken wire many wires were found to be sagging. As this was an early plane in the construction of the chambers, the sagging problem was not seen with the other planes.

For the experiments which require the Hadron detector package, the detector package will be configured with two wire-chambers and dE/E scintillator trigger planes. In order to be able to install the BigBite wire-chambers in the BigBite Hadron package, the Kanya extruded aluminum frame needed to be modified. This change was accomplished this summer by the technicians of the Glasgow group. The detector electronics have been prepared mainly by Bryan Moffit (MIT) with much help from the summer student Gordon Lott (VPI) as well as from Khem Chirapatpimol (UVa), also thanks to John Annand (Glasgow) for his help in debugging the system.

For the electron package, the G_E^n pre-shower and shower lead-glass detectors needed to be repaired. Under the direction of Albert Shahinyan (JLab/Yerivan), the lead-glass detectors were removed, refurbished, returned to the detector package (as shown in Fig. 2, and tested by Kalyan Allada (Kentucky). Also for the electron package, a gas Čerenkov detector is being built by Temple, Rutgers and JLab. In order to hold the new Čerenkov detector, as well as hold all three wire-chambers, Hall A's new designer Macon Hodges has completed a modification plan and ordered the parts to make the modifications.

Figure 1: Shown is a photo by Brad Sawatzky (Temple) of Mitra Hashemi (UVa), Nikos Sparveris (MIT), and Xin Qian (Duke) preparing to repair a plane of a BigBite wire-chamber.

References

[1] S. Gilad, D. Higinbotham, E. Piasetzky, J. Watson and S. Wood, spokespersons, JLab Experiment E01-015, *Studying the internal small-distance structure of nuclei via the triple coincidence* $(e,e'p\mathrm{N})$ measurement.

[2] G. Cates, N. Liyanage and B. Wojtsekhowski, spokespersons, JLab Experiment E02-013, *Measurement of the neutron electric form factor* G_n^E *at high* Q^2.

[3] http://hallaweb.jlab.org/experiment/BigFamily.

[4] J. Annand, D.W. Higinbotham, R. Lindgren, B. Moffit, B.E. Norum and V. Nelyubin, spokespersons, JLab Experiment E04-007, *Precision measurement of electroproduction of* π^0 *near threshold: a test of chiral QCD dynamics.*

[5] J.P. Chen, E. Cisbani, H. Gao, X. Jiang and J.C. Peng, spokespersons, JLab Experiment E06-010, *Measurement of the single target-spin asymmetry in the semi-inclusive* $^3\mathrm{He}(e,e'\pi^{\pm})$ *reaction on a transversely polarized* ^{3}He *target.*

[6] T. Averett, R. Gilman, T. Holmstrom and X. Jiang, spokespersons, JLab Experiment E06-012, *A Parasitic Measurement during E03-004 of the Target Single-Spin Asymmetry in the Inclusive DIS (e,e′) Reaction on a Vertically Polarized* ^{3}He *Target.*

[7] S. Choi, X. Jiang, Z.E. Meziani and B. Sawatzky, spokespersons, JLab Experiment E06-014, *Precision Measurements of the Neutron* d_2*: Towards the Electric and Magnetic Color Polarizabilities.*

[8] T. Averett, J.P. Chen and X. Jiang spokespersons, JLab Experiment E05-015, *Measurement of the Target Single-Spin Asymmetry in Quasi-Elastic* ^{3}He$(\vec{e},e')$.

[9] S. Gilad, D.W. Higinbotham, W. Korsh, B.E. Norum and S. Širca, spokespersons, JLab Experiment E05-102, *Measurement of* A_x *and* A_z *asymmetries in the quasi-elastic polarized* ^{3}He$(\vec{e},e'd)$ *reaction.*

Figure 2: Summer student Emily Sykes (Phebus High School) after she finished re-stacking the refurbished lead-glass shower detectors in the BigBite electron package.

2.3 New Amplifier/Discriminator Cards for Multi-Wire Drift Chambers

Contributed by I. Rachek
in collaboration with W. Gunning, C. Cuevas and B. Wojtsekhowski

Introduction

The amplifier/discriminator cards by LeCroy Research Systems, type 2475 [1] are widely used in wire-chamber read-out systems. The 2475 card is based on LeCroy custom chips: the quad amplifier TRA402 and the quad discriminator MVL407. These cards are used in the Vertical Drift Chambers of the Hall A High Resolution Spectrometers. Unlike the LeCroy 2475 card the N277C card by Nanometric System [2] utilizes commercially available chips. The N277C card has the same geometry and input-output specifications as the LeCroy 2475 card and therefore can replace the latter.

The tracking chambers for the BigBite spectrometer were also designed to be equipped with LRS2475DC/N277C cards. The LeCroy specifications sets the minimum threshold for these cards at 1 μA, but in practice the threshold has to be set at about 5 μA due to feedback of the ECL signals from the outputs of the cards on the sense wires. With such a threshold the working high voltage for the BigBite chambers is 1800 V when the standard gas mixture of argon(65%)+ethane(35%) is used.

However, in many applications the BigBite tracking system has to be able to operate at a very high background rate. For example, in the G_E^n (E02-013) experiment the background rate on the front chamber was 20 MHz/plane. This could result in a high leakage current at the level of 1 mA, which may cause unstable operation and rapid degradation of the chamber. An obvious way out would be to reduce the chamber's gain with a corresponding increase of the sensitivity of an amplifier/discriminator. The latter can not be done with LeCroy/Nanometric cards, a new A/D card is required.

Design

The new A/D card was developed by the G_E^n collaboration and JLab's Electronics Group. The card's geometry (size, positions and types of input/output/power connectors) is exactly the same as for a reference LRS2475DC card, enabling an easy transition to new cards in existing systems equipped with LeCroy/Nanometric cards.

A key element of the new A/D card is the ASIC called MAD, developed by the INFN section of Padua[1]. Both input and output specifications of this chip are preferable to those of the chips used by LeCroy/Nanometric. The charge-sensitive input stage of MAD is several times less noisy than the current-sensitive one of LeCroy/Nanometric. The MAD's output stage works with LVDS signals which are known to produce significantly less feedback than the ECL signals used in the LeCroy/Nanometric cards. These features of the new card make it feasible to set a threshold significantly lower than is achievable with LeCroy/Nanometric cards.

The new card requires only a single (positive) power supply, applied to the same pins on the power connector as for the positive supply voltage of LeCroy card. Several other voltages used by the MAD chips are formed by voltage regulators installed on the card. No negative supply voltage is needed for the new card.

Two main application differences between the new and old cards are *a*) the way how threshold control is arranged; and *b*) specifications of the output signals (LVDS instead of ECL).

[1] see http://www.lecroy.com/lrs/dsheets/2735.htm
[2] see http://www.nanometricsystems.com/n277info.cfm

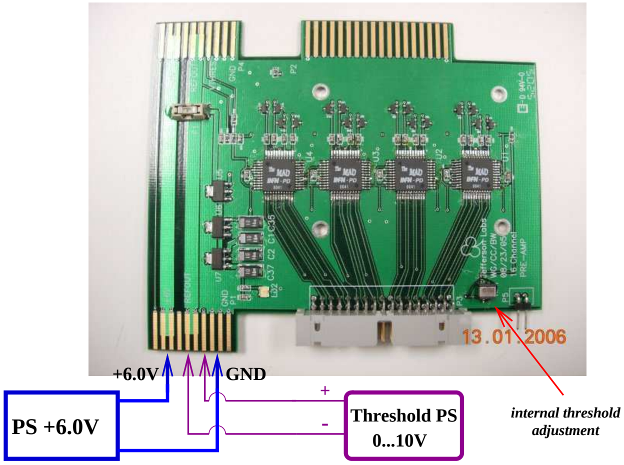

Figure 3: The new A/D card based on MAD ASIC.

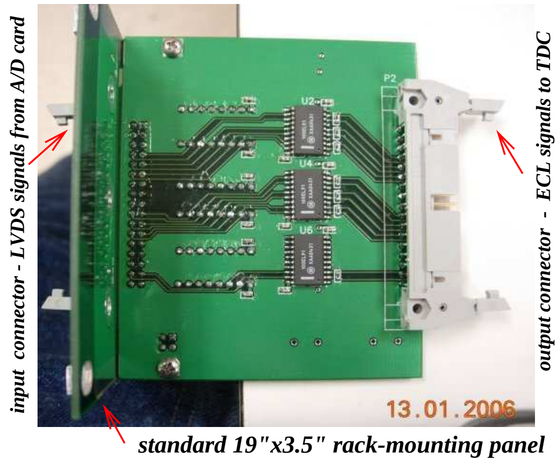

Figure 4: The LVDS to ECL converter panel.

Control of the threshold can be done in two ways: by an on-card potentiometer and by an external source. Unlike for the LeCroy/Nanometric cards, the power supply for remote threshold control for the new card must be isolated from ground – see Figure 3. External and internal threshold voltages are summed, therefore the on-board potentiometer can be used to equalize an actual threshold for all cards on a wire-chamber for a common external threshold voltage.

The outputs of the new card are LVDS signals which can be transmitted by standard twist-and-flat cable up to 40 meters long to novel types of TDCs accepting LVDS levels. In order to use older FastBus/VME TDC modules a special LVDS-ECL level converter has been developed and constructed by the JLab Electronics Group. It is designed as an active patch panel for flat cables, see Fig. 4. Each 19"×3.5" rack-mounting panel houses sixteen 16-channel level converters, placed close to the TDCs.

Performance

A sample of the new card was tested on the wire-chamber of the BigBite tracking system and has shown to be able to operate at a threshold 5-10 times lower than it was possible with the Nanometric N277C card. Figure 5 shows rate vs chamber high-voltage curves measured when the chamber was illuminated by a ^{55}Fe γ-source. One can see that with the new card the high voltage can be reduced by approximately 200 V.

After a successful test of the sample a set of new A/D cards was built and 54 cards were installed on the front MWDC of the BigBite tracking system. The new cards have demonstrated a reliable operation during the two-month G_E^n experiment in Hall A.

References

[1] M. Pegoraro, Proceedings of the Fourth Workshop on Electronics for LHC Experiments, CERN/LHCC/98-36, 1998, p. 257.

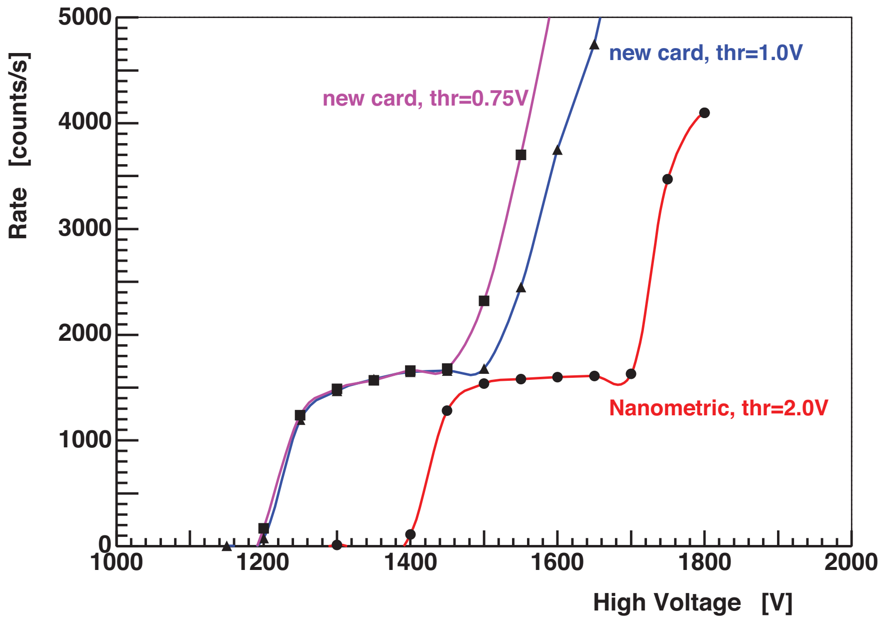

Figure 5: Rate *vs.* high-voltage curves for the old and the new cards mounted on the front chamber of the BigBite tracking system.

3 General Hall Developments

3.1 The Compton Polarimeter Upgrade

Contributed by Sirish Nanda

Overview

The Hall A Compton Polarimeter provides electron beam polarization measurements in a continuous and non-invasive manner via Compton scattering of polarized electrons from polarized photons trapped in a Fabry-Perot cavity. A schematic layout of the Compton polarimeter is shown in Fig. 6. The electron beam is transported through a vertical magnetic chicane consisting of four dipole magnets. At present, a high-finesse Fabry-Perot injected by a 240 mW, 1064 nm infrared laser serves as the photon target. Intra-cavity power remains stable at about 500 W. The Compton back-scattered photons are detected in an electromagnetic calorimeter consisting of lead tungstate crystals. The recoil electrons, separated from the primary beam by the fourth dipole of the chicane, are detected in a silicon micro-strip detector. The electron beam polarization is deduced from the counting-rate asymmetries of the detected particles.

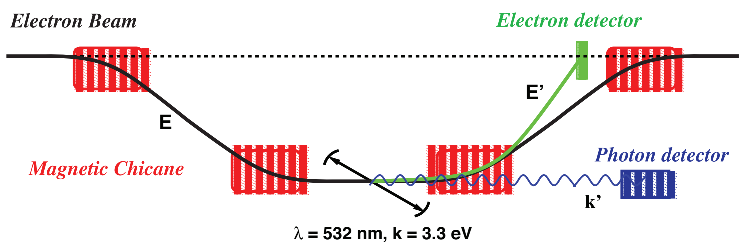

Figure 6: Schematic layout of the Hall A Compton polarimeter.

A performance upgrade of the Compton Polarimeter, in accordance with the conceptual design report[1], is presently under implementation. The upgrade is motivated by upcoming high accuracy experiments with a very demanding requirement on the beam polarization. Defining k as the photon energy and E as the electron beam energy, the Figure Of Merit (F.O.M.) of a Compton measurement scales with $k^2 \times E^2$, making high-accuracy polarimetry a real challenge at low energy. The proposed upgrades are thus driven by the requirement of the Lead Parity experiment[2] of 1% relative accuracy at 850 MeV. The present infra-red system, while capable of achieving such accuracies at higher energy ($\geq$ 6 GeV), falls far short at lower energies. We plan to upgrade the existing Fabry-Perot cavity operating at 1064 nm (IR) with about 1.5 kW power to a 532 nm (green) cavity with similar power.

In addition, improvements to the electron detector and photon calorimeter combined with the development of a new integrated method shows promise of absolute accuracies approaching 1% at 0.85 GeV beam energy. The main parameters of the green Compton upgrade are shown in Table 1. The conceptual design of the green Compton polarimeter utilizes much of the design philosophy and the existing infrastructure of the present Compton polarimeter. In the following, the subsystems under upgrade are described.

Parameter	Present	Upgrade
Wavelength [nm]	1064	532
Cavity Power [W]	1500	1500
Cavity Q	1.0×10^{11}	1.8×10^{11}
FOM (σ.A^2) @ 0.85 GeV	0.57	2.2
Energy Range [GeV]	2 - 6	0.8 - 6
$\delta P_e/P_e$ @ 0.85 GeV	-	1%

Table 1: Main design parameters of the green Compton polarimeter upgrade compared to the present infra-red system.

Electron Detector

The electron detector upgrade is being carried out at the Laboratoire de Physique Corpusculaire IN2P3 of the Université Blaise Pascal, Clermont-Ferrand. The new detector has 4 planes of 192 silicon micro-strips with 240 μm pitch. The expected resolution is about 100 μm. In addition to an improved resolution, the electron detector will be configured to move in a vertical plane so as to facilitate covering the recoil electrons corresponding to the Compton edge over a broad range of energies.

The final design of the electron detector support structures and vacuum chamber was approved for fabrication during the spring of 2007. Fabrication was completed later in the summer. The complete mechanical subsystem was delivered to LPC in the fall. It has been fully assembled and tested at LPC-Clermont and will arrive at Jefferson Laboratory in February 2008 for installation in the beam line.

A high-precision vertical motion of 120 mm for the detector has been incorporated in the design. Presently, the motion control system as well as the remote-control computer interfaces are under development. Illustrated in Fig. 7 is a computer model of the mechanical assembly and in Fig. 8 the electron detector silicon micro-strip assembly.

Photon Detector

The Carnegie Mellon University (CMU) joined the upgrade effort in 2007 and accepted the responsibility for the new photon detector. Simulations for a new high light-output and fast-response calorimeter were completed during the summer of 2007 by Gregg Franklin at CMU. Based on the studies, a single GSO crystal, 60 mm in diameter and 150 mm in length coupled to a 3 inch PMT was chosen for the shower detector of the new calorimeter to replace the present multi-crystal Lead Tungstate array. Full specifications for the GSO crystal were developed and competitive bids for the procurement of the crystal were solicited from three vendors in September 2007. The contract was awarded to Hitachi Chemicals Ltd. for the fabrication, test, and delivery of the GSO crystal. It is expected to be delivered to CMU in the coming weeks.

Further progress was made in the studies of the integrating DAQ with a Flash ADC. Following the analysis of data taken last year, specifications for new flash ADCs were developed in collaboration with CMU. Procurement of the new ADCs is expected to be completed within the coming weeks.

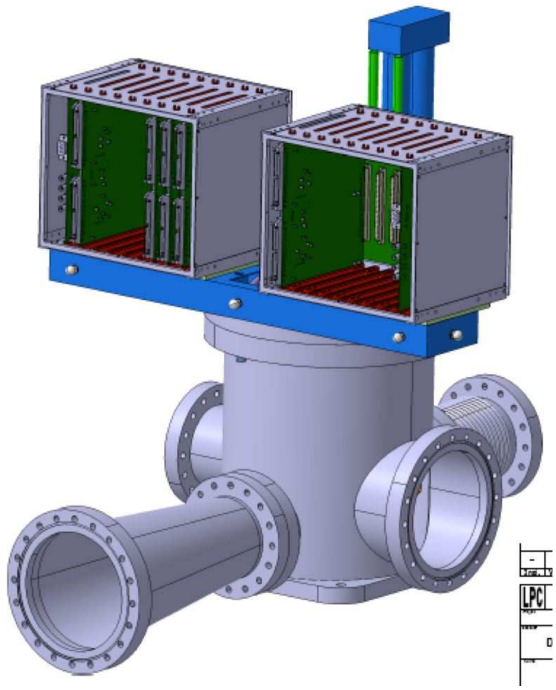

Figure 7: The new electron detector housing and vacuum chamber completed by LPC-Clermont.

Fabry-Perot Cavity

A schematic lay-out of the optical setup for the upgrade is shown in Fig. 9. The heart of the upgrade plan is to replace the infrared cavity with a 532 nm green cavity fed by the new laser. Recent advances in the manufacturing of high-reflectivity and low-loss dielectric mirrors as well as the availability of narrow line-width green lasers facilitates the feasibility of our challenging design goal. High-gain cavities at 532 nm have been successfully constructed by the PVLAS[3] group that has a geometry and gain compatible with our proposed design.

Significant progress has been achieved in the development of the green Fabry-Perot cavity with continuing participation of Botao Jia, Duke University. Our approach to achieve the design goal of 1.5 kW power in the cavity is by sequentially increasing the gain of the cavity by changing the mirrors. For this purpose, we have obtained three sets of mirrors: low-gain mirrors from CVI laser Corp., medium-gain mirrors from LGR Corp. and high-gain mirrors from REO. In the spring of 2008, the cavity was configured with the CVI mirrors in preparation for cavity lock using the Pound-Drever-Hall scheme. We developed a microprocessor-based cavity scan and lock electronics system, the Cavlock, during the summer of 2008. The prototype module of the Cavlock was assembled in-house and tested with the Prometheus laser. A production version of the Cavlock box is now under design in the electronics group. Shown in Fig. 10 is the fully assembled cavity under test in the lab.

We sucessfully acquired cavity-laser lock on the TEM_{00} cavity mode. Illustrated in Fig. 11 is a 40-minute strip-chart recorded with EPICS during lock acquisition. The upper green trace is the photodiode signal from the laser power reflected from the cavity, the blue curve is the photodiode signal from the laser power transmitted through the cavity, the red trace is the error signal fed back to the laser to sustain lock, and the bottom light blue trace is the scan ramp signal used to

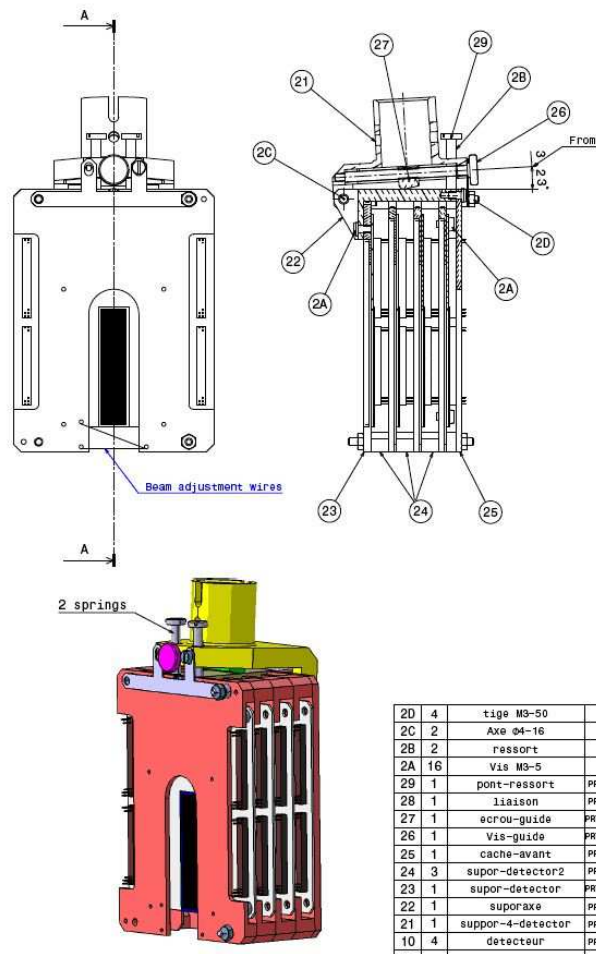

2D	4	tige M3-50	
2C	2	Axe Φ4-16	
2B	2	ressort	
2A	16	Vis M3-5	
29	1	pont-ressort	PF
28	1	liaison	PF
27	1	ecrou-guide	PR
26	1	Vis-guide	PR
25	1	cache-avant	PF
24	3	supor-detector2	PF
23	1	supor-detector	PR
22	1	suporaxe	PF
21	1	suppor-4-detector	PF
10	4	detecteur	PF

Figure 8: The new electron detector silicon micro-strip assembly.

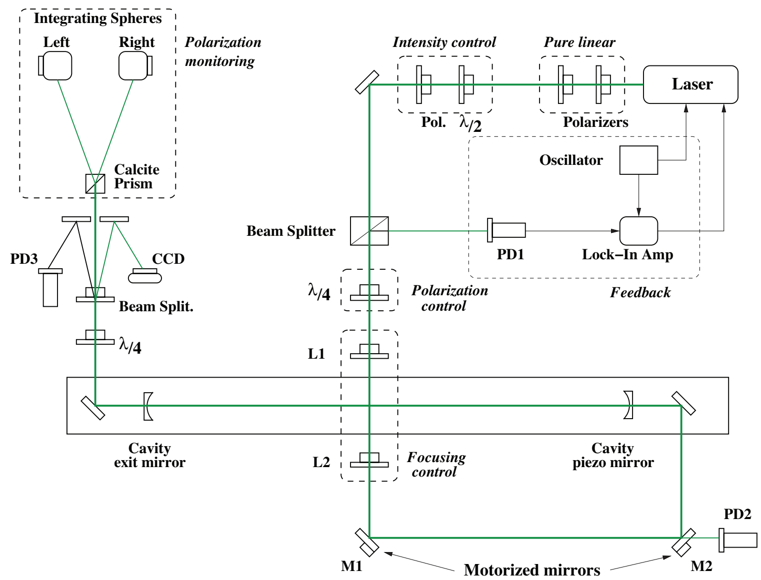

Figure 9: Optics table of the green Compton polarimeter.

Figure 10: Optics table setup showing the assembled Fabry-Perot cavity under test in the Compton Polarimetry Lab.

scan for cavity resonating modes. As evident from the chart, lock durations over 20 minutes were achieved during which the reflected and transmitted powers remain stable at their peaks.

The next higher gain set-up using the LGR mirrors was set up with the help from Abdurahim Rakhman, a graduate student from Syracuse University, in the fall of 2008. We are presently tuning the feed-back loop for this cavity with the Cavlock.

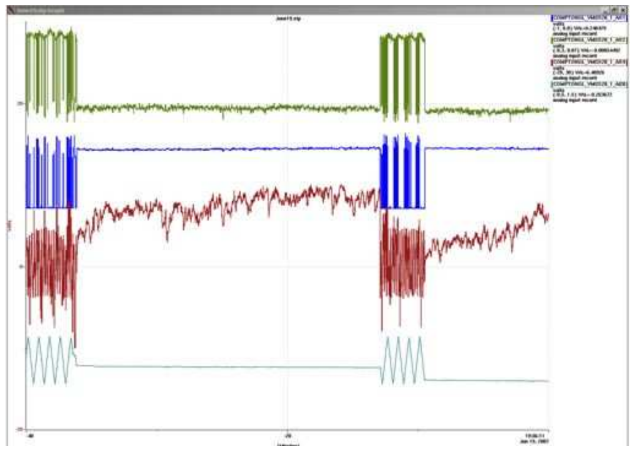

Figure 11: 40-minute strip-chart recorded with EPICS during cavity-laser lock acquisition. The upper green trace is the photodiode signal from the laser power reflected from the cavity, the blue curve is the photodiode signal from the laser power transmitted through the cavity, the red trace is the error signal fed back to the laser to sustain lock, and the bottom light blue trace is the scan ramp signal used to scan for cavity resonating modes.

PPLN green laser

The power available from the Prometheus laser is unlikely to meet our design goal of 1.5 kW of intra-cavity power. This has prompted us to develop our own green laser source. We launched an effort to double the frequency of our existing Lightwave infra-red laser (1064 nm) to produce a 532 nm green beam via second harmonic generation (SHG) using a periodically poled Lithium Niobate (PPLN) crystal. Diana Parno, a graduate student from the Carnegie Mellon University, joined our efforts in February 2008 to investigate SHG in PPLN. We were successful in phase matching the PPLN crystal for SHG by tuning its temperature. In our first attenpt, we obtained about 20 mW of average green power with about 560 mW of pump power. However, the green power was highly unstable due to large temperature fluctuations in the resistive PPLN Oven supplied by HC Photonics. Subsequently, we built an oven based on a thermoelectric element (TEC) controlled by an off-the-shelf TEC controller from Thorlabs. The new system achieved an order of magnitude better temperature stabilities.

Tharanga Jinasundera, a graduate student from the University of Virginia, joined the PPLN studies upon Diana's departure in September 2008. In December 2008, with the new TEC temperature control and improved optics set-up, we were able to produce 38 mW of stable green power with the same pump power as before. Shown in Fig. 12 is the green SHG power generated in the PPLN crystal as a function of the PPLN temperature, with the Lightwave laser pumping 560 mW of infra-red power into the crystal. Quasi-phase matching conditions are reached at a temperature of 62.7° with about 0.6° full-width at half maximum. As expected, the green power (see Fig.13) depends quadratically on the pump IR power.

We plan to couple the Lightwave IR laser through a fiber to an Ytterbium fiber amplifier to produce 10 W of IR power to pump the PPLN crystal. An amplifier for this purpose has been ordered from the IPG. Photonics Corp. With this amplifier we expect green power in the watts regime that will enable us to achieve our design goal for the cavity power.

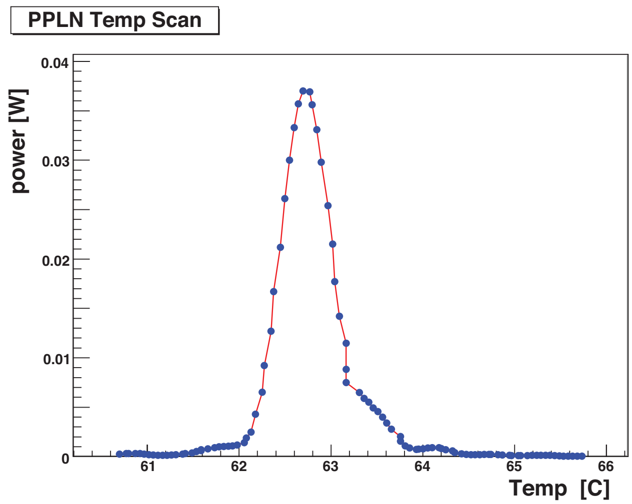

Figure 12: Temperature scan of the PPLN crystal showing a quasi-phase matching temperature of 62.7° for SHG power.

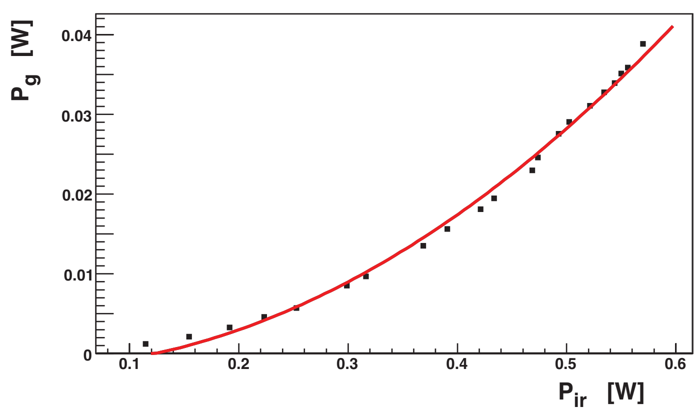

Figure 13: Power scan of the PPLN crystal showing a quadratic dependence of the SHG green power (P_g) on the infra-red (P_{ir}) pump power.

References

[1] S. Nanda and D. Lhuillier, Conceptual Design Report for the Hall A Compton Polarimeter Upgrade, unpublished.

[2] Paul Souder, Robert Michaels and Guido Urciuoli, spokespersons, JLab Experiment E06-002.

[3] M. Bregant *et al.*, Rev. Sci. Instrum. **73**, 4142 (2002); arXiv:hep-ex/0202046.

3.2 Data Analysis

Contributed by J.-O. Hansen

Podd (ROOT/C++ Analyzer)

Our main data analysis software, Podd, saw a number of small yet important improvements over the past year. Aside from minor bug fixes, the following updates were included in the production version (Release 1.4):

- A workaround for the "timezone bug" was implemented. The bug is partly due to a poor design choice in ROOT's `TDatime` class, which always handles time data as local time. This caused a mismatch between time stamps from CODA files and time stamps in the database if the computer used for replay was located in a timezone other than JLab's. The workaround forces the timezone environment of the analyzer process to US/Eastern time regardless of the local setting; then, as long as the database time stamps are also in US/Eastern time, no mismatch occurs.
- The performance of the ROOT file output class, `THaOutput`, was improved as much as possible without a redesign.
- Several bugs in `THaOutput` were corrected, including possibly incorrect scaler data that were written at the beginning of a run, duplicate variables in the tree, and crashes on exit from the analyzer in certain situations. Fortunately, none of these bugs was serious; there is no need to redo old replays.
- Problems with the initialization of the energy-loss physics modules were corrected. The initialization would always fail because of a subtle logic error.
- Support for ROOT 5.16 (which contains significant changes compared to 5.14) was added.
- The build system now supports installation of all required runtime files in a target directory tree ("make install").

All experiments that have run during 2007 have used Podd 1.4. The current production version is 1.4.9.

The release of Podd 1.5 had originally been planned for early to mid 2007. However, the schedule was delayed because of limited manpower and other, more urgent commitments. Nevertheless, a number of major improvements over Podd 1.4 have already been completed and are available in CVS:

- The database system's capabilities were significantly expanded. Now supported are integer and string data, arrays, matrices, continuation lines, and in-line comments. Entries may be up to 16k characters long, up from 256. Error messages are more descriptive. Database keys are now case-sensitive for consistency with ROOT (and C/C++). Multiple variables can now be parsed and loaded with a single database request, resulting in a major simplification of `ReadDatabase` functions, which were often tedious to write in the past.
- Detector maps contain more information. In particular, the support for "reference channels" of pipeline TDCs was expanded. The entire detector map, encoded as a string, can now be read with a single function call. Error checking has been much improved.
- The helicity decoder classes have been restructured for greater clarity. Different helicity decoding schemes are now implemented as independent classes rather than one large catch-all "helicity class".

Since these improvements are mainly interesting for the development of new code, we have not yet released this version for production. Podd 1.5 will probably be released in early to mid 2008 along with the new BigBite tracking software (see next section), which requires the new features.

Because of the success and stability of Podd in the past 2–3 years, we feel that it is time to declare the software "mature" and to end the active development by Hall A staff of new features for the core package. Of course, we will continue to troubleshoot problems with the existing code and port Podd to new platforms as needed. However, major improvements and new features are from now on expected to be contributed by the user community. This has already worked very well in the past, with user groups contributing analysis libraries for their experiment-specific equipment, e.g. the BigBite spectrometer.

Among the open issues with and ideas for improving Podd that should be addressed at some point, we would like to list a few here as suggestions for interested users:

1. *Performance of output.* The time for writing tree variables, histograms etc. to the ROOT output file still usually dominates the total analysis time by a large margin (depending on how judiciously users design the output request). Several code inefficiencies are known; improvements could be readily implemented. Time estimate: 2 man months.
2. *VDC multi-hit analysis.* The current VDC track-reconstruction code does not handle multiple hits and clusters well. Although this is partly a problem inherent in the design of the VDCs, some improvement may come from a more intelligent reconstruction algorithm. Work is needed to (a) fit clusters in the presence of multiple hits per wire intelligently; (b) improve the handling of common time offsets (t_0) of clusters; (c) use a more sophisticated algorithm for combining clusters from different planes (track projections) into 3-D tracks. The algorithm should be tested, and improvements quantified, using the existing `VDCsim` Monte Carlo framework. Estimate: 6–9 man months.
3. *Shower cluster analysis.* The shower reconstruction algorithm should be extended to be able to identify multiple (possibly overlapping) clusters. Well-known approximation algorithms exist in the Computer Science literature for this problem, which ideally should be solved without tracking input (as shower data may be used to assist tracking). Estimate: 3 man months.
4. *EPICS fitter.* We already have the tools to upload EPICS slow-control data to a database in a dedicated analysis pass. Still missing, however, is a general-purpose module that provides the time-dependent information from arbitrary EPICS variables (or other variables in the database) as a fitted, smoothly-varying function of time. Typical examples are the beam position and energy as well as target and beam polarizations. During physics analysis, one would like to have ready access to interpolated values of these variables for the current event. Time estimate: 1 man month.
5. *Abstract database interface (writable) plus SQL implementation.* Our database system is still based on plain text files that are prepared using external scripts or editors. While this approach works well and is popular with users for its simplicity, it would nevertheless be desirable to (a) abstract the database interface fully so that analysis modules do not need to know anything about the actual database implementation; (b) provide the ability not only to read but also to write and edit time-dependent data in the database through this interface; and (c) to have an SQL implementation in addition to the plain text file system. A prototype abstract interface exists. Estimate: 6 man months.
6. *Consistent timestamping.* Convert Podd to use ROOT's `TTimeStamp` class, which keeps time in UTC, instead of `TDatime` to eliminate timezone problems once and for all. Estimate: 1

man month.

7. *Multi-threading.* To improve performance on multiprocessor machines, the code should be multi-threaded. This should be fairly easy to do for the `Decode` and `Reconstruct` stages of the analysis as well as parts of the VDC code whose algorithms are inherently parallel. Other parts of the code (`THaOutput`?) can probably be parallelized with some redesign. Time estimate: 2–3 man months.

Additionally, there is always a need for writing user-friendly documentation. Anyone interested in working on any of these items are welcome to contact us for details.

BigBite Tracking Software

An effort is currently underway to rewrite the track reconstruction software for the BigBite spectrometer (see Section 2.2). The existing BigBite tracking software was developed for the G_E^n experiment, E02-013 (see Section 4.5), by Andrew Puckett of MIT, Seamus Riordan of CMU and others in 2005/2006. It is fairly sophisticated and certainly able to reconstruct tracks with good accuracy from the E02-013 data. However, experience has shown it to be neither very efficient nor scalable. Track reconstruction currently takes $\mathcal{O}(100\ \text{ms})$ per event with memory requirements of $\mathcal{O}(100\ \text{MB})$. Furthermore, the algorithm runs in polynomial time, $\mathcal{O}(N^k)$, where N is the average number of hits per plane (typ. 20–40 in E02-013) and k is proportional to the number of wire planes. Hence, one can expect *significantly* worse performance if all 18 BigBite wire planes are employed (instead of only 15 in E02-013) and/or rates are higher, which could make the analysis of such data with the existing code nearly impossible.

The new reconstruction software uses a recursive template matching algorithm, also known as "Tree Search"[1]. This algorithm has been used for the analysis of the drift chamber data in the HERMES experiment[2] since 1995. As the HERMES tracking system is more complex than that of BigBite, and it was possible already over 10 years ago to analyze the HERMES data at acceptable speed, it can be expected that the BigBite analysis will run very efficiently using the Tree Search algorithm.

In the template matching approach, all physically possible patterns of hits that can occur in the wire chambers for a single track are pre-computed and stored in a database. Computation of the patterns is particularly easy if only straight tracks have to be considered, which is the case for BigBite (to a very good approximation). The main challenge is that, at high spatial resolution, the number of possible templates grows extremely large, $N_t \approx \mathcal{O}(2^{k-2}n^2)$ for $k \geq 2$, where n is the number of bins into which each detector plane is divided. Typically $n = \mathcal{O}(1000)$, so $N_t = \mathcal{O}(10^7)$. Such a vast number of templates would require GB of storage. However, the storage requirements can be dramatically reduced by symmetry considerations: so long as the wire planes are parallel, only patterns originating in one corner of the tracking region need to be stored. The full set of templates can then be reconstructed from these base patterns through translation and/or mirroring [3]. This reduces the storage requirements to approximately $\sqrt{N_t} = \mathcal{O}(10^4)$, i.e. less than a MB.

The second challenge in a template matching algorithm is the lookup speed: in principle, every template must be checked against the hit pattern of an event; and of course $\mathcal{O}(10^7)$ comparisons per event would be extremely slow. An elegant solution to this problem is to use a successive approximation strategy[1]: the tracking area is viewed at increasingly finer resolution (2^i bins at the i-th step). Templates are pre-computed for each resolution level along with a list of "child patterns" that derive from them at the next higher resolution. Then only the child patterns of those patterns that match the hit pattern at a certain level need to be checked at the next level. The search ends when the highest resolution is reached. The hierarchy of parent and child patterns can be visualized as a tree data structure, where the i-th tree level corresponds to a resolution of 2^i bins. The theoretical run time performance of this search is far better than that of the existing BigBite algorithm: Monte Carlo studies suggest a scaling of $\mathcal{O}(N \cdot 2^k)$ (instead of $\mathcal{O}(N^k)$) if most of the N hits per plane are random noise [4]. These studies also show that typically only a few thousand comparisons are needed per event per wire direction at a maximum resolution of 1024 bins. Similar numbers have been obtained in a preliminary analysis of E02-013 data.

At this time, the generator for the pattern database, the raw data decoder, hit pattern class, and the core pattern recognition engine (the template matching tree search) have been written and tested. The output are so-called "roads" (narrow straight paths in which valid tracks may be found), in each of the wire directions. Remaining tasks include (1) fitting of tracks within the roads; (2) combination of 2-D track projections into 3-D tracks in space; (3) rejection of ghost tracks (which may occur due to noise, resolution effects and left-right ambiguities); and (4) target (vertex) reconstruction. Once these steps are implemented, Monte Carlo studies will be done to verify the algorithm's correctness and accuracy. We hope to have the new tracking code ready for the Big Family experiments in the Spring of 2008.

References

[1] M. Dell'orso and L. Ristori, Nucl. Instr. Meth. in Phys. Res. A **287**, 436 (1990).

[2] K. Ackerstaff *et al.*, Nucl. Instr. Meth. in Phys. Res. A **417**, 230 (1998).

[3] W. Wander, Ph.D. thesis, Friedrich-Alexander-Universität Erlangen-Nürnberg, 1996, available from `http://www-hermes.desy.de/notes`.

[4] J.-O. Hansen, "A Tree Search Tracking Algorithm for the Hall A BigBite Spectrometer", in preparation.

3.3 A New Concept for an Adiabatic Light Guide for Scintillator Counters

Contributed by B. Wojtsekhowski
in collaboration with A. Sarty, J. Glister and A. Shahinyan

Introduction

The use of adiabatic light guides (ALG) made of acrylic is a well-known method for light collection from large area thin scintillator counters[1]. ALGs are typically made from polished strips, which are prepared from flat straight bars and then deformed at high temperature to a twisted form to allow for a compact arrangement of the strips at the PMT photocathode. Most commonly, the twisting deformation is made by a 90° rotation of the strip plane.

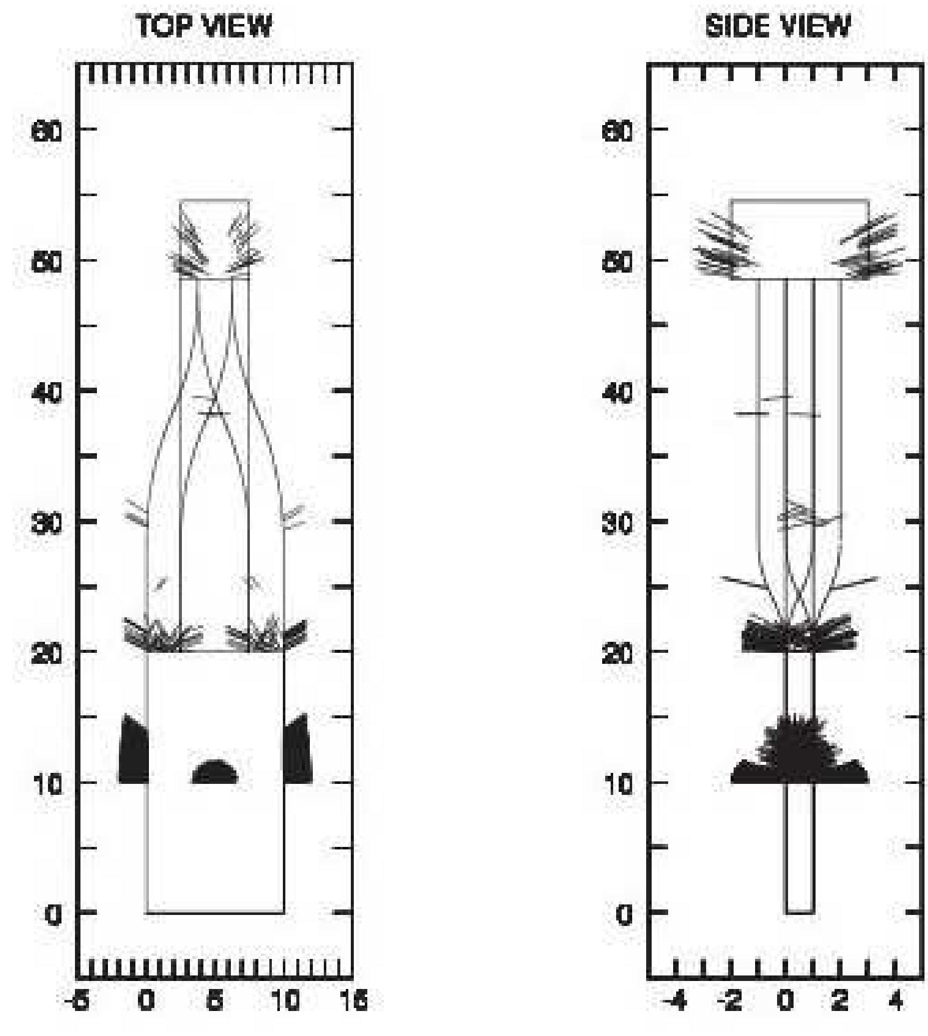

Figure 14: MC simulation of light propagation in the three-strip design of the S-shape light guide. Dimensions are given in cm. Taken from [3].

Such a 90° rotation requires a significant length of light guide, especially for thick light guide strips. A few years ago, we suggested a new option for light guide topology in which the strip deformation is made only in the plane for which the strip size is smallest, and subsequently the bending radius could be made smaller than in the conventional method of twisting. A smaller bending radius allows the possibility of a shorter light guide, and an associated reduced jitter in the photon time propagation, and therfore can lead to a better overall time resolution for a scintillation counter using the smaller-bend light guide.

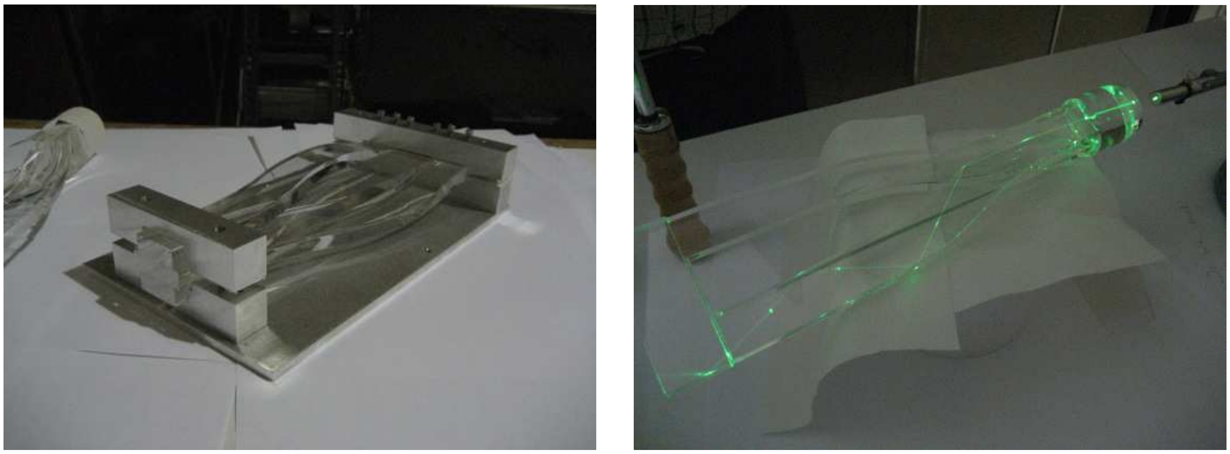

Figure 15: (Left) Construction of the S-shape light guide. (Right) Laser light going through the light guide.

Monte Carlo simulation. With this perspective in mind, we first performed a detailed simulation of a scintillation counter that had an active area of $200 \times 100 \times 10$ mm^3, with light collection by two inch PMTs at two ends, by using the Guide-7 simulation code[2] to track photons through the counter and a new S-shaped, three-strip light-guide configuration. The results of this simulation has demonstrated the adiabatic property of light collection and a good/improved efficiency and timing resolution for this new S-shaped light guide configuration[3, 4]. Figure 14 shows Monte Carlo results for the light guide in two projections[3, 4], and illustrates escape points for scintillation photons which were programmed to originate in the middle of the scintillator. According to that simulation, the collection efficiency is about 97% for light arriving at the corresponding face of the scintillator.

Construction. We have developed equipment to form the strips in the desired shape, and for gluing the light-guide pieces. The first prototype has been constructed in order to test the technological process (see Figure 15).

References

[1] W.R. Leo *"Techniques for Nuclear and Particle Physics Experimnets"*, New York: Springer-Verlag (1987); P. Gorenstein and D. Luckey *"Light Pipe for Large-Area Scintillator"*, Rev. of Sci. Instr. **34**, 196 (1963).

[2] T. Masam *"GUIDE-7: A General Program for Evaluating the Properties of Scintillation and Čerenkov Counter Systems"*, CERN Library.

[3] J. Glister *"Novel Light Guide for Scintillation Counters in Hall A of Jefferson Lab"*, B.Sc. Honour's thesis, Saint Mary's University, Canada, (2005).

[4] J. Glister and A.J. Sarty, *"Design Study of Novel Light Guide Geometry for Scintillation Counters"*, Proc. of the Nova Scotian Institute of Science, Vol. 43, Part 2, p. 227 (2006).

3.4 RICH upgrade

Contributed by E. Cisbani

The measurement of the neutron SSA on π and K (at 2.4 GeV/c) in the upcoming experiment on Transversity E06-010, requires an effective - at the level of 1:1000 - pion-kaon rejection. This will be achieved by the use of the upgraded RICH detector, the original version of which was succesfully operated in the Hypernuclear Spectroscopy Experiment E94-107.

The upgrade is in progress and consists of the extension of the photon-detection surface by a factor of 1.6 with respect to the original version and a longer proximity gap. Both modifications will improve the photon collection efficiency and the reconstructed Čerenkov angle resolution at the same time. A 3D exploded CAD view of the new detector is shown in Fig. 16.

The expected performance has been estimated with a GEANT3 based Monte Carlo code tuned to the real data of the hypernuclear experiment. A pion-kaon angular separation above 4.7σ (corresponding to 1:1000 rejection) is expected over the whole momentum range of the Transversity experiment, as shown in Fig. 17, where two configurations of the upgraded RICH have been simulated for different gap sizes.

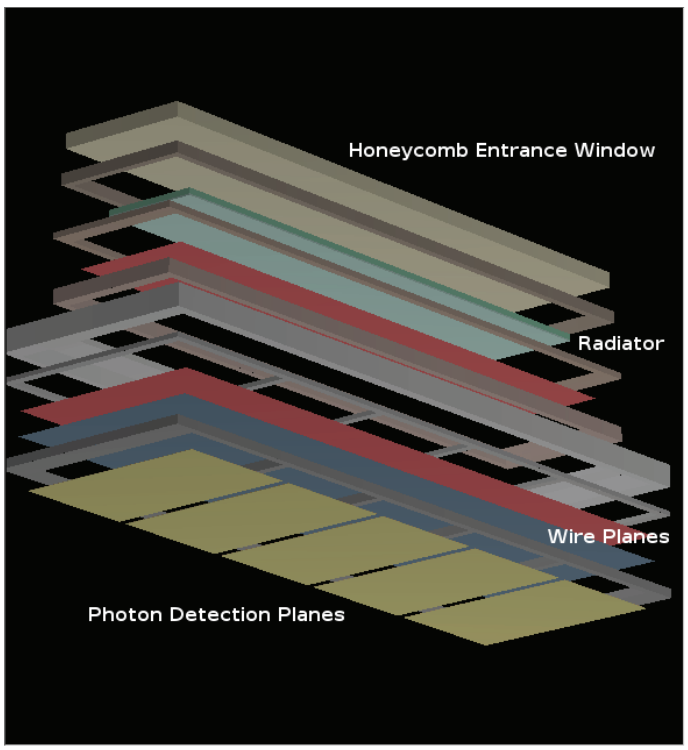

Figure 16: 3D expanded view of the upgraded RICH detector components: the five photon-detection pad planes are the gold-yellow ones on the bottom; the radiator vessel is in light-green-blue on the upper part of the figure.

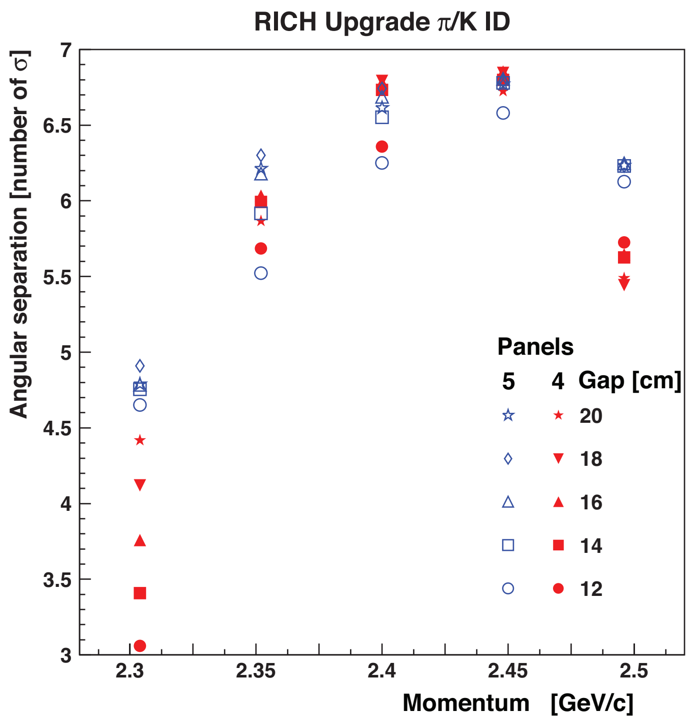

Figure 17: Monte Carlo simulation: expected angular separation (in terms of number of σ) of the upgraded RICH in the Transversity momentum range; the four-panel configuration (filled red symbols) corresponds to a 1.3 larger photon-detection surface with respect to the original RICH, while the five-panel one (open blue symbols) is the adopted (1.6 larger) upgrade solution.

3.5 12 GeV DAQ / Trigger Upgrade Plans

Contributed by R. Michaels and D. Abbott

The 12 GeV upgrade plan includes possible funding for an upgrade of the Hall A HRS DAQ. There are two themes to this upgrade: 1) replace obsolete components, and 2) achieve a much higher DAQ rate using full pipelining, possibly 200 kHz with zero deadtime. Such a rate increase could open the door to a number of new experiments, e.g. PVDIS. The higher rate is achieved essentially by having very large buffers at each stage of the pipeline. However, it is a "paper" estimate which needs to be demonstrated in a test stand.

We need to replace all our Fastbus and CAMAC modules. For the Fastbus, the present plan is to use the JLab-built VME-based F1-TDCs and FADCs, or suitable commercial units. These also have the important upgrade potential of allowing pipelining and higher rates. Some commercially available VME units might become competitive, in particular TDCs and FADCs from CAEN, and the FADCs from SISGmbH. The F1-TDC can be run in either a low-resolution mode (120 ps) or high-resolution mode (60 ps); the former is a replacement for the 1877 Fastbus TDC, while the latter replaces the 1875. The JLab-FADC will be a replacement for the 1881M ADC. This FADC will be a 250 MHz 12 bit unit. We might need preamps and shaping to get the resolution. In the next few years, we will be using the JLab-built units as well as commercial VME units in various setups, e.g. BigBite and the Compton polarimeter. This experience will help us evaluate what is best for the future.

To take full advantage of faster front-end readout we will also need VME64X crates, Gigabit ethernet, and a new Trigger Supervisor that is being designed by the DAQ group. The front-end VME CPUs will need to be fast, multi-core, and have Gigabit ethernet, and will have the option of using embedded Linux.

We also need to replace our CAMAC trigger modules with NIM- and VME-based electronics. It is doubtful that CAMAC has much of a future. Our quantity of spare modules is dangerously low and the modules are either difficult or impossible to fix since they are based on obsolete components. Note, the danger is not quite as bad with Fastbus because we've obtained a large supply of excessed material from other labs, so as the old modules go bad they can be swapped out. This strategy should help us survive the next few years with Fastbus.

We have performed the exercise of identifying replacement items for all the trigger and DAQ modules if we had to buy them "tomorrow". A notable exception is the programmable delay (LeCroy model 4518), for which there is no currently available commercial replacement. Therefore we have requested the JLab electronics group to build a programmable delay module in VME format with slightly improved features over the existing ones.

A report is being written with cost estimates and schematic diagrams of the future electronic layout. The installation can be done either during a significant downtime during 12 GeV construction or phased in over a several-year period. Scenarios for this installation will be available in the final report. At the time of this writing the details have not been completely ironed out.

4 Summaries of Experimental Activities

4.1 Experiment E94-107

High-Resolution Hypernuclear 1p-shell Spectroscopy
Contributed by F. Cusanno

F. Garibaldi, S. Frullani, J. LeRose, P. Markowitz, spokespersons
and
the Hall A collaboration

Experiment E94-107 used a waterfall target for hypernuclear production on oxygen nuclei and simultaneously for the measurement of the elementary cross section in $p(e,e'\mathrm{K}^+)\Lambda$.

Kinematics were set to electron detection at 6° for scattered electrons with a momentum of 1.44 GeV/c, an incident beam energy of 3.66 GeV, a virtual photon energy of 2.2 GeV with $\mathrm{Q}^2 = 0.06$ GeV^2. Scattered kaons were detected with momenta of 1.96 GeV/c at 6°.

Figure 18 shows the preliminary cross-section for the $^{16}_{\Lambda}$N hypernuclear spectrum produced on oxygen nuclei at $\theta_{K^+e} = 6°$. The dotted line is a result of the theoretical calculation using the SLA model for the elementary cross section and the calculations by J. Millener for the hypernuclear structure, the red line that of a fit using the same procedure as for the carbon spectrum. The overall picture shows a very good agreement between the data and the calculations in terms of positions and relative strength of the levels, as reported in Table 2.

The waterfall thickness used during the experiment was 75 mg/cm^2. This value was determined using the known cross section for the elastic reaction on hydrogen.

Table 2: Levels and cross sections obtained by fitting the $^{16}\mathrm{O}(e,e'\mathrm{K}^+)^{16}_{\Lambda}\mathrm{N}$ spectrum compared with theoretical predictions. For comparison with the results in Table 3, the two 0^+ states are predicted at 11.22 and 6.91 MeV.

E_x/E_Λ [MeV]	Width [FWHM, MeV]	Cross section [(nb/sr^2/GeV]	E_x [MeV]	Wave function	J^π	Cross section [nb/sr^2/GeV]
0.0/13.57 ± 0.25	0.992	2.35± 0.47	0.00	$p^{-1}_{1/2} \otimes s_{1/2\Lambda}$	0^-	0.002
			0.03	$p^{-1}_{1/2} \otimes s_{1/2\Lambda}$	1^-	2.38
6.68 ± 0.10	0.800	6.26 ± 1.25	6.71	$p^{-1}_{3/2} \otimes s_{1/2\Lambda}$	1^-	1.56
			6.93	$p^{-1}_{3/2} \otimes s_{1/2\Lambda}$	2^-	4.10
10.80 ± 0.13	1.125	5.52 ± 1.10	11.00	$p^{-1}_{1/2} \otimes p_{3/2\Lambda}$	2^+	2.60
			11.05	$p^{-1}_{1/2} \otimes p_{1/2\Lambda}$	1^+	0.89
17.00 ± 0.09	0.851	7.29 ± 1.46	17.56	$p^{-1}_{3/2} \otimes p_{3/2\Lambda}$	3^+	3.17
			17.56	$p^{-1}_{3/2} \otimes p_{1/2\Lambda}$	2^+	2.96

The measured Λ binding energy in $^{16}_{\Lambda}$N, $B_\Lambda = 13.57 \pm 0.25$ MeV obtained from the first peak is a previously not well-known quantity. A few emulsion events have been observed for the heavier p-shell hypernuclei, but these events tend to have ambiguous interpretations[1]. Also, reactions involving the production of a Λ from a neutron are more difficult to normalize.

Table 3: Comparison of B_Λ values [MeV], with errors in parentheses, and excitation energies for the four peaks observed in $(e, e'\mathrm{K}^+)$, (K^-, π^-), and (π^+, K^+) reactions on ^{16}O.

	$(e, e'\mathrm{K}^+)$ This expt.	(π^+, K^+) KEK	(K^-, π^-) CERN	$(K^-_{\mathrm{stop}}, \pi^-)$ KEK
$B_\Lambda(\#1)$	13.57(25)	12.42(5)	13.28(36)	13.40(40)
$E_x(\#2)$	6.68	6.23	5.96	6.39
$E_x(\#3)$	10.80	10.57	10.62	10.84
$E_x(\#4)$	17.00	16.59	17.15	17.15

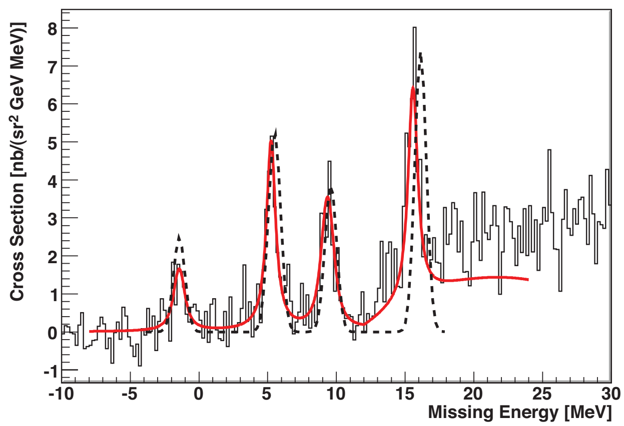

Figure 18: Preliminary data for the $^{16}_{\Lambda}$N missing-energy spectrum.

The preliminary results for the simultaneous measurement of the elementary reaction on hydrogen show a similar agreement between the datum ($\sigma = 30$ nb/sr^2/GeV $\pm$ 30%) and the cross-section value of 36 nb/sr^2/GeV, predicted by the SLA model.

References

[1] D.H. Davis, *LAMPF Workshop on (π, K) Physics*, edited by B.F. Gibson, W.R. Gibbs and M.B. Johnson, AIP Conf. Proc. **224**, 38 (1991).

4.2 Experiment E97-110

The GDH Sum Rule, the Spin Structure of ^{3}He and the Neutron using Nearly Real Photons
Contributed by A. Deur

J.-P. Chen, A. Deur, F. Garibaldi, spokespersons
and
the E97-110 Collaboration.

The goal of the experiment is to measure the generalized Gerasimov-Drell-Hearn integral (GDH) and moments of spin-structure functions at low Q^2 on the neutron and ^{3}He. A brief description of the physics goal and of the running of the experiment was given in the 2003 Hall A report.

The experiment The experiment ran in April-May and July-August 2003. The first part of the experiment (low Q^2, April-May 2003) acquired data with a miss-wired septum magnet. The septum was fixed in June and the experiment was completed in July-August.

Present state and outlook Data analysis is ongoing on the first and second periods. The second period, which contains the bulk of the data, has been the focus of the analysis. Preliminary results are now available for this period (V. Sulkosky): The $g_1^{^3He}$ and $g_2^{^3He}$ spin structure functions and the electroproduction cross sections σ_{TT} and σ_{LT} are available with preliminary radiative corrections. These preliminary data have been integrated to form various moments: the GDH sum on neutron, Γ_1^n and Γ_2^n. These preliminary results are in good agreement with the data at larger Q^2 (from experiment E94-010) in their overlap range. Γ_1^n is also in good agreement with phenomenological models. The Burkhardt-Cottingham sum rule ($\Gamma_2 = 0$) is validated by our preliminary data. Preliminary results on Γ_1^n are shown in Fig. 19.

To finalize these results, more work on radiative corrections (J. Singh) and on the ^{3}He quasi-elastic contamination remain to be done (V. Sulkosky). Other backgrounds are being studied (T. Holmstrom). The HRS/septum acceptance study needs to be finalyzed. Systematic uncertainties have to be precisely estimated. A study on the correct size of the statistical error bars in the case of runs with a large pre-scale factor is also under way (T. Holmstrom).

Analysis of the target polarimetries (NMR and EPR) as well as other target characteristics has to be finalized (J. Singh). Preliminary numbers are available. The elastic cross sections and asymmetries for the various targets used will be analyzed (J. Singh, V. Sulkosky). Such a study will provide results complementary to the polarimetry analysis, an estimate of background and a cross-check of systematic uncertainties. The data analysis for the first period is also underway, mostly done by our Chinese collaborators from USTC. Completion of the data analysis for the first period will be done by USTC.

We plan to have final results on the GDH sum, the first moments Γ_1^n and Γ_2^n, the $g_1^{^3He}$ and $g_2^{^3He}$ spin-structure functions and the electroproduction cross sections σ_{TT} and σ_{LT} in the next few months and the first publication will be prepared once the results have been finalized.

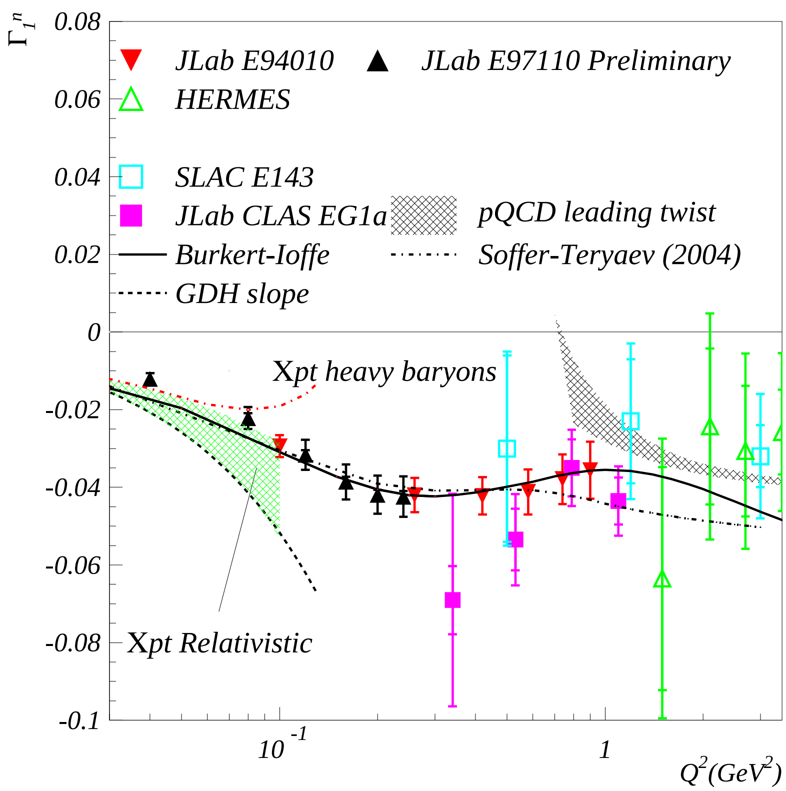

Figure 19: Preliminary results for Γ_1^n. Data from SLAC E143, DESY HERMES, JLab Hall A E94-010 and JLab CLAS EG1a are plotted for comparison. The χPT calculations are from Ji *et al.* (heavy Baryons) and Bernard *et al.* (relativistic). The Burkert-Ioffe and Soffer-Teryaev curves are results from phenomenological models. The GDH sum rule gives the slope at Γ_1^n at $Q^2 = 0$.

4.3 Experiment E00-102

Testing the Limits of the Single-Particle Model in $^{16}O(e, e'p)$
Contributed by J. Lachniet

A. Saha, W. Bertozzi, L.B. Weinstein and K. Fissum, spokespersons,
and
the Hall A Collaboration

Experiment E00-102 is an update to Hall A experiment E89-003: measurement of the cross section, R_{LT}, and A_{LT} for the $^{16}O(e, e'p)$ reaction. Experiment E89-003 made measurements at energy and momentum transfer of $\omega = 0.445$ GeV and $Q^2 = 0.8$ GeV^2, respectively, up to $p_m = 0.345$ GeV/c[1, 2, 3]. This update experiment expands these measurements to $p_m = 0.755$ GeV/c at $\omega = 0.449$ GeV and $Q^2 = 0.902$ GeV^2. The goals of these measurements are to determine:

- the limits of validity of the single-particle model of valence proton knockout;
- the effects of relativity and spinor distortion on valence proton knockout using the diffractive character of the A_{LT} asymmetry; and
- the bound-state wave function and spectroscopic factors for valence knockout.

The cross section will be determined for measurements from $p_m = -0.515$ GeV/c to $p_m = 0.755$ GeV/c, in order to determine the point at which single-knockout calculations fail and two-nucleon effects become important. R_{LT} and A_{LT} will be separated for p_m up to ± 0.515 GeV/c to further test relativistic DWIA calculations. Figure 20 shows the anticipated data from E00-102 for A_{LT} as a function of missing momentum for the 1p-shell states along with data obtained from E89-003, both compared to calculations from Udias *et al.*

Data were taken at a fixed beam energy of 4.620 GeV, $\vec{q} = 1.066$ GeV/c, and $\theta_q = 56.22°$. Throughout the entire experiment, the electron arm (HRS-L) was fixed at 12.5° with a central momentum of 4.121 GeV/c, allowing it to be used as a luminosity monitor. The hadron arm (HRS-R) angle was varied from 28.3° to 96.1° to cover the necessary missing-momentum range. These kinematics are shown in Fig. 21.

Both detector stacks were used in their standard configurations. Each stack contained an additional S0 scintillator to check the trigger efficiency, and the HRS-L contained a pion rejector for e^-/π^- separation. The target used was the Hall A self-normalizing three-foil waterfall target[4, 5]. Each water foil was approximately 200 mg/cm^2 thick and separated by 25.4 mm. The foils were rotated to an angle of 57.4° with respect to the beam direction, as shown in Fig. 22. Using the hydrogen in the water precise calibrations can be made as well as a normalization of the cross section to known $^1H(e, e'p)$ and $^1H(e, e')$ cross sections.

Detector calibrations, beam position and beam energy calibrations have been completed. Optimized detector maps have been created, and the data have been replayed using ESPACE. Analysis of the spectrometer mispointing has been performed. The water foil thicknesses have been determined by comparison of $^{16}O(e, e'p)$ yields to a BeO target of known thickness[6].

Extensive progress has been made at ODU in adapting the ROOT/C++ analyzer to the E00-102 analysis[7]. The ESPACE optics calibration database has been transferred to the new format and tested extensively to demonstrate agreement between ESPACE and the analyzer. A model of the waterfall target has been built into the analyzer to calculate energy-loss corrections. The three-foil target configuration was not supported in ESPACE. The foil-to-foil variation in the elastic peak position has been reduced from 2.5 MeV using ESPACE to less than 0.4 MeV. The C++

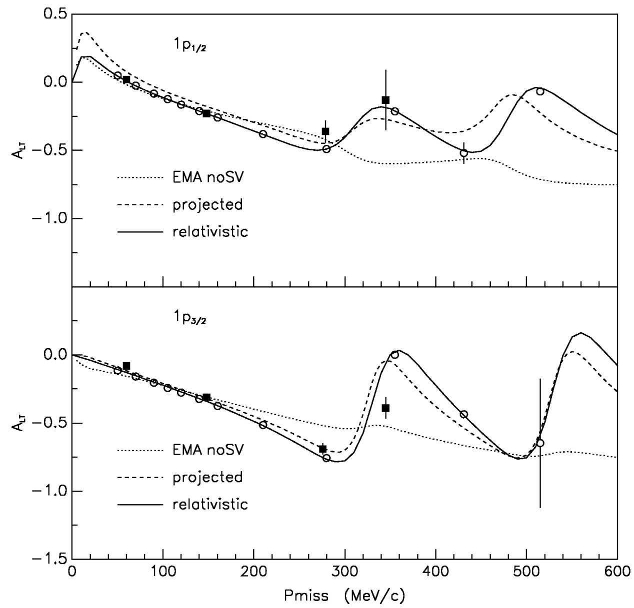

Figure 20: Projected A_{LT} data compared to E89-003 results and calculations of Udias *et al.* Open circles are anticipated data points from E00-102, solid squares are E89-003 data obtained at slightly different kinematics.

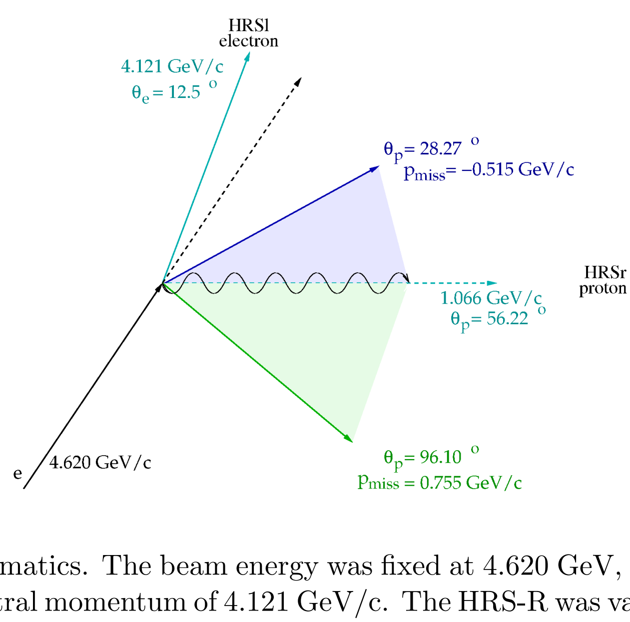

Figure 21: E00-102 kinematics. The beam energy was fixed at 4.620 GeV, and the HRS-L remained fixed at 12.5° with a central momentum of 4.121 GeV/c. The HRS-R was varied around the direction of parallel kinematics to cover the necessary missing momentum range.

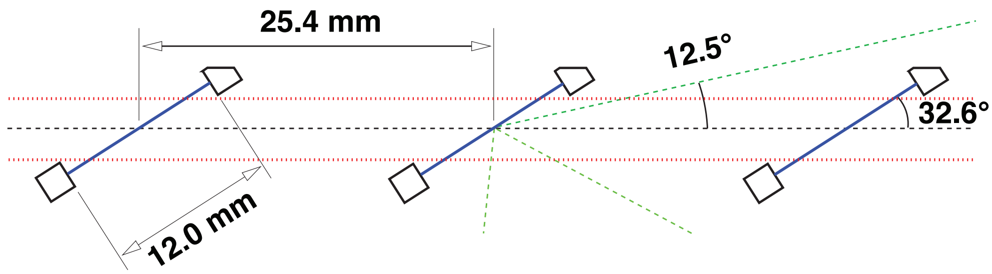

Figure 22: E00-102 waterfall target

analyzer was written for a more modern configuration of the coincidence trigger logic, so a new coincidence time module was written for the analyzer. Results comparable in quality to ESPACE have been obtained, and are illustrated in Fig. 23. The LeRose R-functions were added to the analyzer, giving a new option for detector acceptance cuts and acceptance matching between data and MCEEP-based simulations.

A luminosity monitor based on left-arm singles has been developed. Since the left spectrometer was fixed for the duration of the experiment, measurement of $(e, e'p)$ elastic scattering using the left arm can be used to extract run-to-run variations in target thickness and electronic deadtime. The elastic yield for each run is extracted from a comparison of the measured energy of the scattered electron and the energy expected for an electron elastically scattered at the measured scattering angle. Figure 24 shows a sample ΔE distribution. This technique will be used to provide a measurement of the electronic deadtime which is independent of the pulser system.

The University of Madrid, in collaboration with Lund University, has integrated the Udias RDWIA model[8, 9] into the MCEEP simulation. An interpolatable hyper-cube containing the results of the Udias calculation over a broad range of kinematics was generated and used to weight the MCEEP events. This allows the calculation to be correctly averaged over the finite acceptance of the spectrometers. An in-depth comparison of the MCEEP output and the results of the previous oxygen experiment (E89-003) has been performed[10].

In Fig. 25, the simulated longitudinal-transverse asymmetry A_{LT} for the removal of $1p_{1/2}$-state protons from ^{16}O in E89-003 kinematics is presented. Experimental cuts have been applied to the simulated data. Open red boxes result from the simulations, each box representing a particular (ω, q, p_m) bin. In the top panel, the results of the simulations for the E89-003 acceptances considered in the data analysis are shown. The blue circles represent the average of the A_{LT} values over all of the red (ω, q, p_m) bins corresponding to a given kinematics. It is clear that the averaged simulated A_{LT} values agree reasonably well with the published data. In the bottom panel, the p_m evolution of the results corresponding to "extremely reduced" spectrometer acceptances: ± 0.1 mrad for spectrometer angles and $\pm 0.1\%$ for the electron and ejected proton momenta is shown. It can be noted that, as the acceptances are reduced, the simulated results collapse to the point-acceptance RDWIA calculations.

With the recent improvements in the analysis and simulation tools, a full-scale data analysis is ready to begin. Relative and absolute $^{16}\mathrm{O}(e, e'p)$ cross sections, along with R_{LT} and A_{LT} for the $1p_{1/2}$ and $1p_{3/2}$ states will be extracted. Some preliminary results, showing the $1p_{1/2}$ cross section relative to the $\mathrm{H}(e, e')$ cross section for a one foil subset of the available data, are shown in Fig. 26[11].

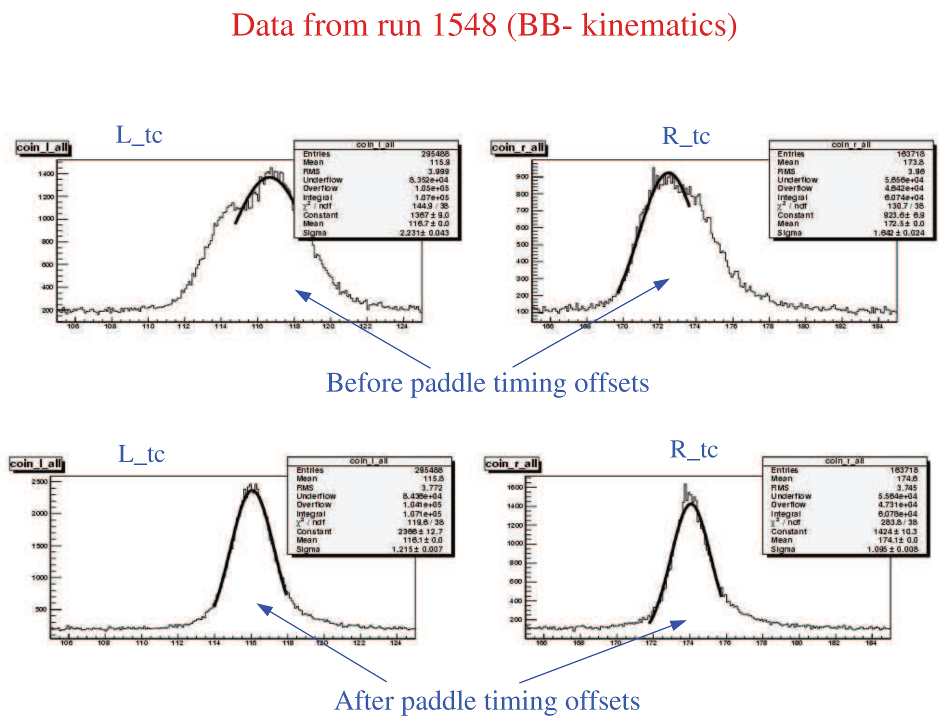

Figure 23: Coincidence time spectra from the ROOT/C++ analyzer before and after the construction of specialized E00-102 coincidence timing code.

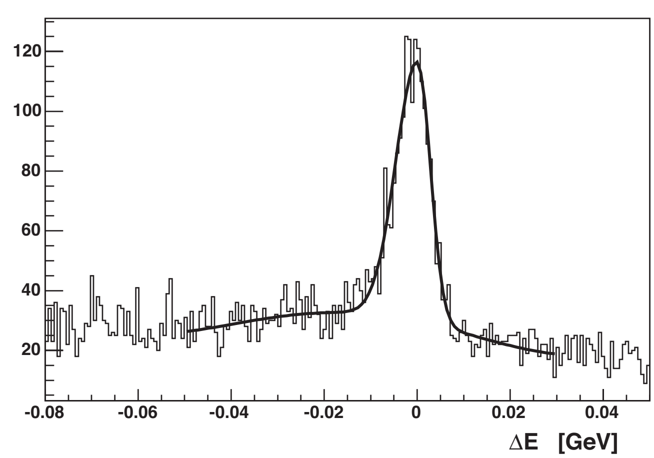

Figure 24: Extraction of the elastic peak from the ΔE spectrum in HRS-L events. ΔE is the difference between the measured electron energy and the energy expected for elastic scattering at the measured scattering angle.

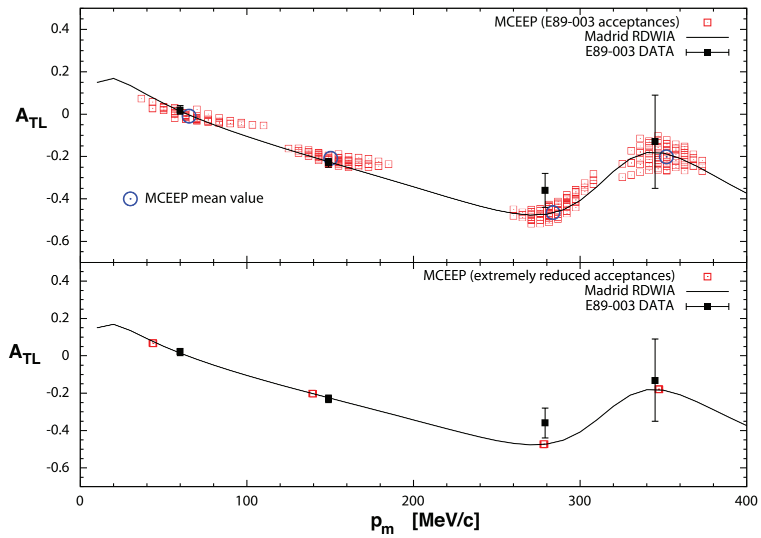

Figure 25: Selected results from the Lund/Madrid MCEEP simulations. See text for details.

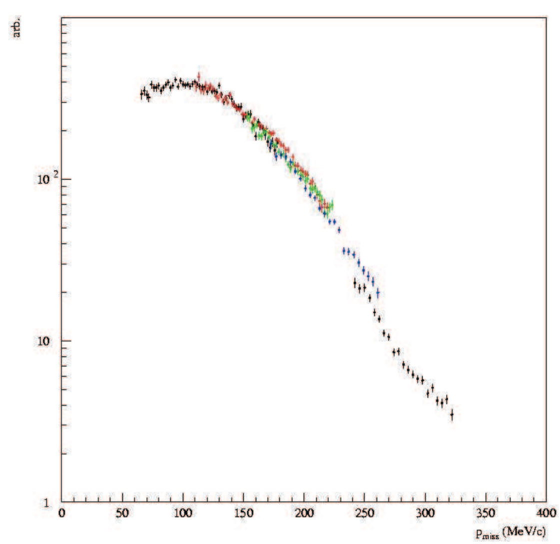

Figure 26: $1p_{1/2}$ cross section relative to the $H(e, e')$ cross section for a one foil subset of the data. The different colors represent data from different kinematic settings (different positions of the right spectrometer).

References

[1] W. Bertozzi, K.Fissum, A. Saha, and L. Weinstein, spokespersons, JLab Experiment E89-003, *Study of the Quasi-Elastic (e,e′p) Reaction in* ^{16}O *at High Recoil Momentum*.

[2] J. Gao *et al.*, Phys. Rev. Lett. **84**, 3265 (2000).

[3] N. Liyanage *et al.*, Phys. Rev. Lett. **86**, 5670 (2001).

[4] F. Garibaldi *et al.*, Nucl. Instrum. Methods. Phys. Res. A **314**, 1 (1992).

[5] E. Cisbani *et al.*, *A Waterfall Target System for Hall A at Jefferson Lab*, INFN/ISS **97/04** (1997).

[6] B. Reitz *et al.*, "E00-102 status report, July 2005"

[7] J. Lachniet, private communication.

[8] J.M. Udias *et al.*, Phys. Rev. Lett. **83**, 5451 (1999).

[9] J.M. Udias, private communication.

[10] J.L. Herraiz, Jefferson Lab Technote JLAB-TN-07-068.

[11] M. Andersson, Lic. Thesis, University of Lund, 2005

4.4 Experiment E01-015

Studying the Internal Small-Distance Structure of Nuclei via $(e, e'p\text{N})$ Measurements
contributed by D. W. Higinbotham

P. Monaghan, R. Shneor, and R. Subedi (Ph.D. Students)
and
the Hall A Collaboration

The attractive short-range component of the nucleon-nucleon force can cause some of the protons inside a nucleus to form pairs. These pairs have a low center-of-mass momentum and a high relative momentum where low and high are relative to the Fermi sea level, which is approximately 220 MeV/c for ^{12}C. Experiment E01-015 sought to indirectly observe this effect by measuring the triple coincidence $(e, e'pn)$ and $(e, e'pp)$ events from carbon at high missing momentum.

The experiment completed data taking in April of 2005. The $^{12}\text{C}(e, e'p)$ data were taken with the two Hall A high-resolution spectrometers and, for each $(e, e'p)$ event, the BigBite spectrometer and a neutron detector ADCs and TDCs were read out. This allowed the experiment to measure the $(e, e'pn)$ and $(e, e'pp)$ channels simultaneously without having to setup a complex multi-arm triggering system.

During the past six months, the first publication from this experiment was published in Phys. Rev. Lett.[1]. This paper presented the results for the $^{12}\text{C}(e, e'p)$ and $^{12}\text{C}(e, e'pp)$ reactions at $Q^2 = 2$ GeV^2, $x_B = 1.2$, and in an $(e, e'p)$ missing-momentum range from 300 to 600 MeV/c. In these kinematics, with a missing momentum greater than the Fermi momentum of nucleons in a nucleus and far from the Δ excitation, short-range nucleon-nucleon correlations were predicted to dominate the reaction. For $(9.5 \pm 2)\%$ of the $^{12}\text{C}(e, e'p)$ events, a recoiling partner proton was observed back-to-back to the $^{12}\text{C}(e, e'p)$ missing-momentum vector, an experimental signature of correlations. These results are shown in Fig. 27.

Also within the past six months, the first Ph.D. student from this experiment, Ramesh Subedi (Kent State University), graduated [2]. The other two students, Ran Shneor (Tel Aviv University) and Peter Monaghan (MIT), are both expecting to be finished within the next six months. These students are analyzing the $^{12}\text{C}(e, e'pp)$ and $^{12}\text{C}(e, e'p)$ results, respectively.

Presently, the collaboration is working on publishing its $^{12}\text{C}(e, e'pn)/^{12}\text{C}(e, e'pp)$ ratio result. This result shows a clear dominance of $p - n$ pairs. This result seems to be unique in that it can thus far only be explained in terms of correlated pairs; where as most experiments which have sought to study correlations end up with controversial or ambiguous results. The collaboration is also reviewing the other channels that were measured during the experiment and currently are investing $(e, e'd)$ events and (e, e') ratios.

References

[1] R. Shneor *et al.*, Phys. Rev. Lett. **99**, 072501 (2007).

[2] R. Subedi, *Studying Short-Range Correlations with the $^{12}C(e, e'pn)$ Reaction*, Kent State University (2007).

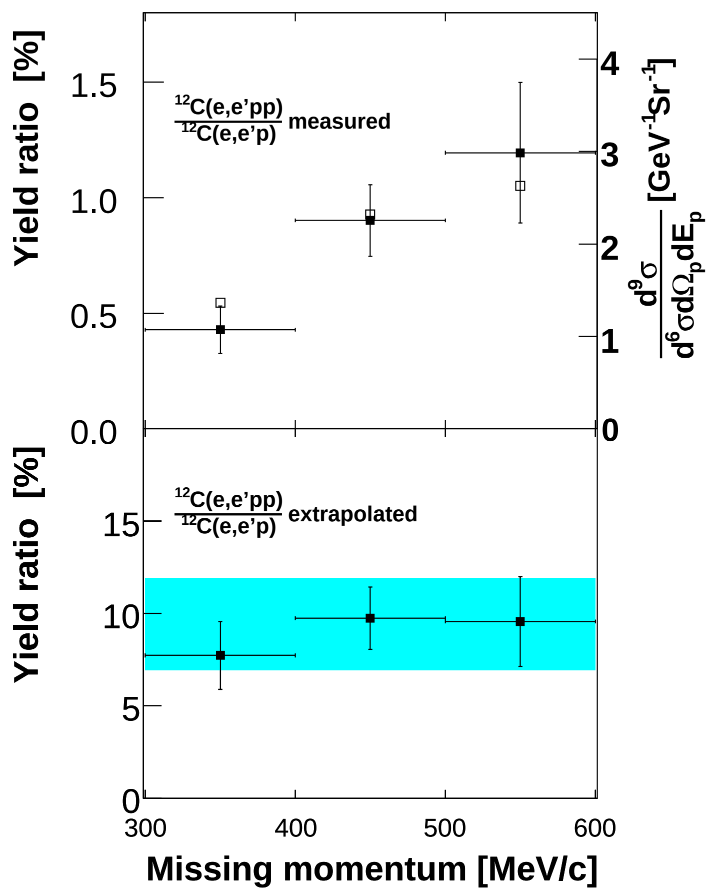

Figure 27: The measured and extrapolated yield ratios for the ^{12}C$(e,e'pp)$ and the ^{12}C$(e,e'p)$ reactions. The full squares are the yield ratios and the open squares are the corresponding ratios of the differential cross sections for the ^{12}C$(e,e'pp)$ reaction to the ^{12}C$(e,e'p)$ reaction. A simulation was used to account for the finite acceptance of BigBite and make the extrapolation to the total number of recoiling proton pairs shown in lower figure. The shaded area represents a band of $\pm 2\sigma$ uncertainty in the width of the c.m. momentum of the pair.

4.5 Experiment E02-013

Measurement of the Neutron Electric Form Factor G_E^n at High Q^2
Contributed by B. Wojtsekhowski

G. Cates, N. Liyanage, and B. Wojtsekhowski, spokespersons
and
the E02-013 and the Hall A Collaborations

Introduction

The nucleon form factors (FFs) are unique testing grounds for hadronic models and a crucial source of information for the development of the parameterization for the Generalized Parton Distributions[1, 2]. The electric form factor of neutron is one of central interest for hadron physics community. Precision measurements of G_E^n will allow for a much more accurate determination of F_1 and especially F_2 of the neutron as well as separation of the FFs for valence u and d quarks. The E02-013 experiment is a measurement of G_E^n via the beam-helicity cross-section asymmetry from quasi-elastic electron scattering from a polarized ^{3}He target.

This year the G_E^n collaboration continued the analysis of the experiment including the calibration of the detectors and the polarized target, and the extraction of the physics results. In 2007 the analysis efforts were focused on the data for the kinematics of 1.7 and 3.4 GeV^2. The first is located a bit higher in Q^2 than a previous experimental point obtained in Hall C[3], Q^2=1.47 GeV^2 and the second, at double the Q^2 value, is located in a region where quark degrees of freedom are expected to dominate. We developed a full analysis procedure for both kinematics and are expecting preliminary results by the spring of 2008.

Experiment overview

Experiment E02-013 measured the electric form factor of the neutron by studying spin asymmetries in quasi-elastic scattering in the reaction $^3\vec{\mathrm{He}}(\vec{e}, e'n)$ at four values of Q^2 up to 3.4 GeV^2. The scattered electron and the recoiling neutron were detected in coincidence using the open-geometry electron spectrometer BigBite (with a solid-angle acceptance of roughly 76 msr) and the large neutron detector BigHAND which (with an active detection area of around 8 m^2) at a distance 9-12 m, provided an adequate acceptance for quasi-elastic neutrons. A diagram of the physics concept is shown in Fig. 28. The asymmetry A_{phys} relates to G_E^n through the equation:

$$A_{phys} = -\frac{2\sqrt{\tau(\tau+1)}\tan(\frac{\theta}{2})G_E^n G_M^n \sin\theta^\star \cos\phi^\star}{(G_E^n)^2 + (G_M^n)^2(\tau + 2\tau(1+\tau)\tan^2(\frac{\theta}{2}))} - \frac{2\tau\sqrt{1+\tau+(1+\tau)^2\tan^2(\frac{\theta}{2})}\tan(\frac{\theta}{2})(G_M^n)^2\cos\theta^\star}{(G_E^n)^2 + (G_M^n)^2(\tau + 2\tau(1+\tau)\tan^2(\frac{\theta}{2}))},$$

where $\tau = Q^2/4M^2$, and θ^* and ϕ^* are the polar and the azimuthal angles between the polarization direction of the ^{3}He target and a vector of momentum transfer, $\vec{q}$. A missing momentum p_m (the difference the between $\vec{q}$ and the momentum of the neutron $\vec{p}_n$, measured through time of flight) is used for selection of the quasi-elastic process. The $p_{m,\perp}$, a component of $\vec{q} - \vec{p}_n$ perpendicular to $\vec{q}$, is the most useful for the selection of quasi-elastic events.

Table 4 shows the kinematics for which data have been taken and the accumulated beam charge.

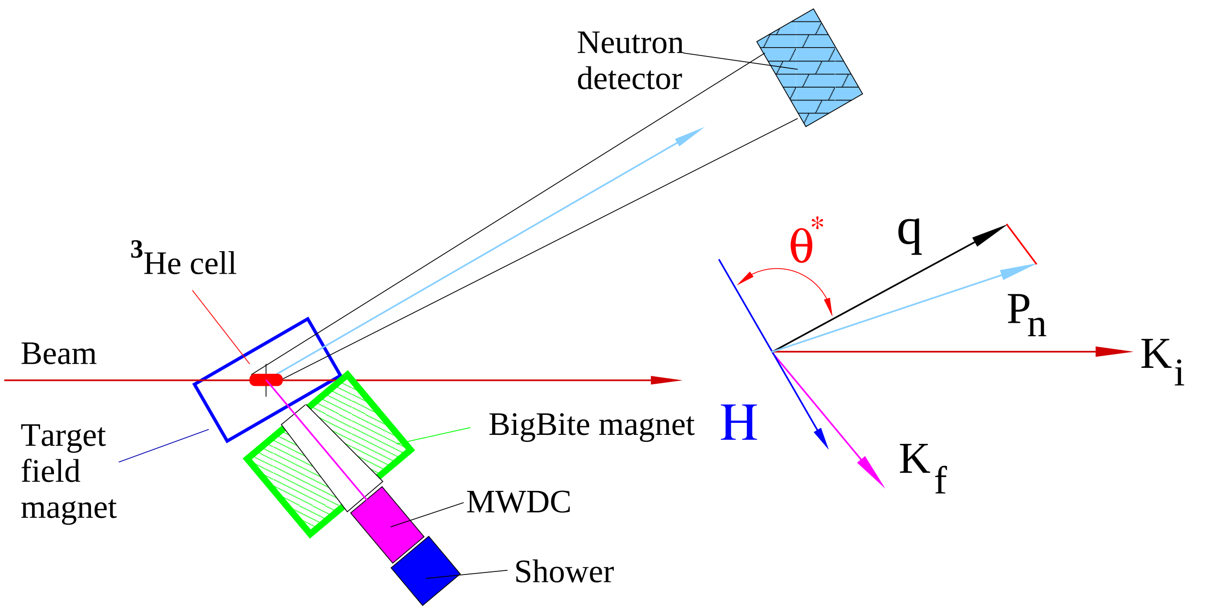

Figure 28: Conceptual lay-out of the E02-013 experiment. Here H shows the target holding magnetic field; K_i and K_f are the initial and final electron momenta; $\vec{q} = \vec{K_i} - \vec{K_f}$ is the momentum transfer; P_n is the neutron momentum, θ^* is the angle between the direction of the magnetic field and the momentum transfer.

kin. #	E_{beam} [GeV]	average $\theta_{e'}$ [degrees]	Q^2 [GeV^2]	Q_{beam} [Coulomb]
1	1.519	56.26	1.2	1.2
2	2.640	51.59	2.5	5.5
3	3.291	51.59	3.4	11.4
4	2.079	51.59	1.7	2.2

Table 4: The four kinematics of G_E^n measurements in E02-013 together with the accumulated beam charge.

Progress of data analysis

The analysis of the G_E^n data is currently underway, and while we have not yet released any numbers on G_E^n itself, we have presented preliminary results from various aspects of the analysis at conferences, including raw asymmetries from one of our kinematic points at $1.7\,\mathrm{GeV}^2$. Major aspects of the G_E^n analysis include tracking in BigBite, calibration of the BigBite calorimeter, timing and position calibration in the neutron arm, target polarimetry, and target polarization direction, and dilution factors.

Target polarization. The results of the target polarization analysis were reported at the 2007 APS/DNP meeting [4]. Figure 29 presents the observed polarization for almost all of the experiment. The polarization was measured to be close to 50% for most of the production period, which

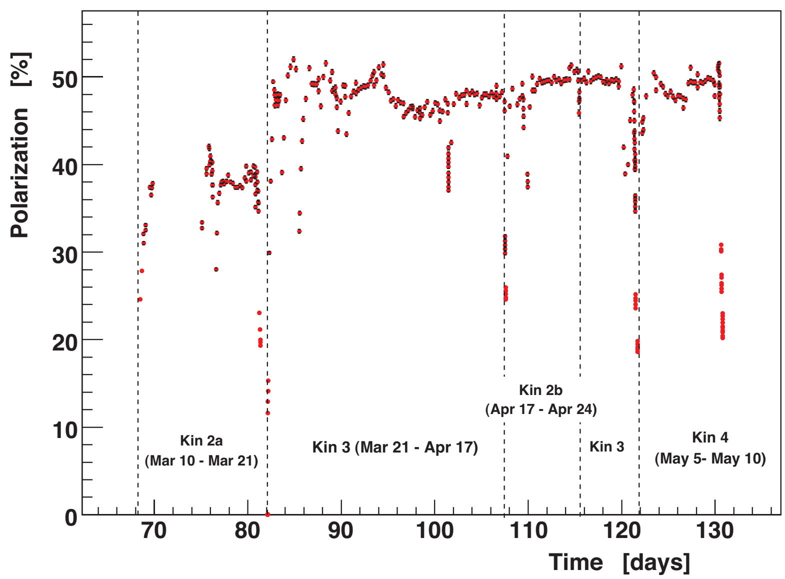

Figure 29: ^{3}He target polarization degree *vs.* day during E02-013.

gave the experiment's productivity a welcome boost.

A significant achievement in the G_E^n setup was the large solid angle of the electron spectrometer, which requires a close proximity of the large magnet to the polarized cell of ^{3}He. The same distance from the target and the BigBite magnet was used in the NIKHEF $^3\vec{\mathrm{He}}(\vec{e}, e'n)$ experiment. However, for an internal target with an atomic dwelling time of the order of milliseconds, the demand for a small field gradient is much less critical. The magnetic holding field at the target defines the direction of the neutron polarization. Its variation was carefully measured by means of a specially designed compass and is taken into account during the analysis of the asymmetry (see Fig. 30).

Helicity information. Our experiment ran in parallel with the G^0 experiment in Hall C, so the beam helicity scheme was the so-called "G^0" set of four pseudo-random groups, such as $+--+$. An additional sign to the helicity was introduced by the "half-wave-plate", which allows for an extra check of systematics and was rotated on average, once per day. The helicity sign was recorded in the data stream every 30 ms when the helicity sign was changed. Off-line analysis allows for decoding

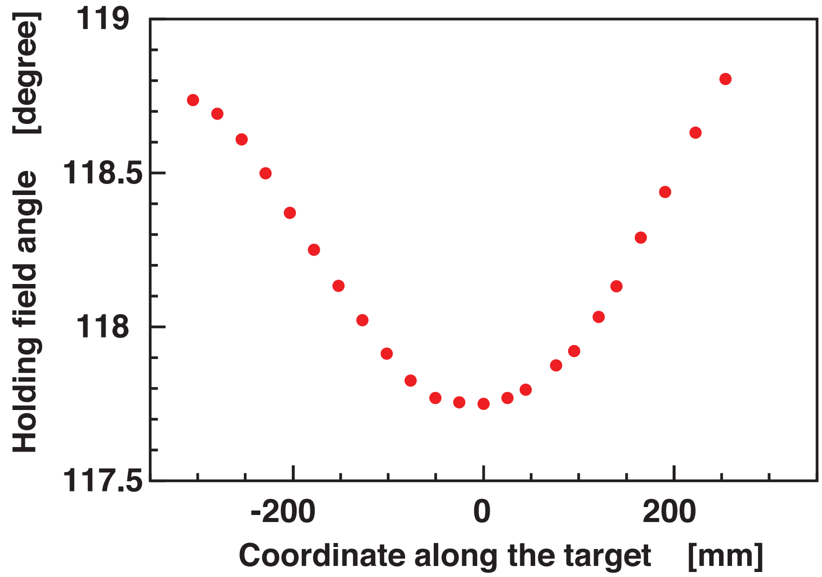

Figure 30: The angle between the beam direction and the holding field direction *vs.* coordinate at the target along the beam.

of the actual sign of the beam helicity for each physics event. An example of a check for correctness of the helicity assignment, as well as the target and half-wave-plate information, is shown in Fig. 31. This is done by using the helicity asymmetry of the raw trigger rates measured in our scalars. It is easy to see in the middle of day 98, the averaged over run asymmetry had dropped. An additional, but statistically less accurate check was done by measuring the helicity asymmetry of the yield of the negative pions detected in BigBite.

BigBite optics. The concept of the BigBite spectrometer with three tracking chambers in a field-free region behind a strong magnet was demonstrated to be very effective. The magnetic field reduces the hit rates in the chambers by a factor of 15. Tracking in the field-free region allows us to find the correct combination of hits even at a hit rate on the level of 20 MHz per plane. Due to the dominant deflection of the trajectory in the vertical direction, the track from behind the magnet and the beam position are sufficient for the determination of the particle momentum, trajectory, and position at the target.

The present implementation of the spectrometer optics is done by using a dipole approximation as a first iteration and first-order corrections for the momentum and Z vertex position. Figure 32 shows the difference between the reconstructed electron momentum, $P_{e,\,magnetic}$, minus the electron momentum $P_{e,\,geometrical}$ (calculated from the value of scattering angle with elastic scattering $e-p$ kinematics) *vs.* P_e. A band of elastically scattered electrons is well aligned and has an overall resolution of about 1%. This implementation has been successful in the reconstruction for over 90% of the spectrometer acceptance.

Neutron arm. The system of 600+ PMTs requires effective tools to keep its combined performance as good as the individual counters. Figure 33 shows the accuracy of the timing offset calibration for kinematic 4. For each detector the marker + shows the accuracy of calibration and the marker X shows the stability of the calibration. The detectors marked as N1 are located in the

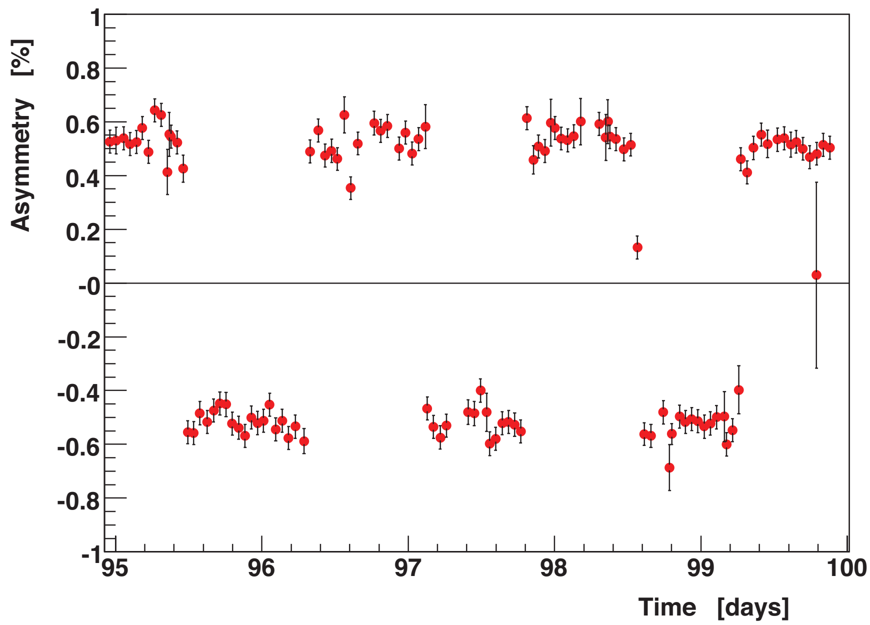

Figure 31: The beam-helicity asymmetry of T2(T3) trigger rates *vs.* run number.

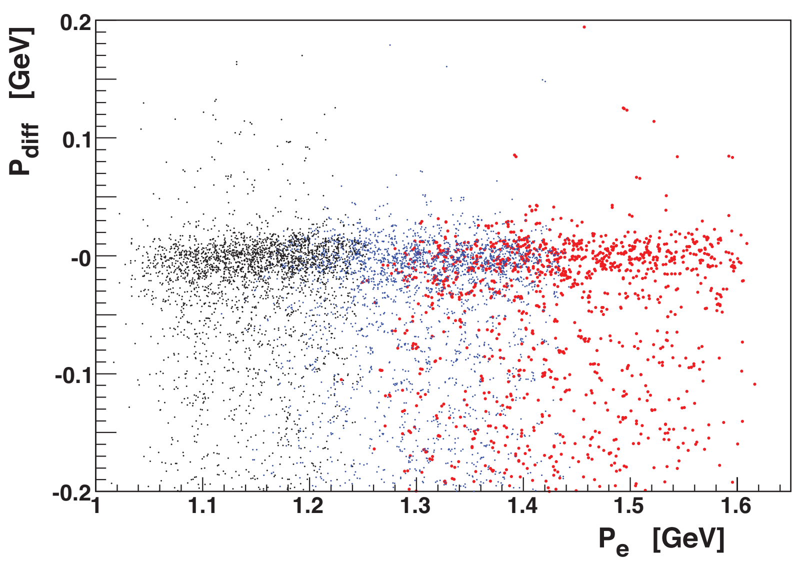

Figure 32: Calibration of the momentum reconstruction by using elastic $e - p$ scattering. See text for details.

front wall of BigHAND. They are calibrated relative to BigBite by using quasi-elastic protons. The detectors marked as N2-N7 are calibrated relative to N1. Clearly, the relative calibration inside BigHAND for most detectors is very good and stable to 50-100 ps. Stability of the N1 calibration is good to the level of 200 ps. A column "Marker" shows the calibration quality of the horizontal coordinate which was tested by using vertically oriented marker counters.

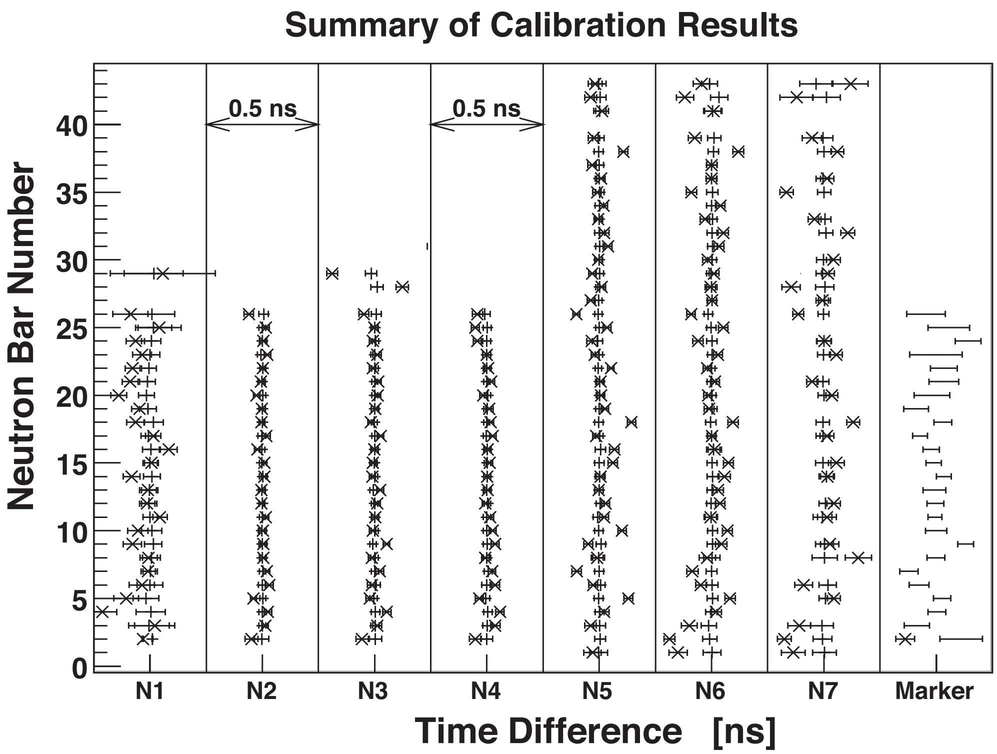

Figure 33: Calibration of the time off-sets for the neutron arm BigHAND.

The development of a GEANT-4 based code for Monte Carlo simulations is in its testing stage. We are using ${}^1\mathrm{H}(e, e'p)$ data obtained with the N-20 setup, which ran parasitically to the SRC experiment in 2005. Figure 34 shows the amplitude spectrum from the first wall of the neutron detectors in MC and experiment. At a threshold of 5 MeV, which was used for timing measurements from individual PMTs, the efficiency is about 60%. The difference between the efficiency value from MC and experiment was estimated to be 2–3% (after taking into account experimental amplitude variations).

Accuracy of the form factor results

The systematic uncertainty of results has several contributions, which are expected to significantly improve with new calculations of FSI effects and new Monte Carlo simulations. An estimate of the statistical accuracy is close to final. Figure 35 presents a plot of the Q^2-values for the E02-013 measurements. For the 1.7 and 3.4 GeV^2 data points the statistical accuracy was obtained from experimental analysis. The curves in this plot are from a light-cone CQM calculation[5]; a recent pQCD prediction which includes the effect of quark orbital momenta[6], normalized to data[3]; and the well-known Galster fit.

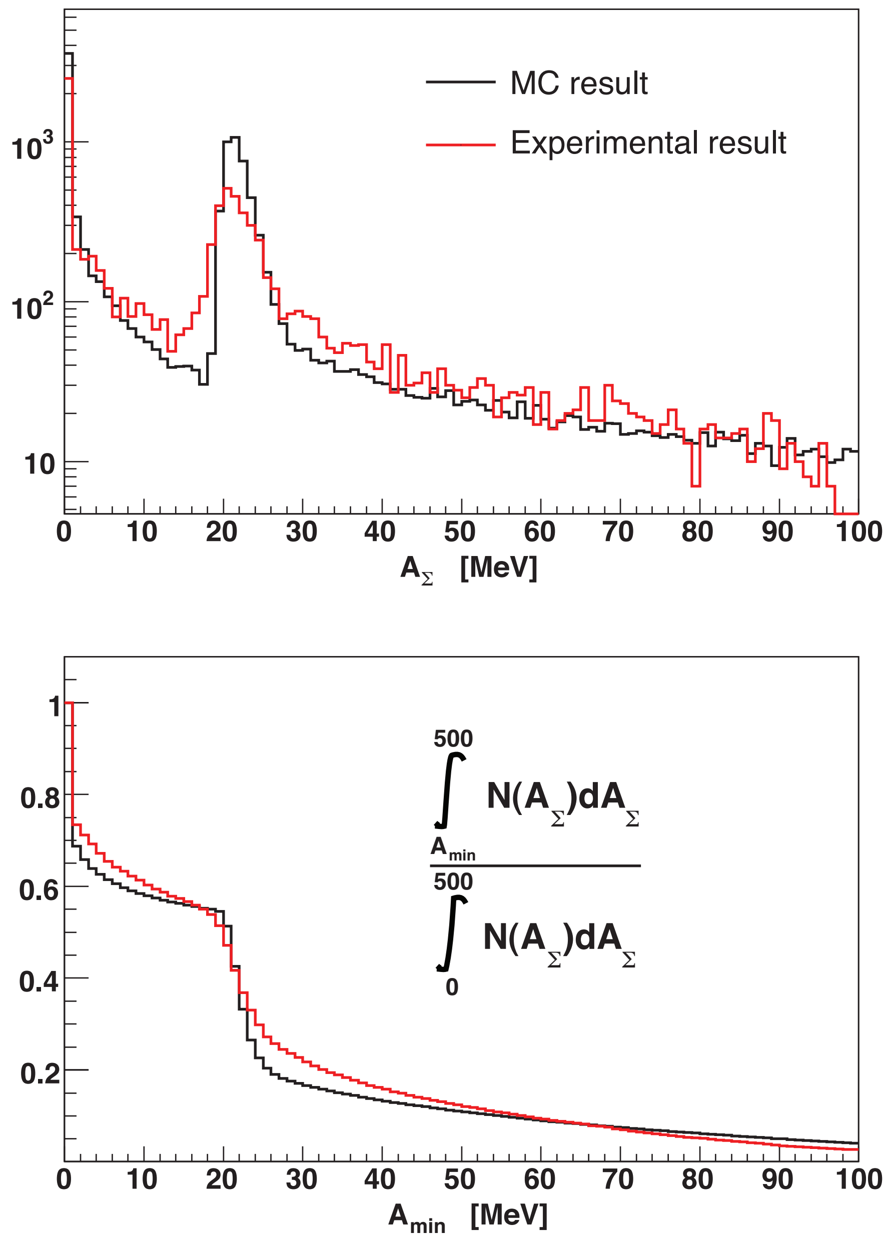

Figure 34: The amplitude spectrum in the front neutron detector of the N-20 setup from MC simulation and experimental data for 2 GeV/c protons. The bottom panel shows the integral of the spectra used to calculate the detection efficiency.

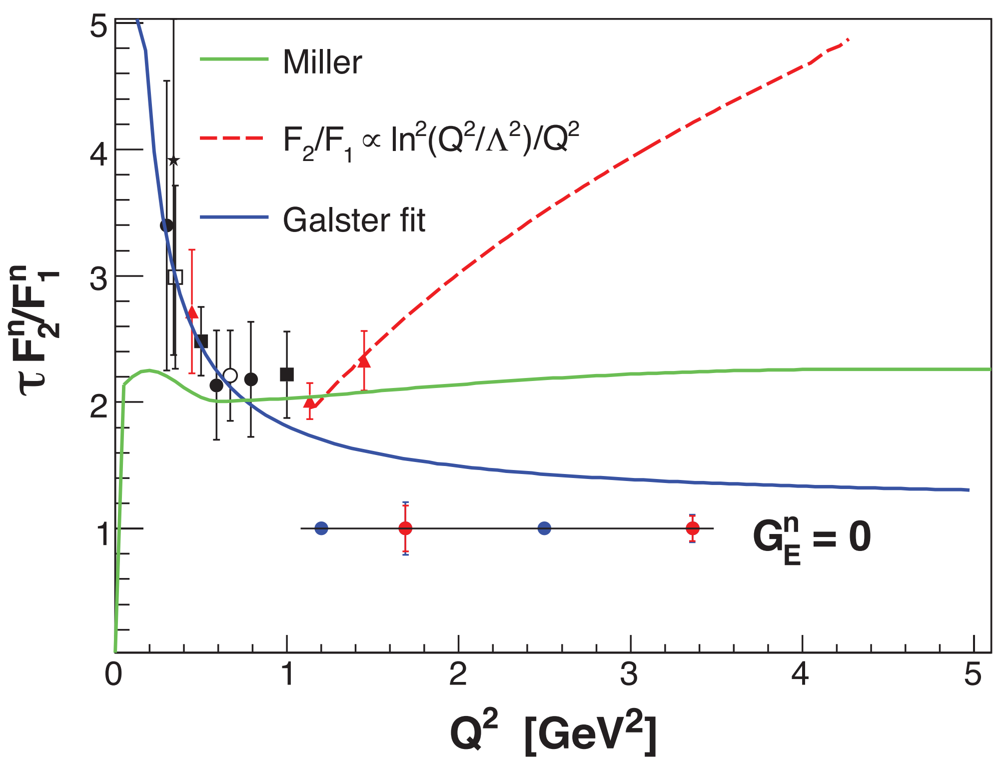

Figure 35: The electric form factor of the neutron with the four Q^2 values for the E02-013 measurements and the observed statistical accuracy for two data points, all points are shown for $G_E^n = 0$.

We would like to thank the E02-013 analysis team for preparing the plots included in this contribution.

References

[1] M. Diehl *et al.*, *Generalized parton distributions from nucleon form factor data*, Eur. Phys. J C **39**, 1 (2005).

[2] M. Guidal *et al.*, *Nucleon form factors from generalized parton distributions*, Phys. Rev. D **72**, 054013 (2005).

[3] R. Madey *et al.*, Phys. Rev. Lett. **91**, 37 (2003).

[4] A. Kelleher, *Polarized* ^{3}He *target*, DNP/APS fall meeting, October 2007.

[5] G. A. Miller, Phys. Rev. C **66**, 032201 (2002).

[6] A. Belitsky, X. Ji and F. Yuan, Phys. Rev. Lett. **91**, 092003 (2003).

4.6 Experiment E03-101

Hard pp Photodisintegration using γ^3He$\rightarrow pp + n$
Contributed by R. Gilman

Experiment E03-101, that ran during June 2007, has one Ph.D. student: I. Pomerantz from Tel Aviv University.

The goal of E03-101[1] was to determine the cross section for hard two-proton disintegration of ^{3}He. The motivaton rests in the extensive measurements of pn photodisintegration in the reaction $\gamma d \rightarrow pn$[2].

While modern hadronic theory provides, with some exceptions, a good explanation of measured deuteron photodisintegration at low energies[3], the underlying dynamics of photodisintegration above about 1 GeV have remained elusive. The cross-section data have led to the development of five quark-based[4, 5, 6, 7, 8] models of the reaction. Four models are based on the idea that an incoming high-energy photon is absorbed by a pair of quarks interchanged between the two nucleons; in two of these four models[6, 8] the photodisintegration cross section is directly related to measured nucleon-nucleon elastic scattering data. The fifth model, the quark-gluon string (QGS) model[5], uses Regge theory to evaluate the three-quark exchange diagram, and is based on the dominance of planar diagrams in quantum chromodynamics.

Polarization observables provide further support for some of these models at high energy, but the underlying dynamics are not clear since none of the models have predicted all measurements, some are not absolutely normalized, and the agreement with cross-section data remains more qualitative than quantitative. The benefit of pp photodisintegration[9] is that the models provide firmer predictions for the ratio of pp to pn disintegration: some predict pp disintegration is significantly smaller, but others predict pp disintegration is similar in size or even a few times larger.

The cross section was measured for $\theta_{c.m.} = 90^\circ$ pp disintegration at 8 beam energies, from 0.8 to 4.7 GeV, as shown in Fig. 36. The red points indicate the ^{3}He data taken during E03-101. The vertical position is arbitrary, since the Monte Carlo simulation that will be used to extract the final cross-section values is not sufficiently developed to show cross-section data at this time. Still, the analysis is sufficiently advanced that the statistical uncertainties are known. Overall systematic uncertainties are likely to be around 10%.

The black points shown are earlier, preliminary data from Hall B CLAS[10]. The curves shown represent three very different models: the reduced nuclear amplitudes (RNA) model[4] has been multiplied by 1/20 to fit in this plot, the hard rescattering model (HRM)[6] predicts oscillations in the cross section versus energy arising from oscillations in the pp elastic scattering, and QGS[5] predicts that pp disintegration is smaller than pn disintegration. For comparison, deuteron photodisintegration above 1 GeV would appear at $s^{11} d\sigma/dt \approx 0.4$ kb$\cdot$GeV^{20} on this plot.

In addition, Fig. 36 shows a series of light blue triangular points, for hard two-proton photodisintegration of ^{12}C. These points were taken on a solid target to provide spectrometer pointing information. They will also provide information on the effects of three- (or more-) body photodisintegration.

At this point in the analysis, the Monte Carlo is being tuned, and preliminary cross-section values should be available within several months. The final analysis will likely require of order a year. The data appear to be in good shape, except possibly for the 4.7 GeV point. At this energy, a problem with Q3 caused us to run with this magnet turned off, a non-standard spectrometer optics. We have not yet evaluated the effect of having Q3 off on our ability to make appropriate cuts in analyzing the data.

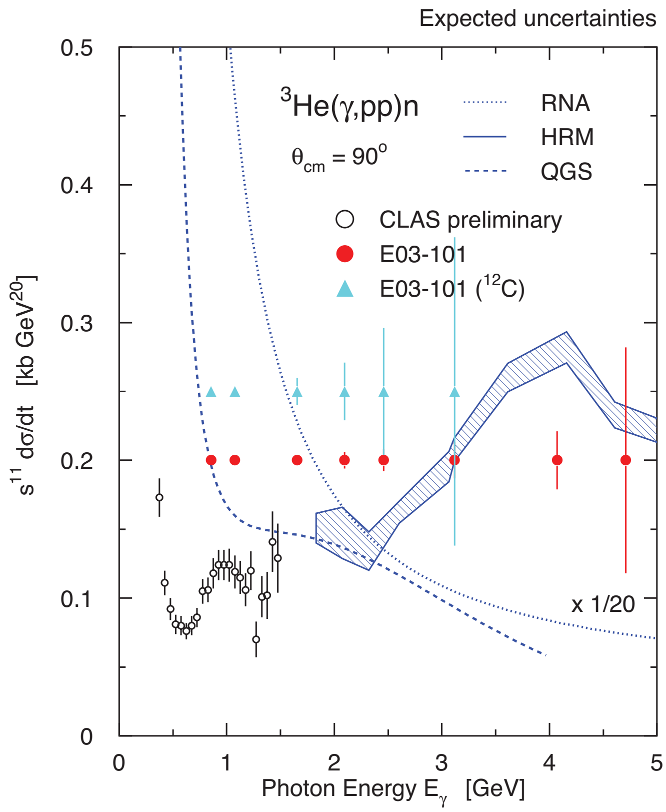

Figure 36: The cross section as a function of energy for ^{3}He photodisintegration. The cross-section values are multiplied by s^{11} to remove the strong energy dependence expected in perturbative QCD. See text for details.

References

[1] R. Gilman, E. Piasetzky *et al.*, spokespersons, JLab experiment E03-101; and I. Pomerantz *et al.*, to be published.

[2] Recent work includes E.C. Schulte *et al.*, Phys. Rev. Lett. **87**, 102302 (2001); E.C. Schulte *et al.*, Phys. Rev. C **66**, 042201R (2002); M. Mirazita *et al.*, Phys. Rev. C **70**, 014005 (2004); and X. Jiang *et al.*, Phys. Rev. Lett. **98**, 182302 (2007).

[3] R. Gilman and F. Gross, *Electromagnetic Structure of the Deuteron*, J. Phys. G **28**, R37 (2002).

[4] S.J. Brodsky and J.R. Hiller, Phys. Rev. C **28**, 475 (1983).

[5] E. De Sanctis *et al.*, Few Body Syst. Suppl. **6**, 229 (1992); L. A. Kondratyuk *et al.*, Phys. Rev. C **48**, 2491 (1993); V.Yu Grishina *et al.*, Eur. Phys. J. A **10**, 355 (2001); V.Yu Grishina *et al.*, Eur. Phys. J. A **18**, 207 (2003); V.Yu Grishina *et al.*, Eur. Phys. J. A **19**, 117 (2004).

[6] L.L. Frankfurt, G.A. Miller, M.M. Sargsian and M.I. Strikman, Phys. Rev. Lett. **84**, 3045 (2000); L.L. Frankfurt, G.A. Miller, M.M. Sargsian and M.I. Strikman, Nucl. Phys. A **663**, 349 (2000); M.M. Sargsian, Phys. Lett. B **587**, 41 (2004).

[7] A. Radyushkin, private communication.

[8] B. Julia-Diaz and T.-S. H. Lee, Mod. Phys. Lett. A **18**, 200 (2003).

[9] S.J. Brodsky *et al.*, Phys. Lett. B **578**, 69 (2003).

[10] S. Strauch, private communication; B.L. Berman *et al.*, CLAS run g3a.

4.7 Experiment E03-104

Probing the Limits of the Standard Model of Nuclear Physics with the $^4\mathrm{He}(\vec{e}, e'\vec{p})^3\mathrm{H}$ Reaction
Contributed by Steffen Strauch

Experiment E03-104 ran in Hall A from October 3 to November 9, 2006 and its analysis is now underway. Michael Paolone from the University of South Carolina is the Ph.D. student analyzing the polarization transfer data while Simona Malace, a postdoctoral fellow with the University of South Carolina, is working in particular on the induced polarization extraction.

The polarization-transfer double ratio, $R = (P'_x/P'_z)_{^4\mathrm{H}}/(P'_x/P'_z)_{^1\mathrm{H}}$, in the $^4\mathrm{He}(\vec{e}, e'\vec{p})^3\mathrm{H}$ reaction in quasi-elastic kinematics is shown in the left panel of Fig. 37. The preliminary data of the present experiment E03-104 (filled circles) are consistent with our previous data from E93-049 [1] and MAMI [2] (open symbols). The final systematic uncertainties from E03-104 are expected to be much smaller than those shown here. The data are compared with relativistic distorted-wave impulse approximation (RDWIA) calculations from the Madrid group [3]. The RDWIA calculation (dashed curve) overpredicts the data by about 6%. After including the density-dependent medium-modified form factors as predicted by Lu *et al.*[4] in the RDWIA calculation (solid curve) good agreement with the previous data is obtained[3]. This agreement has been interpreted as a possible evidence of proton medium modifications[1]. This interpretation is based on the more effective description of the data in a particular model in terms of medium modifications of nucleon form factors and requires excellent control of the inherent many-body effects, such as meson-exchange currents (MEC) and isobar configurations (IC). In addition, when probing nuclear structure, one has to deal with final-state interactions (FSI). Indeed, the observed suppression of the polarization-transfer ratio has been equally well described in a more traditional calculation by Schiavilla[5] using free form factors by including charge-exchange final-state interactions and two-body charge and current operators (shaded band). Yet, the choice of the parameters for the charge-exchange FSI is not well constrained by data. The preliminary results from E03-104 possibly hint at an unexpected trend in the Q^2-dependence of R. This is particularly interesting as other calculations of in-medium form factors suggest a different Q^2-dependence than that of the QMC model. The high statistics of the data from E03-104 will allow for a study of the individual polarization observables as a function of missing momentum up to about 120 MeV/c.

The difference in the modeling of final-state interactions is the origin of the major part of the difference between the results of the calculations by Udias *et al.* [3] and Schiavilla *et al.* [5] for the polarization observables. Effects from final-state interactions can be studied experimentally with the induced polarization, P_y. E03-104 took dedicated high-precision data to extract P_y.

In this context, an ongoing effort aimed at devising a method to minimize false asymmetries will make possible the precise extraction of the induced polarization P_y. Our studies show that false asymmetries are partly caused by what appears to be highly inefficient regions ("bad" regions) in the FPP rear chambers. The "mirror test" method was developed to deal with this issue: an event for which a rear track is reconstructed is used for the polarization extraction only if its "mirror" (*i.e.* its 180° symmetric in the azimuthal angle distribution) does not cross a "bad" region of the FPP rear chambers. However, the success of this method in reducing false asymmetries relies on having a reconstruction of the "mirror" track as good as the reconstruction of the real track. While the real rear track reconstruction is based on wire hits in the rear chambers, the "mirror" track reconstruction relies additionally on the knowledge of the location of the proton-Carbon interaction

[3] A Glauber-based calculations by Ryckebusch[6] gives R/R_{PWIA} of about one and is not shown here. We also do not show a chiral-soliton model calculation of the in-medium form factors by Smith and Miller[7], which gives results similar to the QMC results.

vertex. It was found that due to multiple scattering in the Carbon analyzer this location is not known with enough accuracy to have comparable resolution in the reconstruction of the real and "mirror" track. Therefore this method does not allow the extraction of P_y with the expected accuracy [8]. This study triggered, however, a revision of the FPP tracking algorithm. We are working on an alternative tracking algorithm for improved tracking efficiency at the expense of track resolution.

At this stage in the analysis, P_y in $^4\mathrm{He}(\vec{e}, e'\vec{p})^3\mathrm{H}$ is extracted by correcting for false asymmetries via $^1\mathrm{H}(\vec{e}, e'\vec{p})$ subtraction and the preliminary results are shown in the right panel of Fig. 37. This experiment's preliminary data are presented together with the published results of E93-049 and it can be seen that the acceptance-corrected induced polarization is small in $^4\mathrm{He}(\vec{e}, e'\vec{p})^3\mathrm{H}$, about -0.03 in absolute value. The sizable systematic uncertainties for E03-104 are due to possible instrumental asymmetries. The data are compared with theoretical calculations from Udias *et al.*[9] and Schiavilla *et al.*[5] at a missing momentum of about zero. The data have been corrected for spectrometer acceptance to facilitate this comparison. As mentioned above, the two theoretical calculations use different ingredients to parameterize the FSI. Presently, the data suggest that the magnitude of the induced polarization (and thus the final-state interaction) is overestimated in the model of Schiavilla *et al.* However, for a definite conclusion a more accurate extraction of P_y is necessary. Taking advantage of the high statistics accumulated in E03-104 we expect, through our study of false asymmetries, to reduce the shown preliminary systematic uncertainties by a factor of 2.

A comparison of the model calculations in Fig. 37 shows that the in-medium form factors (solid curves) mostly affect the ratio of polarization-transfer observables, not the induced polarization. It is a key element of E03-104 to have access to both of these observables.

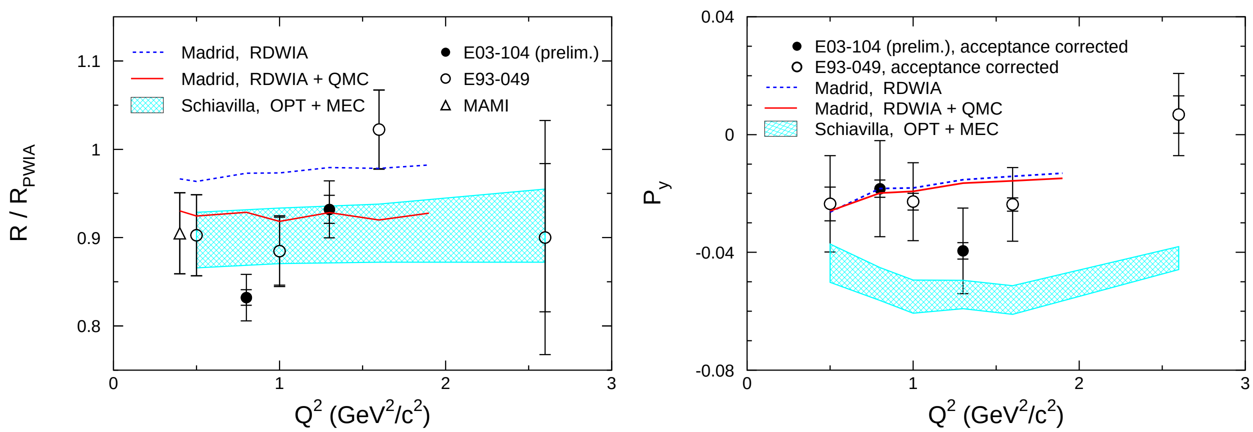

Figure 37: Recoil-polarization data as a function of Q^2 from Mainz[2] and Jefferson Lab experiment E93-049 (open symbols)[1] along with preliminary results from experiment E03-104 (filled circles), compared to calculations from the Madrid group[3] and Schiavilla *et al.*[5]. Left panel: Super-ratio R/R_{PWIA}, where R is the ratio of transverse to longitudinal polarization of the recoiling proton in $^4\mathrm{He}(\vec{e}, e'\vec{p})^3\mathrm{H}$ compared to the same ratio for $^1\mathrm{H}(\vec{e}, e'\vec{p})$. The baseline R_{PWIA} is the value of R obtained in a plane-wave calculation, to account for the "trivial" effects of free *vs.* moving proton. Right panel: Induced polarization P_y for missing momentum $p_m \approx 0$; note that the experimental data have been corrected for the spectrometer acceptance.

References

[1] S. Strauch *et al.*, Phys. Rev. Lett. **91**, 052301 (2003).

[2] S. Dieterich *et al.*, Phys. Lett. **B500** 47 (2001).

[3] J.M. Udias *et al.*, Phys. Rev. Lett. **83**, 5451 (1991); J.A. Caballero, T.W. Donnelly, E. Moya de Guerra and J.M. Udias, Nucl. Phys. **A632**, 323 (1998); J.M. Udias and J.R. Vignote, Phys. Rev. C **62**, 034302 (2000).

[4] D.H. Lu *et al.*, Phys. Lett. **B417**, 217 (1998) and Phys. Rev. C **60**, 068201 (1999).

[5] R. Schiavilla *et al.*, Phys. Rev. Lett. **94**, 072303 (2005).

[6] P. Lava *et al.*, Phys. Rev. C **71**, 014605 (2005).

[7] J.R. Smith and G.A. Miller, Phys. Rev. C **70**, 065205 (2004).

[8] J. DeGange, S. Malace, M. Paolone, S. Strauch and D. Tedeschi, for the Jefferson Lab Hall A Collaboration, "*Study of Instrumental Asymmetries in a Focal Plane Polarimeter (CEU Poster Session)*", Bull. Am. Phys. Soc. **52**, No. 9, 55 (2007).

[9] J.M. Udias *et al.*, Phys. Rev. C **51**, 3246 (1995).

4.8 Experiment E03-106

Deeply Virtual Compton Scattering off the Neutron
Contributed by M. Mazouz

P.-Y. Bertin, C.E. Hyde, F. Sabatié and E. Voutier, spokespersons,
and the Hall A Collaboration.

Motivations and goals

Experiment E03-106 studied the beam-helicity dependence of the deeply virtual Compton Scattering process off the neutron (n-DVCS) at $Q^2 = 1.9$ GeV^2 and $x_B = 0.36$ [1]. At leading order, DVCS allows to extract the generalized parton distributions (GPDs) which unify form factors and parton distributions and access the contribution of orbital angular momentum of the quarks (and gluons) to the nucleon spin[2, 3, 4]. The GPDs correspond to the amplitude for removing a parton of momentum fraction $x+\xi$ and restoring it with momentum fraction $x-\xi$ resulting in a momentum transfer t. Experimentally DVCS interferes with the Bethe-Heitler (BH) process where the real photon is radiated by the incident or the scattered electron instead of the struck quark as in the DVCS case. The $N(e,e'\gamma)N$ helicity-dependent cross section accesses the imaginary part of this interference which is proportional, in the Bjorken limit, to a linear combination of GPDs at $x = \pm\xi$:

$$\frac{1}{2}\left[\frac{d^5\sigma^+}{d^5\Phi} - \frac{d^5\sigma^-}{d^5\Phi}\right] = \Gamma^{\Im}\, \Im\mathrm{m}\left[\mathcal{C}^{\mathrm{I}}\right]\, \sin(\phi_{\gamma\gamma})\,, \tag{1}$$

where $\phi_{\gamma\gamma}$ is the angle between the hadronic and leptonic planes; $d^5\Phi = dQ^2 dx_{\mathrm{B}} dt d\phi_e d\phi_{\gamma\gamma}$ is the detection hypervolume, and $\Gamma^{\Im}$ is a kinematical factor depending of the BH propagators [5]. $\Im\mathrm{m}\left[\mathcal{C}^{\mathrm{I}}\right]$ depends on the interference of the BH amplitude with the set $\mathcal{F} = \{\mathcal{H},\, \mathcal{E},\, \widetilde{\mathcal{H}}\}$ of twist-2 Compton form factors (CFFs):

$$\mathcal{C}^I = F_1\mathcal{H} + \xi(F_1+F_2)\widetilde{\mathcal{H}} - \frac{t}{4M^2}F_2\mathcal{E}\,, \tag{2}$$

where $F_1(F_2)$ is the Dirac(Pauli) form factor entering the BH amplitude. The imaginary part of twist-2 CFFs is determined by the $x = \pm\xi$ points of the GPDs, for example:

$$\Im m\,[\mathcal{E}] = \pi \sum_q e_q^2 \left(E_q(\xi,\xi,t) - E_q(-\xi,\xi,t)\right)\,, \tag{3}$$

where the sum $q \in \{u,d\}$ runs over the flavor content of the nucleon, and e_q is the quark charge in unit of the elementary charge. The goal of E03-106 was to determine the imaginary part of Eq. 2, mostly sensitive to the contribution of the GPD E_q in the neutron case[6, 7]; this same quantity is dominated by the GPD H_q for a proton target. The knowledge of the least constrained GPD E_q is mandatory in order to access the quark orbital angular momentum with Ji sum rule[4]:

$$J_q = \frac{1}{2}\Delta\Sigma_q + L_q = \frac{1}{2}\int_{-1}^{+1} dx\, x\left[H_q(x,\xi,t=0) + E_q(x,\xi,t=0)\right]\,. \tag{4}$$

Experimental apparatus and analysis technique

A 15-cm long liquid D_2 target was used as a quasi-free neutron target. The beam energy was 5.75 GeV with a 76% polarization and a 4 μA intensity yielding a luminosity of 4×10^{37} cm$^{-2}\cdot$s^{-1}.

The scattered electrons of 2.94 GeV/c were detected at 19.3° in the HRS-L and the photons above a 1.2 GeV energy threshold were detected at 18.3° in a calorimeter made of 11×12 array of 3×3×18.6 cm^3 PbF$_2$ blocks. Three DVCS processes are possible within the impulse approximation:

$$\begin{aligned} \mathrm{D}(\vec{e}, e'\gamma)X &= d(\vec{e}, e'\gamma)d + n(\vec{e}, e'\gamma)n + p(\vec{e}, e'\gamma)p + \ldots \\ &= d{-}DVCS + n{-}DVCS + p{-}DVCS + \ldots \end{aligned} \tag{5}$$

where meson production channels are also contributing as background. The missing mass is used to remove this inclusive background and identify DVCS events. The n-DVCS and d-DVCS contributions are determined after a subtraction of the p-DVCS contribution from $\mathrm{H}(\vec{e}, e'\gamma)p$ events recorded during the p-DVCS experiment (E00-110). A systematic error was introduced since the H$_2$ and D$_2$ data are not taken simultaneously. Events where a high-energy photon, from a π^0 decay, is detected in the calorimeter mimic DVCS events. The contamination of these events was treated as a systematic error[1].

E00-110 showed strong evidence of DVCS scaling for Q^2 as low as 2 GeV^2[8]. This important result allows to write the experimental helicity-dependent cross-section as[5, 9]

$$\frac{d^5\Sigma_{\mathrm{D-H}}}{d^5\Phi} = \frac{1}{2}\left(\frac{d^5\sigma^+}{d^5\Phi} - \frac{d^5\sigma^-}{d^5\Phi}\right) = \left(\Gamma_d^{\Im}\,\Im\mathrm{m}\left[\mathcal{C}_{\mathrm{d}}^{\mathrm{I}}\right]^{\mathrm{exp}} + \Gamma_{\mathrm{n}}^{\Im}\,\Im\mathrm{m}\left[\mathcal{C}_{\mathrm{n}}^{\mathrm{I}}\right]^{\mathrm{exp}}\right)\sin(\phi_{\gamma\gamma})\,, \tag{6}$$

where only twist-2 terms from n-DVCS and d-DVCS contribute to the cross section (Eq. 1). $\Im\mathrm{m}\left[\mathcal{C}_{\mathrm{n}}^{\mathrm{I}}\right]^{\mathrm{exp}}$ and $\Im\mathrm{m}\left[\mathcal{C}_{\mathrm{d}}^{\mathrm{I}}\right]^{\mathrm{exp}}$ are then simultaneously extracted in each t-bin taking advantage of their kinematic $\Delta M_X^2 \simeq t/2$ separation. This extraction is based on a fit of a Monte-Carlo simulation with the kinematic weights of Eq. 6 to the experimental distribution obtained after the D$-$H subtraction.

Results

Figure 38 (Left) displays $\Im\mathrm{m}\left[\mathcal{C}_{\mathrm{n}}^{\mathrm{I}}\right]^{\mathrm{exp}}$ and $\Im\mathrm{m}\left[\mathcal{C}_{\mathrm{d}}^{\mathrm{I}}\right]^{\mathrm{exp}}$ as a function of t [1]. Both n-DVCS and d-DVCS contributions are compatible with zero. The deuteron results are in agreement with the rapid decrease of the deuteron form factors at high $-t$. n-DVCS results are compared to three different calculations of the VGG model[6, 7] where the GPD E_q is parametrized by the contributions J_u and J_d of up- and down-quarks, respectively to the proton spin. This comparison indicates that the results are accurate enough to constrain GPD models and in particular the GPD E_q parametrization. Figure 38 (Right) shows a correlated constraint on J_u and J_d extracted from a fit of the VGG model to the neutron data[1]. The model dependence of this analysis should be stressed: n-DVCS data involve GPDs at one point $x{=}\pm\xi$ and $t \neq 0$ while the Ji sum rule (Eq. 4) is an integral over x extrapolated to t=0. A similar constraint obtained from HERMES preliminary $\vec{\mathrm{p}}$-DVCS data[11] illustrates the complementarity between n-DVCS and p-DVCS experiments.

Future

The complementarity between p-DVCS and n-DVCS experiments is a key feature for future experimental programs investigating DVCS and GPDs. The measurement of n-DVCS and d-DVCS unpolarized cross sections, which are sensitive to the GPD integral over x, is the next step of this experimental program. A proposal was submitted to PAC33 in order to achieve this measurement. At leading twist, the total cross section reads

$$\frac{d^5\sigma_{D-H}^{exp}}{d^5\Phi} = \frac{d^5\sigma(|BH|_n^2)}{d^5\Phi} + \frac{d^5\sigma(|BH|_d^2)}{d^5\Phi} \tag{7}$$

$$+ \quad \Gamma_n^{DVCS}\, \mathcal{C}_n^{DVCS} + \frac{1}{\mathcal{P}_1\mathcal{P}_2}\Big(\{\Gamma^{\Re}_{0,n} - \cos(\phi_{\gamma\gamma})\Gamma^{\Re}_{1,n}\}\Re\mathrm{e}\left[\mathcal{C}_n^I\right] + \Gamma^{\Re}_{0,\Delta,n}\Re\mathrm{e}\left[\mathcal{C}_\mathrm{n}^\mathrm{I} + \Delta\mathcal{C}_\mathrm{n}^\mathrm{I}\right]\Big)$$

$$+ \quad \Gamma_d^{DVCS}\, \mathcal{C}_d^{DVCS} + \frac{1}{\mathcal{P}_1\mathcal{P}_2}\Big(\{\Gamma^{\Re}_{0,d} - \cos(\phi_{\gamma\gamma})\Gamma^{\Re}_{1,d}\}\Re\mathrm{e}\left[\mathcal{C}_d^I\right] + \Gamma^{\Re}_{0,\Delta,d}\Re\mathrm{e}\left[\mathcal{C}_\mathrm{d}^\mathrm{I} + \Delta\mathcal{C}_\mathrm{d}^\mathrm{I}\right]\Big)\,.$$

where $\mathcal{C}_{n,d}^{DVCS}$, $\Re\mathrm{e}\left[\mathcal{C}_{n,d}^I\right]$ and $\Re\mathrm{e}\left[\mathcal{C}_\mathrm{n,d}^\mathrm{I} + \Delta\mathcal{C}_\mathrm{n,d}^\mathrm{I}\right]$ represent the six GPD combinations (linear and bilinear) to be extracted from the data. This simultaneous extraction requires two different beam energies. Figure 39 shows the projected results with 400 hours of D_2 data and 120 hours of H_2 data from the future p-DVCS experiment[12]. Systematic errors will be strongly reduced by performing frequent swaps between H_2 and D_2 data taking and by improving the trigger capabilities to allow for a better π^0 background subtraction.

References

[1] M. Mazouz *et al.*, Phys. Rev. Lett. **99**, 242501 (2007).

[2] D. Mueller, D. Robaschik, B. Geyer, F.M. Dittes and J. Horejsi, Fortschr. Phys. **42**, 101 (1994).

[3] A.V. Radyushkin, Phys. Rev. **D56**, 5524 (1997).

[4] X.-D. Ji, Phys. Rev. Lett. **78**, 610 (1997).

[5] A.V. Belitsky, D. Mueller and A. Kirchner, Nucl. Phys. **B629**, 323 (2002).

[6] M. Vanderhaeghen, P.A.M. Guichon and M. Guidal, Phys. Rev. **D60**, 094017 (1999).

[7] K. Goeke, M.V. Polyakov and M. Vanderhaeghen, Prog. Part. Nucl. Phys. **47**, 4001 (2001).

[8] C. Muñoz Camacho *et al.*, Phys. Rev. Lett. **97**, 262002 (2006).

[9] A. Kirchner and D. Mueller, Eur. Phys. J. **C32**, 347 (2004).

[10] F. Cano and B. Pire, Eur. Phys. J. **A19**, 423 (2004).

[11] Z. Ye, Proc. of the XIVth International Workshop on Deep Inelastic Scattering, Tsukuba (Japan), April 20-24, 2006; F. Ellinghaus *et al.*, Eur. Phys. J. **C46**, 729 (2006).

[12] C. Muñoz Camacho, P.-Y. Bertin, C.E. Hyde and J. Roche, spokespersons, JLab Experiment E07-007 .

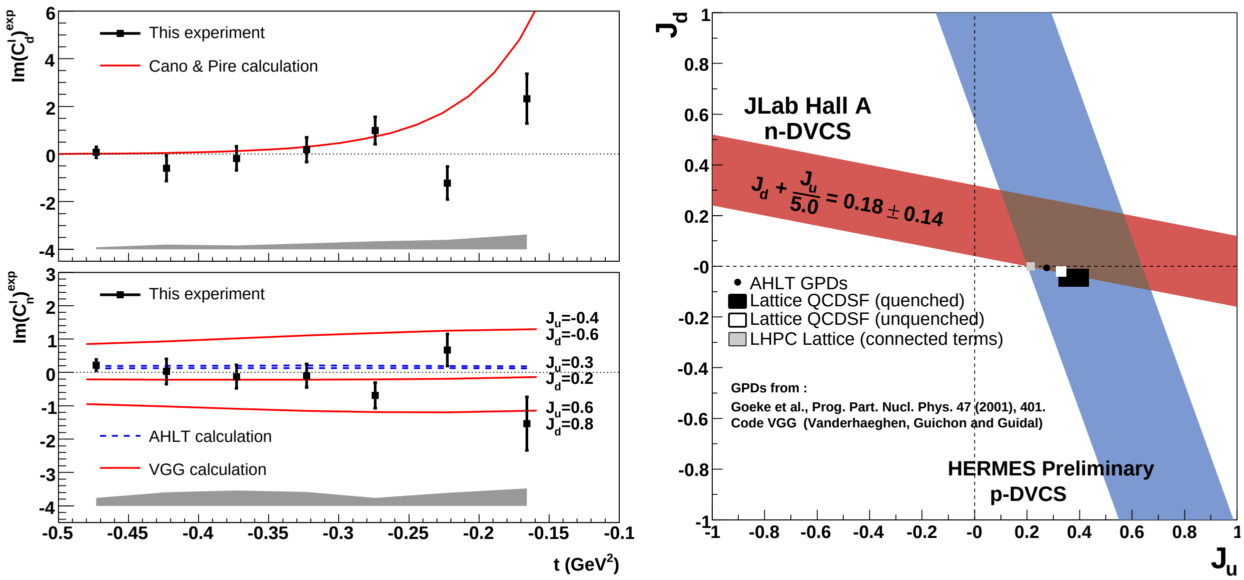

Figure 38: (Left) $\Im\mathrm{m}\left[\mathcal{C}_{\mathrm{n}}^{\mathrm{I}}\right]^{\mathrm{exp}}$ and $\Im\mathrm{m}\left[\mathcal{C}_{\mathrm{d}}^{\mathrm{I}}\right]^{\mathrm{exp}}$ as a function of t; the shaded bands represent the systematic errors; the results are compared to GPD models for the deuteron and the neutron[1]. (Right) A model-dependent extraction from the n-DVCS results of the contributions J_u and J_d of up- and down-quarks to the proton spin; similar constraint from the HERMES collaboration as well as four LQCD-based calulations are also shown[1].

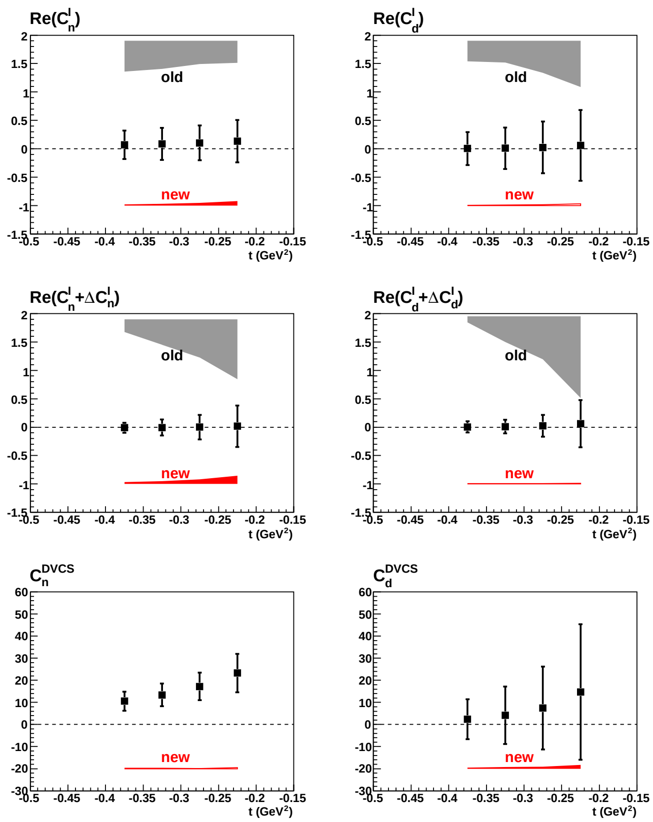

Figure 39: Expected results and statistical errors of the extracted coefficients for n-DVCS (left) and d-DVCS (right). Systematic errors are indicated by the bottom red bands assuming a 5% total systematic uncertainty on the cross section. For comparison, E03-106 systematic errors are indicated by the top shaded bands.

4.9 Experiment E04-018

Elastic Electron Scattering Off ^{3}He and ^{4}He at Large Momentum Transfers
Contributed by G. G. Petratos

A. Camsonne, J. Gomez, A. T. Katramatou and G. G. Petratos, spokespersons,
and
the Hall A Collaboration

Measurements of the elastic form factors of the few-body nuclear systems (deuteron, ^{3}He, tritium and ^{4}He) are of crucial importance in understanding their electromagnetic structure[1, 2]. They offer unique opportunities to study the short-range nucleon-nucleon interaction, few-body wave functions, meson-exchange currents (MEC), isobar configurations (IC) and three-body force contributions, and effects from possible quark-cluster wave-function admixtures. Large momentum transfer measurements can test "nuclear chromodynamics" predictions based on quark dimensional scaling and perturbative Quantum Chromodynamics (pQCD)[3].

There have been extensive experimental investigations of the form factors of the few-body systems over the past 50 years at almost every electron accelerator laboratory. Comprehensive and exhaustive reviews are given in Refs. [2, 4] for the deuteron case and Ref. [5] for the three- and four-body systems. Experimentally, the few-body form factors are determined from elastic electron scattering studies with high intensity beams, high-density targets and magnetic spectrometer systems capable of resolving elastic events with only scattered electron detection or also detection of recoil nuclei in coincidence. The Hall A Facility of JLab completed last Summer an extensive set of elastic electron scattering measurements off the ^{3}He and ^{4}He isotopes, which are in the analysis phase. These measurements are complementary to previous measurements on elastic scattering from the deuteron in Halls A and C[4].

The cross section for elastic electron scattering from the spin one-half ^{3}He nucleus is given, in the one-photon exchange approximation, by:

$$\frac{d\sigma}{d\Omega}(E,\Theta) = \frac{(Z\alpha)^2 E'}{4E^3 \sin^4\left(\frac{\Theta}{2}\right)} \left[A(Q^2)\cos^2\left(\frac{\Theta}{2}\right) + B(Q^2)\sin^2\left(\frac{\Theta}{2}\right)\right], \tag{8}$$

where α is the fine-structure constant, Z is the nuclear charge, E and E' are the incident and scattered electron energies, Θ is the electron scattering angle, $Q^2 = 4EE'\sin^2(\Theta/2)$ is the squared four-momentum transfer, and $A(Q^2)$ and $B(Q^2)$ are the ^{3}He elastic structure functions, given in terms of the charge, F_C, and the magnetic, F_M, form factors as:

$$A(Q^2) = \frac{F_C^2(Q^2) + (1+\kappa)^2 \tau F_M^2(Q^2)}{1+\tau}, \tag{9}$$

$$B(Q^2) = 2\tau(1+\kappa)^2 F_M^2(Q^2), \tag{10}$$

where $\tau = Q^2/4M^2$ with M being the mass of the target nucleus, and κ is the anomalous magnetic moment of the nucleus. The two form factors of ^{3}He are determined by measuring the elastic cross section at least at two different angles using different beam energies for the same fixed Q^2 (Rosenbluth separation).

The cross section for elastic electron scattering from the spin-zero ^{4}He nucleus is free of a magnetic contribution and is given, in the one-photon exchange approximation, by:

$$\frac{d\sigma}{d\Omega}(E,\Theta) = \frac{(Z\alpha)^2 E' \cos^2\left(\frac{\Theta}{2}\right)}{4E^3 \sin^4\left(\frac{\Theta}{2}\right)} F_C^2(Q^2). \tag{11}$$

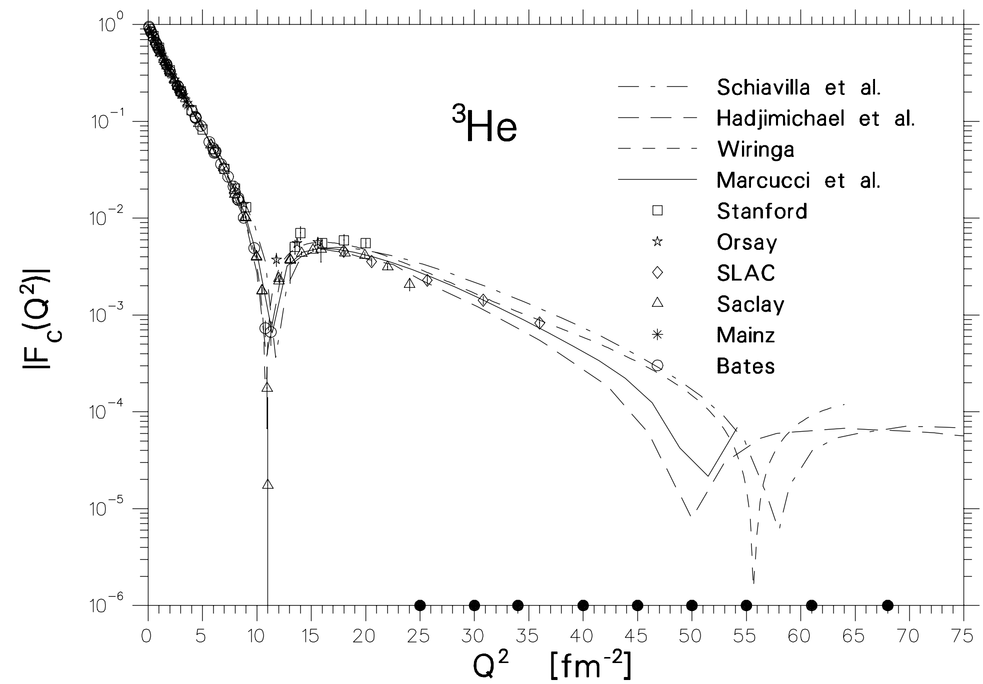

Figure 40: ^{3}He F_C data compared to four different calculations based on the IA with inclusion of MEC[9]. The solid black circles indicate the Q^2 values of new JLab measurements by experiment E04-018 under analysis[9].

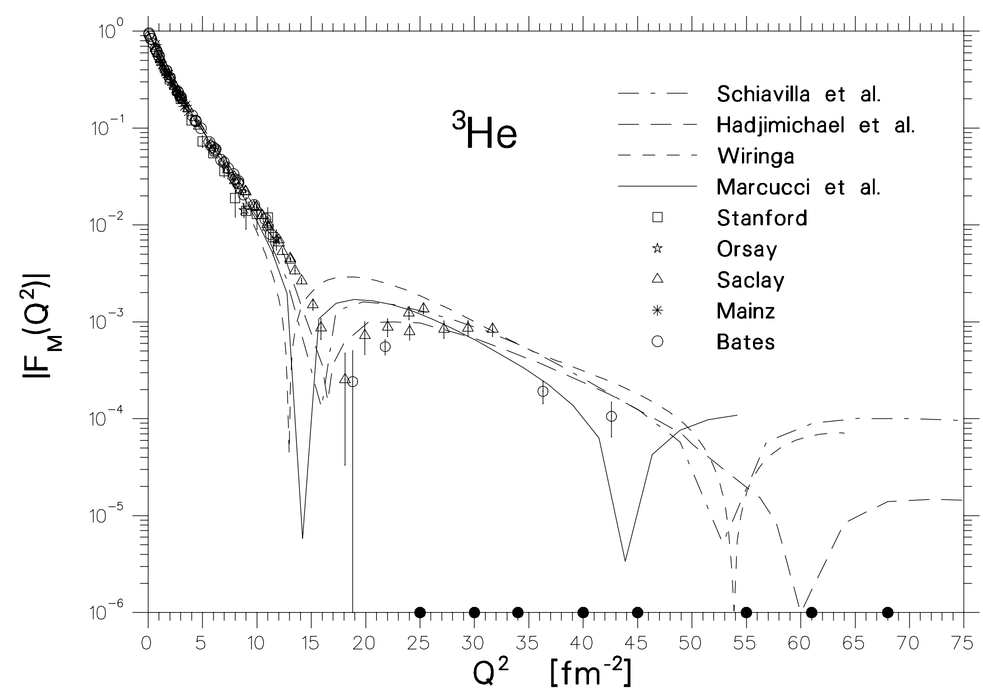

Figure 41: ^{3}He F_M data compared to four different calculations based on the IA with inclusion of MEC[9]. The solid black circles indicate the Q^2 values of new JLab measurements by experiment E04-018 under analysis[9].

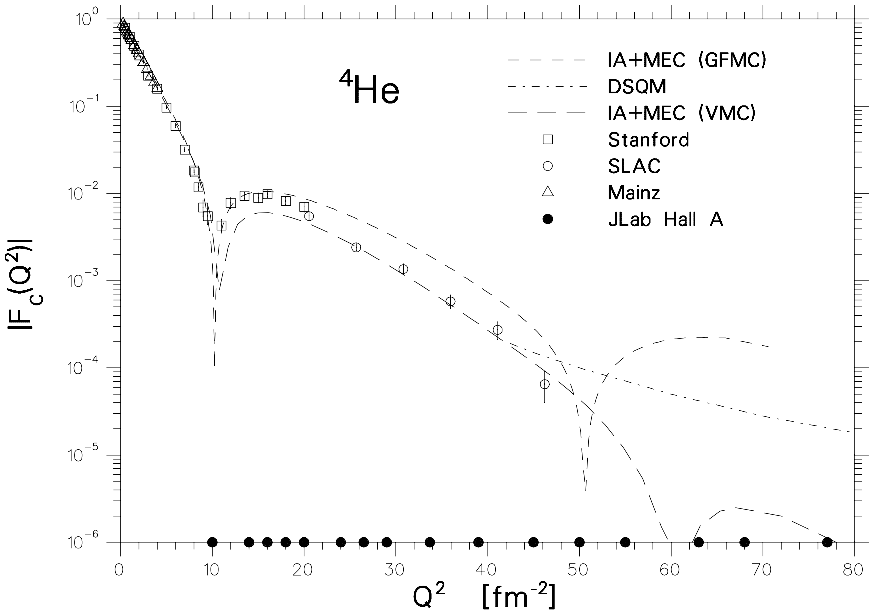

Figure 42: ^{4}He F_C data compared to two IA calculations with inclusion of MEC using Green's Function Monte Carlo (GFMC) and Variational Monte Carlo (VMC) techniques[9]). also shown is the asymptotic DSQM prediction[8]. The solid black circles indicate the Q^2-values of new JLab measurements by experiment E04-018 under analysis[9].

The ^{4}He charge form factor, F_C, is determined at a given Q^2 by a single-angle cross-section measurement using, to maximize the counting rate, the highest possible beam energy.

The conventional theoretical approach of elastic electron scattering from few-body systems is based on the impulse approximation (IA), where the electron interacts with one of their nucleons. The few-body form factors are then convolutions of the nuclear wave function with the form factors of the constituent nucleons. It has long been understood and overwhelmingly supported by the available data that these form factors are sensitive to the presence of MEC and IC that augment the IA picture[1]. At large momentum transfers, the effects of relativity cannot be ignored and either IA corrections or fully relativistic approaches are necessary[2, 6].

It is widely recognized that at distances much less than the nucleon size, the underlying quark substructure of the nucleons cannot be ignored. This has lead to the formulation of so-called hybrid quark models[7] that treat few-body nuclei as quark clusters when the internucleon separations become smaller than ∼1 fm. At sufficiently "large" Q^2, the few-body form factors are expected to be described in terms of only quarks and gluons within the framework of pQCD. The first attempt at such a description was based on the dimensional-scaling quark model (DSQM)[8], where the underlying dynamical mechanism during elastic scattering is the hard rescattering of the constituent quarks via the exchange of hard gluons. The Q^2-dependence of this process was then predicted by simply counting the number n of gluon propagators. For example, for the ^{3}He case (n=8), the $A(Q^2)$ elastic structure function should follow the power scaling law $\sqrt{A(Q^2)} \sim (Q^2)^{-8}$, and its deuteron counter part ($n = 5$) should scale as $\sqrt{A(Q^2)} \sim (Q^2)^{-5}$.

The conventional theoretical calculations for the three- and four-body nuclei are based on the IA, where the problem of solving for the nuclear ground states relies on using the Faddeev-Yakubosky equations, correlated hyperspherical harmonic functions or Green's function and variational Monte Carlo methods. The existing data on the charge and magnetic form factors, F_C and F_M, of ^{3}He are

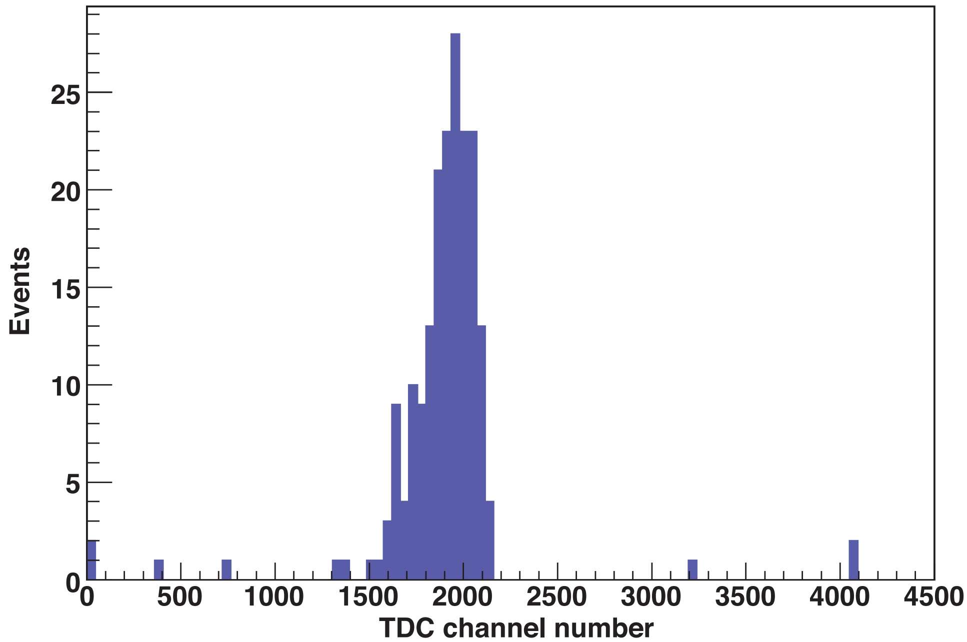

Figure 43: Raw time-of-flight (TOF) spectrum between the electron and recoil spectrometer triggers for elastic $e-{}^4$He scattering at $Q^2 = 34$ fm^{-2}. The observed peak corresponds to elastic events (electron-helium coincidences).

shown in Figs. 40 and 41, and on the charge form factor of ^{4}He in Fig. 42. All three form factors exhibit a diffractive structure (shown in the Figures), in qualitative agreement with theoretical calculations based on the IA, augmented by MEC, whose inclusion, as for the deuteron case, brings the theory in better agreement with the data. To obtain a very good agreement with the data, the theory must by augmented by phenomenological contributions from multi-quark clusters[7].

The recently completed JLab experiment E04-018[9] measured all three helium form factors at large momentum transfers. The experiment was carried out in the Fall 2006 and Spring and Summer 2007 in JLab's Hall A Facility. Elastic electron scattering off ^{3}He was measured at forward and backward electron scattering angles to extract its F_C and F_M form factors using the Rosenbluth separation method. For ^{4}He, only forward elastic electron scattering was measured to extract directly its F_C form factor. The experiment used high-intensity electron beams with an energy in the range between 0.7 and 4.4 GeV, and a high-density cryogenic helium and hydrogen (for calibration) target systems. Scattered electrons and recoil nuclei were detected in coincidence in the Electron and Hadron High Resolution Spectrometers (HRS), respectively. Electrons were identified using a Čerenkov counter and an electromagnetic calorimeter. Both spectrometers used two planes of scintillation counters, for triggering and timing purposes, and two sets of drift chambers for the reconstruction of the kinematical parameters of the detected particles. The identification of electron-nucleus coincidences was accomplished by double-arm time-of-flight (TOF) measurements between the electron and recoil detector electronic trigger signals. Electron-proton elastic scattering was also measured for normalization and calibration purposes. A Monte Carlo simulation model was developed to calculate the double-arm solid angle with radiative corrections, needed for the determination of the cross sections. Data have been obtained in the Q^2-range from 25 to 65 fm^{-2} for ^{3}He, and from 10 to 75 fm^{-2} for ^{4}He, as indicated by the solid black circles in Figs. 40,

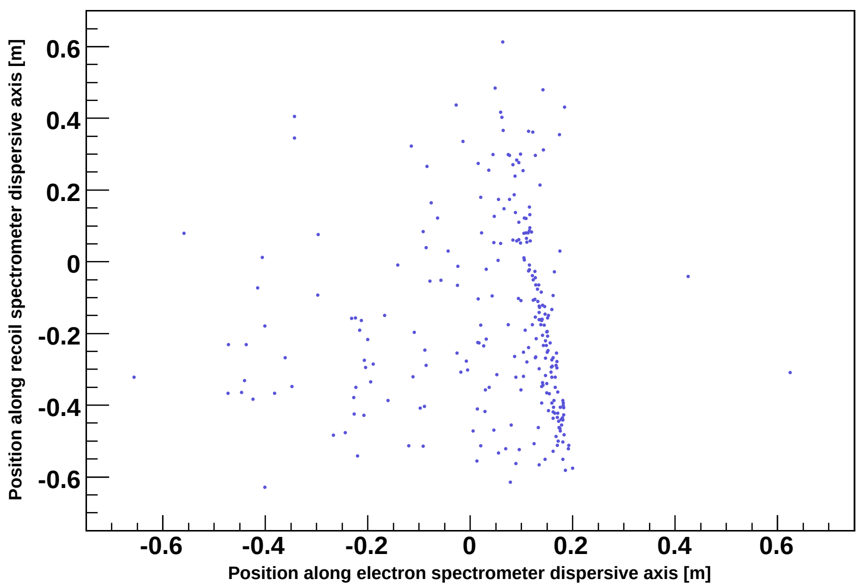

Figure 44: Raw “elastic stripe” with radiation tail (and some background) for elastic $e-{}^4$He scattering at $Q^2 = 34$ fm^{-2}. The quantity plotted in the left(bottom) axis is proportional to the momentum of the recoil(electron) spectrometer detected particle. The stripe corresponds to elastic events. The events to the left of the stripe are mainly elastic events where the incident or scattered electrons have suffered radiation and/or ionization losses in the target.

41 and 42. On-line results for elastic electron-proton are in good agreement with previous world measurements. A selected on-line analysis of helium elastic data has shown that they are consistent with previous measurements from other laboratories such as SLAC. Figures 43 and 44 show two on-line plots indicating clear identification of elastic events via the time-of-flight method and the kinematical correlation of the momenta of the scattered electrons and recoil helium nuclei. This experiment is the Ph.D. thesis topic of one graduate student from Kent State University, Mrs. Elena Khrosinkova. The data analysis is in progress and preliminary results are expected within a year. The experimental work on E04-018 was supported in part by the US Department of Energy and the National Science Foundation.

References

[1] J. Carlson and R. Schiavilla, Rev. Mod. Phys. **70**, 743 (1998).

[2] R. Gilman and F. Gross, J. Phys. **G28**, R37 (2002).

[3] C. E. Carlson, J. R. Hiller and R. J. Holt, Annu. Rev. Nucl. Part. Sci. **47**, 395 (1997).

[4] M. Garcon and J. W. Van Orden, Adv. Nucl. Phys. **26**, 293 (2001).

[5] I. Sick, Prog. Part. Nucl. Phys. **47**, 245 (2001).

[6] F. Gross, A. Staedler and M. Pena, Phys. Rev. **C69**, 034007 (2004).

[7] H. Dijk and B. L. G. Bakker, Nucl. Phys. **A494**, 438 (1989); W.-H. Ma and L. .S. Kisslinger, Nucl. Phys. **A531**, 493 (1991); and references therein.

[8] S. J. Brodsky and G. R. Farrar, Phys. Rev. Lett. **31**, 1153 (1973); V. A. Matveev, R. M. Muradyan and A. N. Tavkhelidze, Lett. Nuovo Cimento **7**, 719 (1973); S. J. Brodsky and B. T. Chertok, Phys. Rev. **D14**, 3003 (1976); B. T. Chertok, Phys. Rev. Lett. **41**, 1155 (1978).

[9] G. G. Petratos *et al.*, spokespersons, JLab Experiment E04-018.

4.10 Experiments E05-103 & E05-004

Low-Energy Deuteron EXperiments
Contributed by Ph.D. students J. Glister, B.W. Lee and G. Ron

R. Gilman, D. Higinbotham, X. Jiang, A Sarty and S. Strauch, spokespersons

Two Low-Energy Deuteron EXperiments (LEDEX) ran in Hall A during July – September, 2006 with a short extension to measure elastic Li and B which ran in February 2008: E05-004, $A(Q)$ at Low Q in *ed* Elastic Scattering and E05-103, Low Energy Deuteron Photodisintegration. The experiments have three Ph.D. students analyzing the data, J. Glister from St. Mary's and Dalhousie Universities, Canada, G. Ron from Tel Aviv University, Israel, and B.W. Lee from Seoul National University, Korea.

4.10.1 E05-103

The goal of E05-103[1] was to obtain recoil-proton polarization observables in deuteron photodisintegration over a range of angles and energies near 300 MeV. Current hadronic interaction models are in excellent agreement with deuteron photodisintegration data up to a few hundred MeV. The models are based on meson, nucleon and Δ degrees of freedom and include meson-exchange currents, final-state interactions and relativistic corrections[2]. The modern calculations include a series of technical advances over older ones, such as modeling the pion with finite velocity, nonperturbative treatment of the Δ resonance, and mutual interaction in the πNN system[3]. A striking disagreement emerges at roughly 300 MeV, where the calcuations predict that the induced recoil-proton polarization near $\theta_{cm} = 90°$ will approach 0, yet the data grow in magnitude to nearly -1 at 500 MeV. This large peak in the induced polarization has been known, but not explained, for 30 years.

The existing data set consists of measurements taken at different labs, with varying bins in energy and angle. Also, no polarization transfer data had been taken below ∼500 MeV. We proposed to obtain a systematic set of recoil-polarization observables, both transferred and induced, at lower energies, in order to identify precursors of what causes the disagreement at 500 MeV. The experiment covered an angular range of $\theta_{cm} = 20° - 120°$, generally in 10° steps, although some intermediate angles were skipped due to time constraints. A photon energy range of 270 – 360 MeV was covered at each angle using two spectrometer momentum settings, except at the two largest angles and one of the intermediate ones. All measurements were taken above pion production threshold.

Due to the relatively low energy, the older McNaughton Analyzing Power parameterization[4] was not sufficient and *ep* elastic scattering measurements were taken to obtain a new parameterization. The proton elastic form factor ratio, $\mu G_E^p/G_M^p$, was also extracted from the low energy *ep* data, demonstrating a ratio less than unity at low Q^2, shown in Fig. 45. It was found that this deviation was primarily due to G_E^p being smaller than the dipole parameterization[5].

Some preliminary polarization transfer data (P_x^c and P_z^c) and previous induced polarization data (P_y)[15]-[17] are shown in Fig. 46. The new Analyzing Power parameterization, spectrometer mispointing corrections and background subtraction of electron and target wall contamination were all considered. The Pentchev[14] spin-precession method was used to precess the protons through the magnetic field of the spectrometer. The new induced polarization data are not shown, as they need a more careful treatment of false asymmetries than is currently available. The error bars are statistical only; the systematic uncertainty analysis remains to be completed. The calculations are from [2] (solid line) along with recent, unpublished improvements from [3] (dashed line). The calculations are in general agreement with the data, although the older calculations appear to have

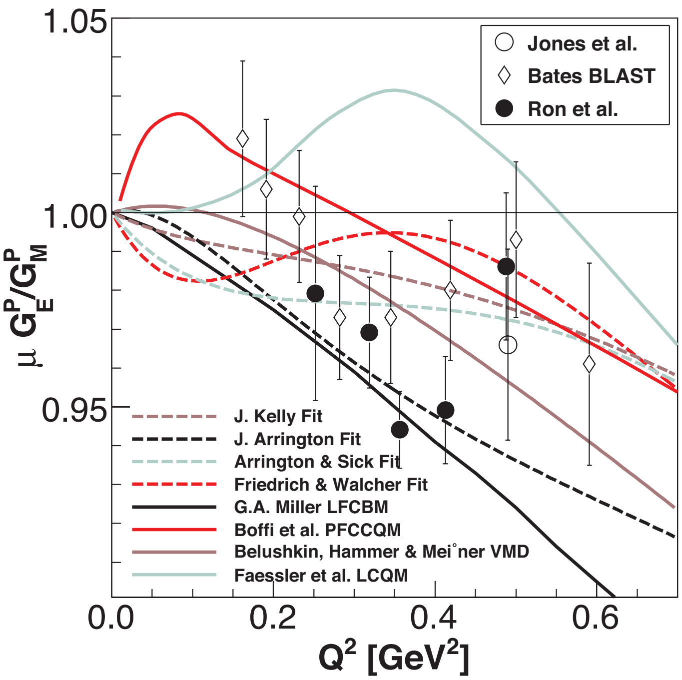

Figure 45: The proton form-factor ratio as a function of Q^2 shown with world data. The broken lines are fits[6]-[9] while the solid lines are calculations[10]-[13].

better agreement with the transferred polarization data. It remains to be determined whether the differences are consistent with the theoretical and systematic uncertainties, or whether they are indicative of something missing or poorly modelled in the calculations.

4.10.2 E05-004

The goal of E05-004[18] was to resolve a discrepancy of about 10% between two high-precision data sets, from Mainz[19] and Saclay[20], in the region $Q = \sqrt{Q^2} = 0.2 - 0.4$ GeV. The best conventional non-relativistic calculations tend to lie between the two data sets, with relativistic calculations tending to increase the prediction slightly towards the Mainz data. The best chiral perturbation theory calculations agree well with the Saclay data. It has been found that extractions of the deuteron form factors from the recent Bates tensor polarization[21] data vary by a few σ depending on whether $A(Q)$ is assumed to follow the Saclay or the Mainz data. Thus, it is important to resolve the discrepancy to determine the sign of the leading relativistic corrections at low Q, the level of convergence of chiral perturbation theory calculations, and the deuteron form factors with improved confidence.

The experimental technique was based on scattering electrons from tantalum, aluminum, carbon, hydrogen, and deuterium targets. The tantalum is used primarily for kinematics fits to determine the beam energy. The aluminum is used to subtract backgrounds in the hydrogen and deuterium data. The carbon provides a check of our ability to measure cross sections from a solid target; the carbon cross section was previously measured at NIKHEF to ~1%. Hydrogen provides a similar check of our ability to measure the cross section, with the advantage of having the same extended target geometry as the deuterium, along with a greater sensitivity to target heating. One

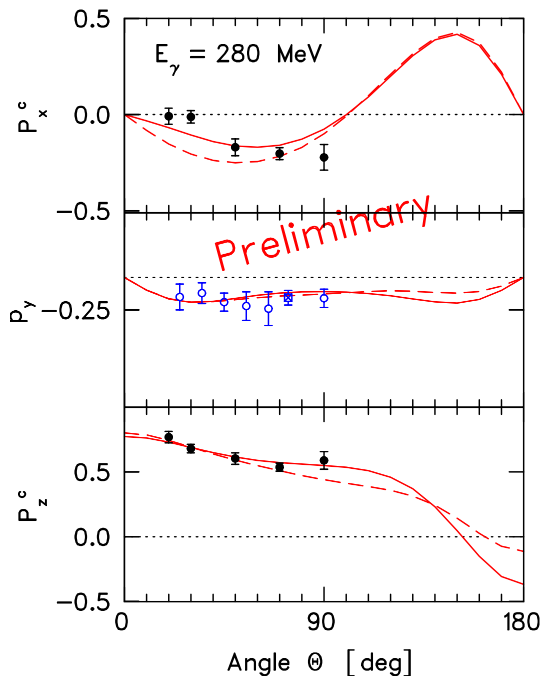

Figure 46: Angular distributions for recoil-proton polarizations in deuteron photodisintegration, for $E_\gamma = 280 \pm 10$ MeV. See text for details.

spectrometer was used as a luminosity monitor while the other spectrometer measured the angular distribution.

To better understand the solid angle, new ∼1 and 2 msr collimators were fabricated and mounted on the front of the spectrometers. To better understand the integrated beam charge for the low currents needed for these experiments, the Hall A BCM electronics were upgraded, and a new beam calorimeter was installed in the beam line. Initial comparisons among the various BCM read-outs indicate the point-to-point variations in beam current are about 0.3%. Initial studies of the absolute current calibration using the beam calorimeter as a calorimeter, versus as a Faraday cup, indicate that the absolute current calibration is better than 1%, down to a few tenths of 1 μA.

The initial analysis of the data is underway. Spectra from the 687 MeV run in late September look clean, but some spectra on solid targets at 362 MeV indicate that the beam might have been striking the aluminum target frames. At this point, no issues have arisen which would prevent us from reaching the experimental goals of 2–3% absolute cross sections and better than 1% point-to-point cross sections.

References

[1] R. Gilman, A. Sarty and S. Strauch *et al.*, spokespersons, JLab Experiment E05-004; and J. Glister *et al.*, to be published.

[2] M. Schwamb and H. Arenhövel, Mod. Phys. Lett. **A 18**, 190 (2003); preprint nucl-th/0209083; M. Schwamb and H. Arenhövel, Nucl. Phys. **A 696**, 556 (2001); preprint nucl-th/0105033; and M. Schwamb and H. Arenhövel, Nucl. Phys. **A 690**, 682 (2001); preprint nucl-th/0008034.

[3] M. Schwamb, Habilitation thesis, Johannes Gutenberg Universität, Mainz, 2006.

[4] M. McNaughton *et al.*, Nucl. Inst. Meth. in Phys. Res. **A 241**, 435 (1985).

[5] G. Ron, J. Glister, B. Lee *et al.*, Phys. Rev. Lett. **99**, 202002 (2007); arXiv:0706.0128v1.

[6] J. Friedrich and T. Walcher, Eur. Phys. J. **A 17**, 607 (2003).

[7] J. Arrington, Phys. Rev. **C 69**, 032201 (2004).

[8] J. J. Kelly, Phys. Rev. **C 70** 068202 (2004).

[9] J. Arrington and I. Sick (2006), Phys. Rev. C **76**, 035201 (2007); nucl-th/0612079.

[10] M. A. Belushkin, H. W. Hammer, and U. G. Meissner, Phys. Rev. **C 75**, 035202 (2007).

[11] G. A. Miller, Phys. Rev. **66**, 032201 (2002).

[12] S. Boffi, P. Demetriou, M. Radici and R. F. Wagenbrunn, Phys. Rev. **C 60**, 025206 (1999).

[13] A. Faessler, Th. Gutsche, V. E. Lyubovitskij and K. Pumsa-ard, Phys. Rev. **D 73**, 114021 (2006).

[14] L. Pentchev (2003), JLAB TN-03-024.

[15] F. F. Liu *et al.*, Phys. Rev. **165**, 1478 (1968).

[16] R. Kose *et al.*, Z. Phys. **220**, 305 (1969).

[17] A. A. Zybalov *et al.*, Nucl. Phys. **A 533**, 642 (1991).

[18] R. Gilman, D. Higinbotham and X. Jiang *et al.*, JLab Experiment E05-004.

[19] G.G. Simon *et al.*, Nucl. Phys. **A 364**, 285 (1981).

[20] S. Platchkov *et al.*, Nucl. Phys. **A 510**, 740 (1990).

[21] J. Calarco, private communication.

4.11 Experiment E05-110

A Sodium Iodide calorimeter for the Hall A High Resolution spectrometer

S. Choi, J.-P. Chen, and Z.-E. Meziani, spokespersons,
and
the Hall A Collaboration
Contributed by A. Camsonne

The Coulomb Sum Rule experiment

The Coulomb Sum Rule experiment E05-110 will use the HRS spectrometers for the first time in a momentum range of 0.1 to 0.5 GeV/c. From a test run we determined the resolution of the pion rejector in the HRS-L to be $3.1/\sqrt(E)$ (E in MeV) which gives 30% at 100 MeV/c to 26% at 140 MeV/c, as shown in Fig. 47. In order to reduce the systematic error generated by the low-energy electron background a higher resolution calorimeter was added to the HRS-L focal-plane detector package. It was built reusing the NaI(Tl) crystals from the Crystal Box which was used at the now completed LEGS experiment at Brookhaven.

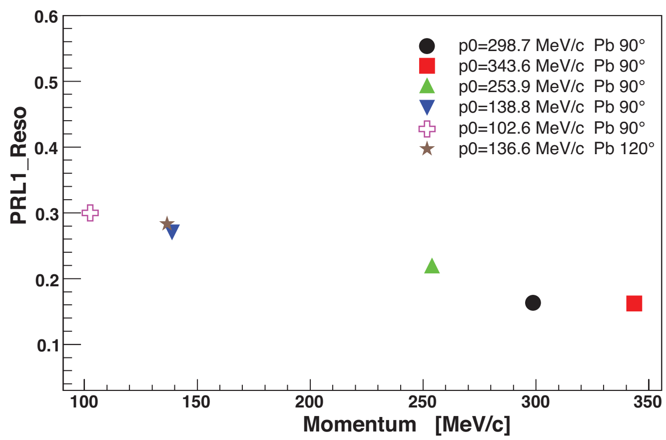

Figure 47: Energy resolution of the pion rejector in the HRS-L spectrometer for momentum settings in the 100 to 350 MeV/c range.

The Crystal box

The Crystal Box was a large acceptance detector, with a close to 4π coverage, initially built at Los Alamos[1]. It constituted of 396 NaI crystals:

- 360 crystals, 2.5 x 2.5 x 12 in^3 each, in four 90 block sides surrounding the target.
- 36 long crystals put in the corners to obtain a full hermiticity

The detector was brought from Brookhaven to Jefferson Laboratory at the end of March. Sodium Iodide doped with Thallium, NaI(Tl), is one of the best inorganic scintillator materials, producing of the order of several hundreds of photoelectrons per MeV. It is widely used when very good energy resolution is needed at lower energy. A major drawback, however, is the hygroscopy of NaI, which requires special handling, since the crystal would dissolve in ambient humidity.

The detector reconfiguration

Dry room and detector dismounting The original detector is described in the article about the Crystal Box[1]. With the help of Alexandre Lukhanin from Temple, a dry room was set up in order to have a regulated humidity of around 3% using air dryers. Setting up the dry room, dismounting the detector and unloading the crystals was done in July. In order to keep the humidity low while working on the crystals full-body air-supplied suits were worn by the workers, with the humid atmosphere from the workers drained to an exhaust line. With this kind of set-up the humidity level could be kept at a tolerable level for the crystals during the dismounting of the original detector and the assembling of the new detector.

Block polishing The RICH glove box was lent to us by INFN Sanita to process the crystals. It allowed to work on the crystals in a dry nitrogen atmosphere. We followed the polishing method from the technical note[2] with a slight modification of the polishing process. The coarse polishing was done using polishing oil which limited the scratching of the blocks and the release of NaI dust when using sandpaper. Final polishing was done using 0.3 μm Alumina. The crystals were processed in about one month from August to September. Once polished, the crystal were wrapped in millipore paper and mylar, ready for the final mounting.

Box mounting In order to fit into the spectrometer detector package, the detector was reconfigured in three individual boxes, each holding 90 crystals. The design of these boxes by Alan Gavalya and Joyce Miller can be seen in Fig. 48. It reused some elements of the original box. After processing the crystal were loaded in each individual box allowing safe and independent handling of the crystals. In order to couple crystals with the PMT keeping the box completely sealed, the company Alpha Spectra was hired to mount the glass windows making the individual interface between the PMT and the crystal using their proprietary technique to seal each box as shown in Fig. 49.

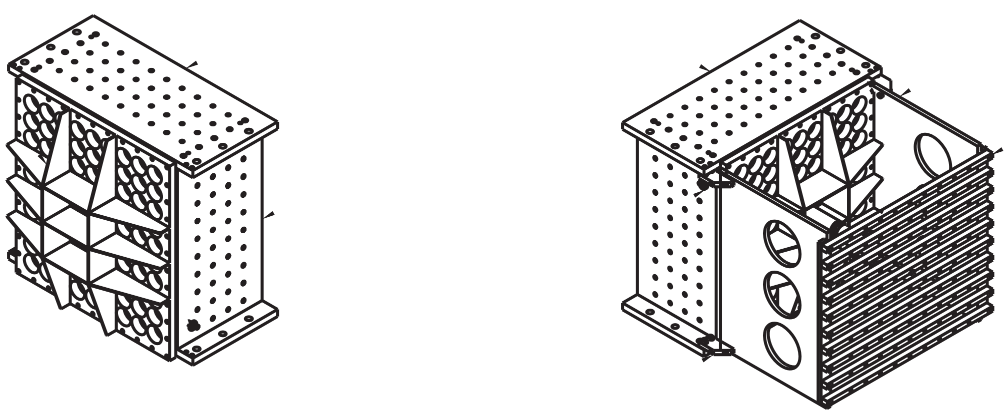

Figure 48: Schematic of one individual box holding 90 crystals.

Detector mounting

Detector frame In order to keep the detector stack unmodified a calorimeter frame was designed to mount the NaI detector inside the carbon doors of the Focal Plane Polarimeter using a hydraulic

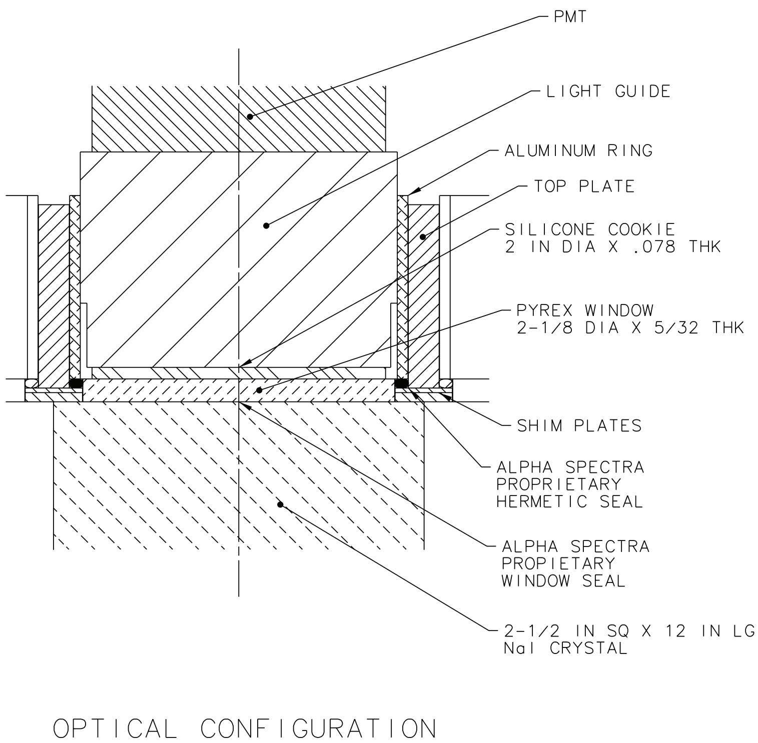

Figure 49: Schematics of the optical coupling between a PMT and a NaI(Tl) crystal.

system designed by Ed Folts. The three boxes were first assembled and cabled on the frame on the floor of the Hall and then the complete set was craned into the spectrometer.

Spectrometer lay-out The detector was first placed in the detector stack and then pushed into the FPP carbon doors to allow mounting of S2 and the Gas Čerenkov. The detector was cabled to the LEGS electronics boxes which provide a delay of 440 ns and amplification as well as a fan-out for the analog signal. The 270 PMTs were powered using a 1440 Lecroy HV crate which provided 256 channels and the remaining channels were plugged into the existing HV channel of the spectrometer crate. All the additional electronics was located on the right side of the detector stack.

Preliminary results

The Coulomb Sum Rule experiment used a wide range of spectrometer momentum settings, from 100 MeV/c up to a 4.2 GeV/c. The calibration of the detector turned out to be trickier than expected: the code that had been used previously for the shower and preshower[4], has not yielded good results yet, most likely due to bad blocks, energy leakage and the aluminum interface between the different boxes. A more limited study using a simple minimization procedure of the response from the 25 blocks centered on block 202 has provided preliminary results on the detector performance. Several runs for different electron momenta were processed to study the momentum dependence. The results are summarized in Table 5 and Fig. 52.

The resolution of around 8% obtained at low momentum is similar to the result of a test run. At these low momentum settings, the NaI(Tl) calorimeter performs three to four times better than the pion rejector, shown in Fig. 47. At higher energies (not shown in the plot) the resolution

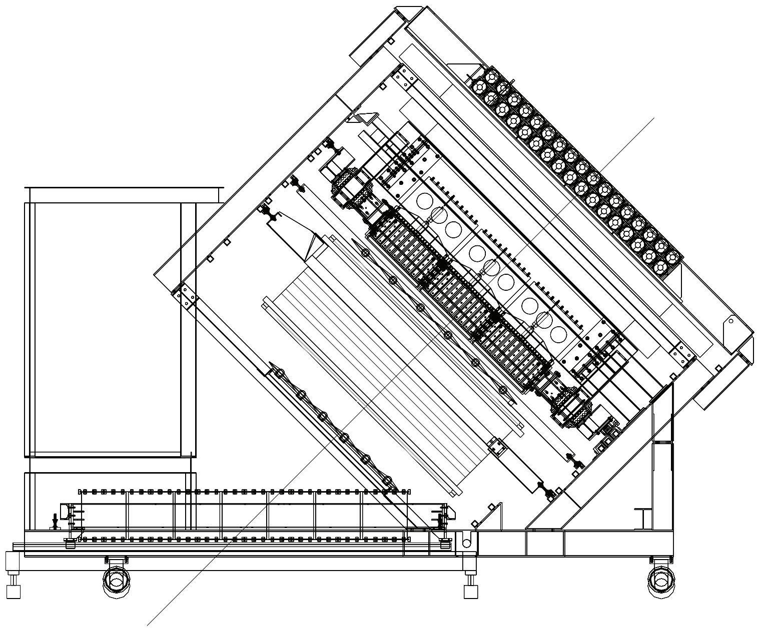

Figure 50: A schematic lay-out of the HRS-L detector stack, showing the CSR NaI(Tl) calorimeter mounted in its final position.

is worsening a bit, maybe because of leakage. In addition, the resolution can change from one kinematic to the other depending on the background. A more detailed study including all detectors blocks as well as the pion rejector is expected to yield a more reliable result but this will have to wait for the final analysis: the different contributions to the resolution still need to be understood since the resolution does not follow the usual $E^{-1/4}$ dependence, with E the incident particle energy.

Run 4094 which was at a momentum setting of 420 MeV/c with a beam energy of 739 MeV, yielded the best resolution, see Fig. 53. For the lowest momentum of 121 MeV/c at a beam energy of 729 MeV the resolution of the pion rejector is three times that of the sodium iodide, see Fig. 54. The contribution of the low-energy tail represents about 2.7% of the events in the peak. We expect the background to be worse at the lowest energies 400 MeV and 528 MeV data. The systematic error for the background quoted in the proposal was 0.5%[3].

Conclusion

The Crystal Box detector was moved from Brookhaven, refurbished and reconfigured to be fitted in the left High Resolution Spectrometer of Hall A in a time span of 6 months. It was the first time such a large scale of NaI was processed at Jefferson Laboratory. Thanks to the huge effort from people of Temple University, Jefferson Laboratory and the CSR collaboration, the detector could be finished in time for the start of the experiment. The crystals were re-polished and show a performance similar to the one quoted in the original paper. The resolution obtained will be essential for an extensive study of the low-energy background of the Coulomb Sum Rule experiment.

References

[1] S. L. Wilson *et al.*, Nucl. Instrum. Meth. A **264**, 263 (1988).

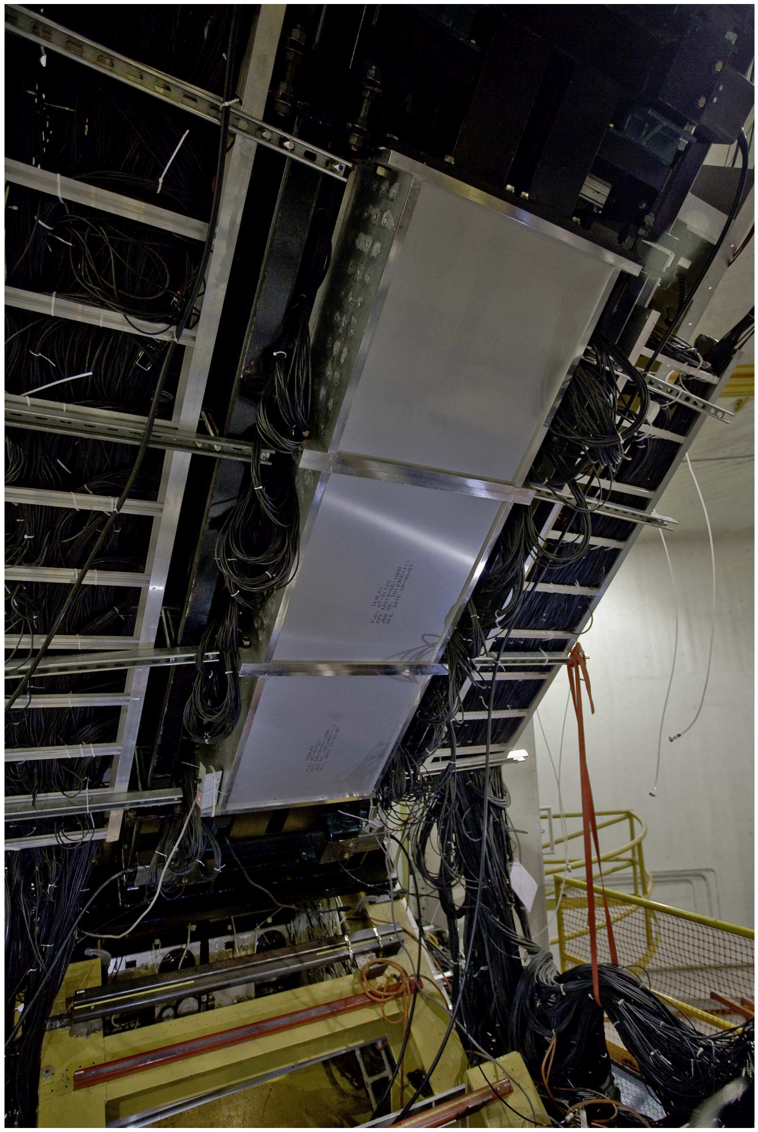

Figure 51: The CSR NaI(Tl) calorimeter mounted inside the FPP doors.

[2] *Surface polishing process for NaI Crystals*, SLAC technical notes : SLAC TN-82-2

[3] S. Choi, J.-P. Chen, and Z.-E. Meziani, spokespersons, JLab experiment E05-110, *Precision Measurement of Longitudinal and Transverse Response Functions of Quasi-Elastic Electron Scattering in the Momentum Transfer Range 0.55 GeV/c < q < 0.9 GeV/c*

[4] Hai-Jaing Lu, *Shower Calibration & Efficiency for E97-110*

Table 5: Resolution of the detector after calibration done on 25 blocks and a fit of the sum of those 25 blocks.

Run	Momentum	Resolution	Error
4421	3092.4	9.6	+-0.033
4311	2228.9	6.41	+-0.012
4584	0.459	4.52	+-0.011
4590	0.428	4.88	+-0.037
4593	0.399	5.09	+-0.05
4603	0.372	5.10	+-0.038
4609	0.347	5.44	+-0.037
4614	0.323	5.58	+-0.032
4621	0.301	5.76	+-0.035
4630	0.281	5.84	+-0.04
4100	0.100	8.4	+-0.023
3673	0.110.9	8.1	+-0.055

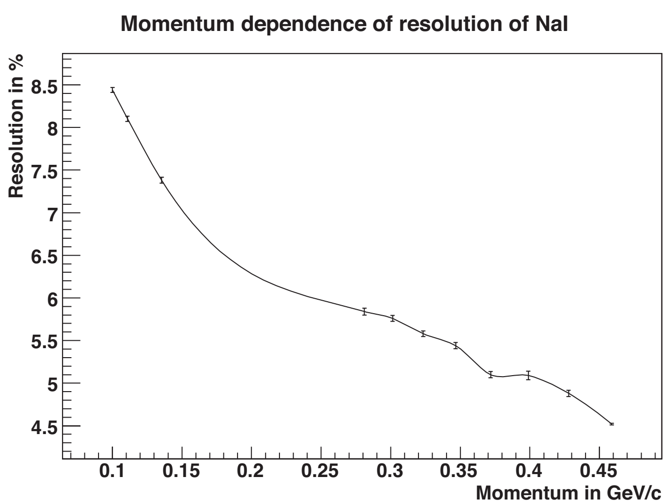

Figure 52: Preliminary results for the calorimeter resolution as a function of momentum.

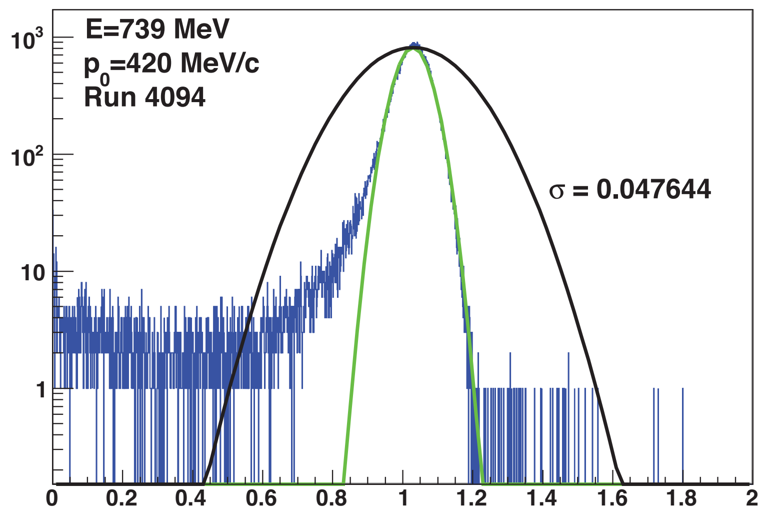

Figure 53: Run 4094 at a beam energy of 739 MeV and a 420 MeV/c momentum setting. In black the resolution expected from the pion rejector is shown.

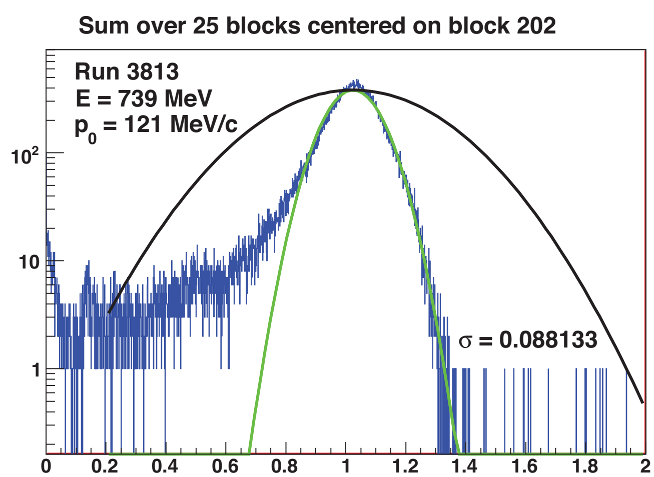

Figure 54: Sum over 25 blocks at 121 MeV/c electron momentum at a beam energy of 739 MeV. In black the resolution expected from the pion rejector is shown.

4.12 Experiment E06-002

PREX Tests

Contributed by R. Michaels

The Lead Radius Experiment (PREX), experiment E06-002, uses the parity-violating weak neutral interaction to probe the neutron distribution in ^{208}Pb, thus measuring the RMS neutron radius to 1% accuracy, which has an important impact on nuclear theory, with widespread applications including neutron star structure. The experiment will be performed by the HAPPEX collaboration. Several activities have occurred in 2007:

- New 18-bit integrating ADCs, designed at JLab by Fernando Barbosa and Ed Jastrzembski, have been tested. These replace our obsolete 16-bit ADCs from the HAPPEX-I era and provide improvements in pedestal sampling and bit resolution.
- A lead/diamond target was used during experiment E06-007. It is the same basic design as for PREX, though there were some differences, e.g. thinner lead. The target ran well at 55 μA (PREX is proposed for 50 μA) but melted somewhere between 55 and 85 μA. A final design of our lead target ladder is being built for tests in early 2008. The experiment E06-007 will also get a few days of beam time with this target. The target will have improved cooling and the thicker foils needed by PREX.
- A new room-temperature septum magnet is being designed by Paul Brindza and the JLab engineering staff. It will allow us to run at 6° scattering angle at 850 MeV. Since the energy is low, a simple room-temperature design suffices. The magnet will be built at JLab over the next year.
- The HAPPEX collaboration is contributing manpower to the Compton polarimeter upgrade.
- New quartz-tungsten detectors are being made by the University of Massachusetts and Smith College. They will be tested in the Møller apparatus in early 2008. The scattered electrons from the Møller target are used as an energy-analyzed test beam.
- The linearity of our PMTs have been studied, leading to a better understanding of how to adjust the input light level and high voltages to achieve good linearity.
- The electronics for the cavity monitor BPMs and BCMs near the target are being upgraded by John Musson. Some errors in the firmware have been corrected and they will have better channel isolation. Also they will have sensitivity to much lower currents (50 nA).

In early 2008 we will have facility development time. A number of tests are planned. The goals are as follows.

- Tests of the PREX target at full current.
- Check the PREX detector in the Møller setup as mentioned above.
- Study a new integration method for the Compton polarimeter. Integration of the photon signal will eliminate the systematic errors from thresholds and deadtime. A new photon detector made from a GSO crystal is being built by Carnegie Mellon; this crystal has a large light yield and is very fast. A custom-made flash ADC from Struck SISGmbH will digitally integrate the data with zero deadtime using a simple on-board algorithm to reject background.

- Studies of noise and linearity with the luminosity monitors.
- Check the interaction of Hall A and Hall C beams, i.e. the impact that one hall has on the "parity quality" of another hall's beam.
- Test a new low-current (50 nA) mode of the cavity BPM and current monitors.

4.13 Experiment E06-007

Impulse Approximation Limitations to the $(e, e'p)$ Reaction on ^{208}Pb, identifying Correlations and Relativistic Effects in the Nuclear Medium
Contributed by K. Aniol

K. Aniol, A. Saha, J. Udias and G. Urciuoli, spokespersons,
and
the Hall A Collaboration

Physics motivation

Experiment E06-007 ran from March 3 until March 26, 2007, to study the $^{208}\text{Pb}(e, e'p)^{207}\text{Tl}$ and $^{209}\text{Bi}(e, e'p)^{208}\text{Pb}$ reactions at kinematical conditions $x_B = 1$, $q = 1$ GeV/c, $\omega = 0.433$ GeV and $\text{Q}^2 = 0.81$ to 1.97 GeV^2.

The question we wish to address in this measurement is " How well do we understand nuclear structure? ". The nucleus is a dense system of fermions whose motion to first order can be treated as independent particles moving in a mean field. The ^{208}Pb nucleus is the textbook example of a nucleus amenable to such an approach. This nucleus has been studied in the past at NIKHEF-K and Saclay by the $(e, e'p)$ reaction[1]. Spectroscopic factors were obtained from missing momenta less than 300 MeV/c and analyzed in the Impulse Approximation both with a non-relativistic and relativistic treatment[2]. Deviations from independent-particle motion for orbits near the Fermi energy are clearly present and are attributed to various correlations. Measurements[3] on this nucleus at high missing momentum, $p_m > 300$ MeV/c, attribute the excess strength in the cross section as determined by a non-relativistic analysis to long-range correlations. However, a relativistic analysis of the bound and free nucleon states shows no need to invoke long-range correlations [4]. In the relativistic treatment of the $(e, e'p)$ reaction the spinor distortions of the lower component of the nucleon wave function account for the cross section at high missing momentum in the case of the measurement of [3]. In that experiment the measurement was done far from quasi-elastic conditions due to limitations of beam energy. At Jefferson Lab we can measure $(e, e'p)$ on ^{208}Pb at $x_B = 1$, for which both non-relativistic and relativistic treatments predict the same high missing-momentum cross sections when the spectroscopic factors are properly normalized. Excess strength at high p_m can then be attributed to long-range correlations.

The asymmetry A_{TL}, accessible in $(e, e'p)$ reactions, is a relatively new and as yet little exploited observable for low-lying excited states. It was not possible to measure this quantity at previous laboratories. Our measurement is the first one to measure the cross section at negative p_m (angles forward of the three momentum transfer). For missing momenta below 300 MeV/c the mean-field potential is primarily responsible for the nucleon's state and other mechanisms are negligible. A_{TL} is sensitive to the theoretical approach (non-relativistic *vs.* relativistic) employed and is of prime interest in this measurement.

It has been claimed[5, 6], from the comparison of $(e, e'p)$ data in ^{12}C at different momentum transfers, that the spectroscopic factors as measured in $(e, e'p)$ reactions at exclusive conditions display a dependence on the momentum transfer. This dependence would saturate at a Q^2-value of around 1 GeV^2[6]. Subsequent studies on ^{16}O including data from 0.2 to 0.8 GeV^2 did not find evidence for such Q^2-dependence (see for instance ref. [7]). This experiment at Hall A can settle this issue since we can efficiently measure the cross section for low p_m at Q^2 between 0.81 to 1.97 GeV^2.

Objectives

(I) Long-Range Correlations search
a) Measure spectroscopic factors for states near the Fermi level. Spectroscopic factors depend on short-range correlations (SRC) and long-range correlations (LRC).
b) Measure cross sections for these low-lying states to 500 MeV/c in p_m. Excess strength here is theoretically identified as due to LRC.
c) Search for a Q^2-dependence of spectroscopic factors.
(II) Identify dynamical relativistic effects in nuclear structure.
Measure the cross-section asymmetry A_{TL} around the three momentum transfer. Relativistic mean-field theory predicts an A_{TL} dependence for $p_m < 300$ MeV/c due to a dynamical enhancement of the lower component of the nucleon wave function. Calculations which do not include the enhancement of the lower component predict a substantially different A_{TL} behavior.

Run time experiences

Optics Studies
The low-lying states of ^{207}Tl, which are the principal focus of this experiment, are the ground state ($3s_{1/2}$), 0.351 MeV ($2d_{3/2}$), 1.348 MeV ($1h_{11/2}$), 1.683 MeV ($2d_{5/2}$), and 3.470 MeV ($1g_{7/2}$). These states are close enough in energy that the best resolution possible with the Hall A high-resolution spectrometers is essential. GEANT simulations predict that if a FWHM for the missing-energy spectrum of 1 MeV is achieved then given a reasonable number of counts in these states a peak-fitting procedure can be exploited to separate the states. This required receiving a beam spot from the accelerator with a vertical size less than 100 μm and $dE/E < 2.5 \times 10^{-5}$. In addition detailed optics studies of the HRS-R and HRS-L were undertaken:
with internal and external sieve slits in/out, for delta scans from -4% to 4% and with the raster on/off at

- 2 pass, E = 1.343 GeV, for HRS-R and HRS-L
- 4 pass, E = 2.649 GeV, for HRS-L

The simulations of the elastic scattering showed that the best resolution to be expected for the elastic scattering would be between 400 keV to 500 keV at E = 1.343 GeV depending on the spectrometer. Work on the optics databases is still in progress. An example of the improvement in resolution is shown in the comparison of Fig. 55, the on-line database, and Fig. 56, the current database. An example of the angle reconstruction is shown in Fig. 57 for HRS-L using the sieve slit. The other major factor in energy resolution is the raster correction. The heavy metal targets required a large raster pattern, 4 x 4 mm^2. A significant effort in the collaboration is being expended to determine the best way to correct for the raster.

Target performance and Data collected
The heavy metal targets (0.2 mm thick) were sandwiched between thin (0.15 mm) sheets of CVD diamond and held in a ladder frame which was actively cooled by flowing 20 K helium gas through the frame. This experiment was the first to subject heavy metal targets to extended periods of bombardment using large beam currents. Our first lead target failed after a few days running at 80 μA. There is a suspicion that this target suffered a cracked diamond foil on assembly, but this was not evident until after the rupture occurred. Our second lead target performed perfectly for 2 weeks with 50 μA beam. Our bismuth target was subjected to 85 μA but as a precaution we also

ran this target at 50 μA. Table 6 shows the number of Coulombs desired and the number actually obtained.

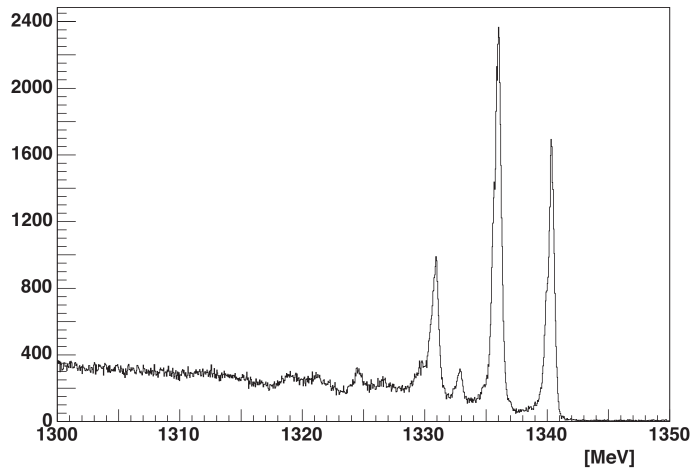

Figure 55: Electron scattering on ^{12}C measured in the HRS-R using the on-line optics database.

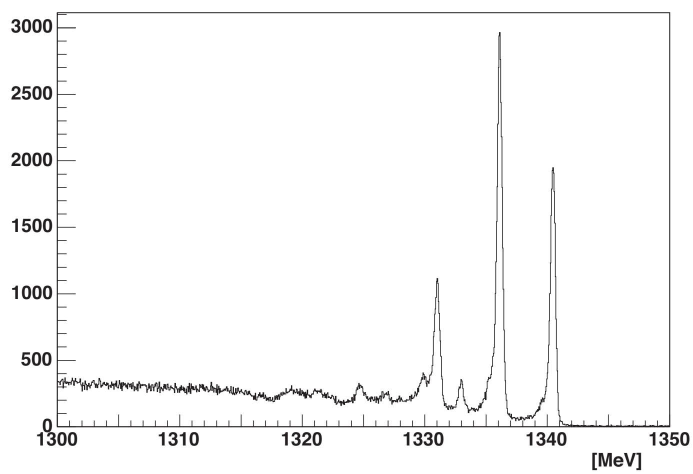

Figure 56: Electron scattering on ^{12}C measured in the HRS-R using the improved optics database.

Preliminary spectra

In Fig. 58 we show the overlay of the spectra of ^{208}Pb$(e, e'p)^{207}$Tl for $p_m = 0$, 100 and 200 MeV/c. The spectra follow the shapes expected from the theoretical predictions. Eventually we hope to perform peak fitting to try to extract the individual Tl states. The challenge with the heavy metal targets lies in compensating for the large raster pattern's effect on the resolution. As we showed in the original proposal even the summed spectra for the Tl states will reveal dynamical relativistic effects in the asymmetry A_{TL} and the presence or absence of long-range correlations at large missing momenta. Besides the shifting overall spectral shapes we also see evidence for structure in the Tl

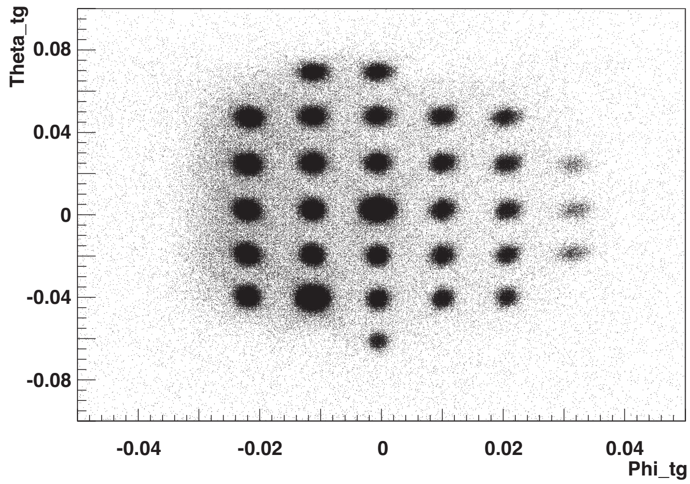

Figure 57: Electron scattering on ^{12}C measured in the HRS-L using the improved optics database seen through the sieve slit.

spectra as compared to the GEANT simulations. For example, in Fig. 59 there is a shoulder on the low E_m side of the peak around 5 MeV, which is predicted by the simulation seen in Fig. 60.

The simulations give a very good shape for E_m in the case of $^{12}C(e, e'p)^{11}B$, where it is assumed that the raster correction is perfectly made. In Fig. 61 we show the spectral decomposition for the carbon target, unrastered and with a small angular acceptance using the nominal spectrometer resolutions. The shape predicted by GEANT, with an 850 keV resolution in E_m can be used unaltered to decompose the spectra.

References

[1] E. Quint, *Limitations of the mean-field description for nuclei in the Pb-region, observed with the $(e, e'p)$ reaction*, Ph.D. thesis, Universiteit van Amsterdam, 1988, unpublished, NIKHEF-K Nr. 1313.

[2] J. M. Udias *et al.*, Phys. Rev. C **48**, 2731 (1993).

[3] I. Bobeldijk *et al.*, Phys. Rev. Lett. **73**, 2684 (1994).

[4] J. M. Udias *et al.*, Phys. Rev. C **51** 3246 (1996).

[5] L. Lapikas *et al.*, Phys. Rev. C **61** 064325 (2001).

[6] L. Frank *et al.*, Phys. Lett. B **503** 73 (2001).

[7] J. M. Udias *et al.*, Phys. Rev. C **64** 024614 (2001).

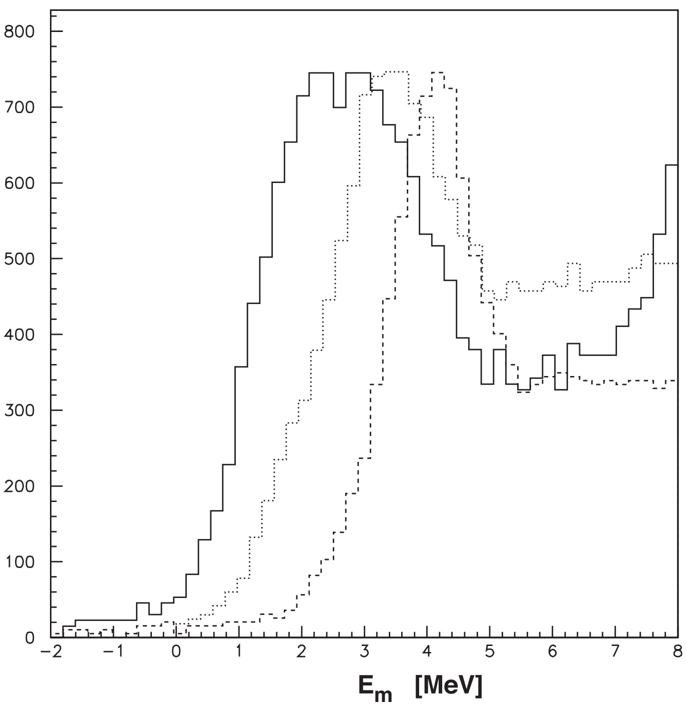

Figure 58: Overlay of E_m spectra for ^{208}Pb$(e, e'p)^{207}$Tl for $p_m = 0$, 100 and 200 MeV/c. The shape of the spectra follows that predicted by the theoretical expectations.

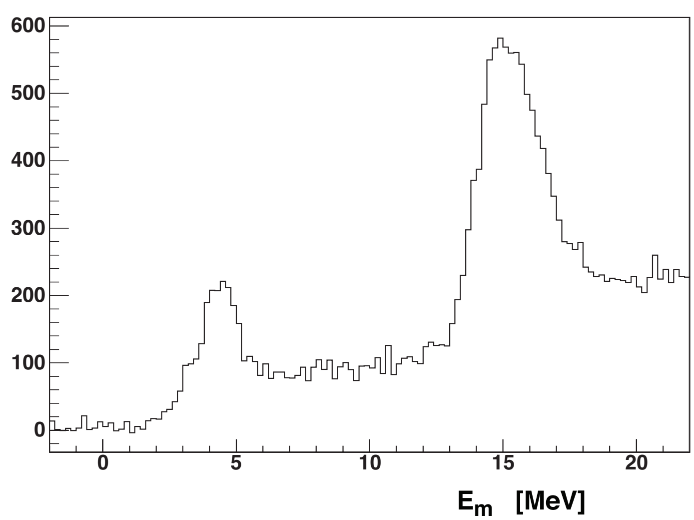

Figure 59: ^{208}Pb$(e, e'p)^{207}$Bi at $p_m = 300$ MeV/c for an electron beam energy of 2.649 GeV. The beam is rastered and full acceptances for the spectrometers were used. There is a shoulder on the low E_m side of the peak at about 5 MeV which is predicted by the simulation.

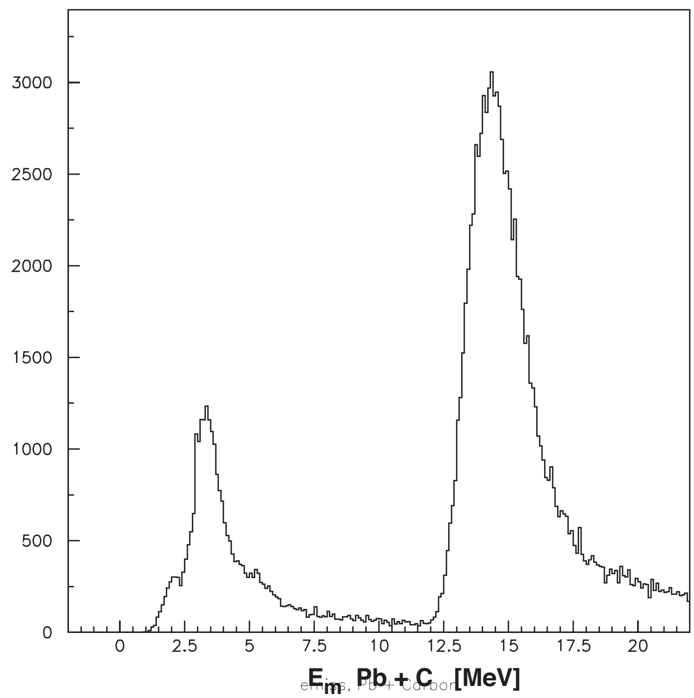

Figure 60: Simulation of $^{208}\text{Pb}(e, e'p)^{207}\text{Tl}$ at $p_m = 300$ MeV/c for an electron beam energy of 2.649 GeV. The GEANT simulation assumes the nominal spectrometer resolutions, no excited states in Tl above 3.5 MeV and only the ^{11}B ground state excited from the diamond foils.

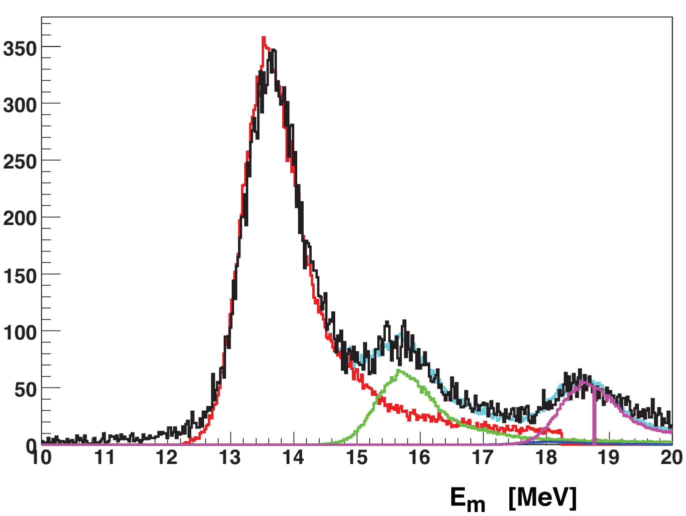

Figure 61: $^{12}\text{C}(e, e'p)^{11}\text{B}$ at $p_m = 100$ MeV/c for an electron beam energy of 2.649 GeV. The beam is unrastered and small acceptances for the spectrometers were used. The curves are shapes from the GEANT simulation assuming the nominal spectrometer resolutions. The predicted and measure resolution in E_m is 850 keV.

Table 6: Coulombs collected and goal for the March 2007 run. On/Off refers to the raster condition for the carbon target. p_m is in MeV/c and Q^2 is in GeV^2

kin	p_m	Q^2	Pb goal	Pb collected	C goal	C collected	Bi goal	Bi collected
01	0	0.81	0.70	0.66	0.1	0.12		
02	+100	0.81	2.2	2.0	0.1	0.12	0.36	0.386
03	-100	0.81	1.8	1.87	0.1	0.13	0.36	0.347
04	+200	0.81	2.16	2.26+1.0	0.36	0.563	8.6	2.8
05	-200	0.81	1.3	1.5	0.1	0.11	0.72	0.87
06	+300	0.81	4.3	4.40	0.1	0.11	0.72	0.75
07	-300	0.81	3.2	3.27	0.14	0.082(off),0.13(on)	0.72	0.35
08	+400	0.81	7.2	2.72	0.29	0.36		
09	-400	0.81	10.8	0.8				
10	+500	0.81	8.6	2.4	0.29	0.34		
11	-500	0.81	8.6	0.8				
12	0	1.40	1.8	1.14	0.14	0.105		
13	0	1.97	6.8	1.29	0.14	0.2		

5 Hall A Collaboration Member List

Armando Acha	*Florida International University*
Zafar Ahmed	*Syracuse University*
Kalyan Allada	*University of Kentucky*
Bryon Anderson	*Kent State University*
Konrad A. Aniol	*California State University*
John Annand	*University of Glasgow*
David S. Armstrong	*College of William and Mary*
John Arrington	*Argonne National Laboratory*
Todd Averett	*College of William and Mary*
Elizabeth Beise	*University of Maryland*
Hachemi Benaoum	*Syracuse University*
Fatiha Benmokhtar	*University of Maryland*
Jacques Berthot	*Laboratoire de Physique Corpusculaire, Clermont-Ferrand*
Pierre Bertin	*Laboratoire de Physique Corpusculaire, Clermont-Ferrand*
Bill Bertozzi	*Massachusetts Institute of Technology*
Louis Bimbot	*Institut de Physique Nucléaire, Orsay*
Werner Boeglin	*Florida International University*
Alexander Borissov	*University of Glasgow*
Ed Brash	*Christopher Newport University*
Vincent Breton	*Laboratoire de Physique Corpusculaire, Clermont-Ferrand*
Herbert Breuer	*University of Maryland*
Nathanial Bubis	*Tel Aviv University*
Etienne Burtin	*DAPNIA/SPhN, CEA, Saclay*
John Calarco	*University of New Hampshire*
Alexandre Camsonne	*Jefferson Laboratory*
Larry Cardman	*Jefferson Laboratory*
Gordon D. Cates	*University of Virginia*
Christian Cavata	*DAPNIA/SPhN, CEA, Saclay*
George Chang	*University of Maryland*
Nicholas Chant	*University of Maryland*
Jian-Ping Chen	*Jefferson Laboratory*
Khem Chirapatpimol	*University of Virginia*
Seonho Choi	*Seoul National University, Korea*
Eugene Chudakov	*Jefferson Laboratory*
Evaristo Cisbani	*INFN/Sezione Sanità*
Luminita Coman	*Florida International University*
Marius Coman	*Florida International University*
Juan Carlos Cornejo	*Universidad Complutense, Madrid*
Brandon Craver	*University of Virginia*
Benjamin Crowe	*North Carolina Central University*
Francesco Cusanno	*INFN/Sezione Sanità*
Dan Dale	*University of Kentucky*
Areg Danagoulian	*Los Alamos National Laboratory*
Piotr Decowski	*Smith College*
Raffaele De Leo	*INFN/Sezione Bari*

Alexandre Deur	*Jefferson Laboratory*
Nicole d'Hose	*DAPNIA/SPhN, CEA, Saclay*
Rachele di Salvo	*INFN/Sezione Roma2*
Pibero Djawotho	*College of William and Mary*
Frank Dohrmann	*Argonne National Laboratory*
Jean-Eric Ducret	*DAPNIA/SPhN, CEA, Saclay*
Chiranjib Dutta	*University of Kentucky*
Dipangkar Dutta	*Duke University/TUNL*
Kim Egiyan	*Yerevan Physics Institute* (deceased)
Martin B. Epstein	*California State University*
Catherine Ferdi	*Laboratoire de Physique Corpusculaire, Clermont-Ferrand*
Robert Feuerbach	*Johns Hopkins University*
Mike Finn	*College of William and Mary*
Kevin Fissum	*University of Lund*
Hélène Fonvieille	*Laboratoire de Physique Corpusculaire, Clermont-Ferrand*
Luis Mario Fraile	*Universidad Complutense, Madrid*
Gregg Franklin	*Carnegie Mellon University*
Bernard Frois	*DAPNIA/SPhN, CEA, Saclay*
Salvatore Frullani	*INFN/Sezione Sanità*
Haiyan Gao	*Duke University*
Franco Garibaldi	*INFN/Sezione Sanità*
David Gaskell	*Jefferson Laboratory*
Ashot Gasparian	*Hampton University*
Gagik Gavalian	*Old Dominion University*
Olivier Gayou	*Allegheny General Hospital, Pittsburgh*
Shalev Gilad	*Massachusetts Institute of Technology*
Ron Gilman	*Rutgers, The State University of New Jersey*
Alexander Glamazdin	*Kharkov Institute of Physics and Technology*
Charles Glashausser	*Rutgers, The State University of New Jersey*
Jackie Glister	*Saint Mary's University*
Javier Gomez	*Jefferson Laboratory*
Viktor Gorbenko	*Kharkov Institute of Physics and Technology*
Tim Gorringe	*University of Kentucky*
Jacqueline Glister	*Saint Mary's University*
Keith Griffioen	*College of William and Mary*
Brian Hahn	*College of William and Mary*
David Hamilton	*University of Glasgow*
Ole Hansen	*Jefferson Laboratory*
David Hayes	*Old Dominion University*
Mitra Hashemi Shabestari	*University of Virginia*
Joaquin Lopez Herraiz	*Universidad Complutense, Madrid*
Bill Hersman	*University of New Hampshire*
Doug Higinbotham	*Jefferson Laboratory*
Wendy Hinton	*Norfolk State University*
Richard Holmes	*Syracuse University*
Harry Holmgren	*University of Maryland*
Tim Holmstrom	*Randolph Macon College*
Maurik Holtrop	*University of New Hampshire*

Tanja Horn	*Jefferson Laboratory*
Edik Hovhannisyan	*Yerevan Physics Institute*
Calvin Howell	*Duke University*
Jin Huang	*Massachusetts Institute of Technology*
Garth Huber	*University of Regina*
Charles Hyde	*Old Dominion University*
Hassan Ibrahim	*Old Dominion University*
Ru Igarashi	*University of Saskatchewan*
Mauro Iodice	*INFN/Sezione Sanità*
Riccardo Iommi	*INFN/Sezione Sanità*
Dave Ireland	*University of Glasgow*
Kees de Jager	*Jefferson Laboratory*
Stephanie Jaminion	*Laboratoire de Physique Corpusculaire, Clermont-Ferrand*
Yi Jiang	*University of Science and Technology of China (USTC)*
Xiaodong Jiang	*Rutgers, The State University of New Jersey*
Sudirukkuge Tharanga Jinasundera	*University of Virginia*
Mark K. Jones	*Jefferson Laboratory*
Joe Katich	*College of William and Mary*
Seigo Kato	*Yamagata University*
Mina Katramatou	*Kent State University*
Lisa Kaufman	*University of Maryland*
James Kellie	*University of Glasgow*
James Kelly	*University of Maryland* (deceased)
Sophie Kerhoas	*DAPNIA/SPhN, CEA, Saclay*
Armen Ketikyan	*Yerevan Physics Institute*
Elena Khrosinkova	*Kent State University*
Kouichi Kino	*Tohoku University*
Norm Kolb	*University of Saskatchewan*
Ameya Kolarkar	*University of Kentucky*
Wolfgang Korsch	*University of Kentucky*
Serge Kox	*Laboratoire de Physique Subatomique et de Cosmologie, Grenoble*
Alexander Kozlov	*University of Regina*
Kevin Kramer	*Duke University*
Laird Kramer	*Florida International University*
Elena Kuchina	*Rutgers, The State University of New Jersey*
Krishna S. Kumar	*University of Massachusetts*
Gerfried Kumbartzki	*Rutgers, The State University of New Jersey*
Geraud Lavessiere	*Laboratoire de Physique Corpusculaire, Clermont-Ferrand*
Byungwuek Lee	*Seoul National University*
John LeRose	*Jefferson Laboratory*
Mark Leuschner	*University of New Hampshire*
David Lhuillier	*DAPNIA/SPhN, CEA, Saclay*
Richard Lindgren	*University of Virginia*
Ken Livingston	*University of Glasgow*
Nilanga Liyanage	*University of Virginia*
George Lolos	*University of Regina*
Robert Lourie	*Renaissance Technology*
Hai-jiang Lu	*University of Science and Technology of China (USTC)*

Richard Madey	*Kent State University*
Kazushige Maeda	*Tohoku University*
Vahe Mamyan	*Yerevan Physics Institute*
Mark Manley	*Kent State University*
Demetrius Margaziotis	*California State University*
Pete Markowitz	*Florida International University*
Jacques Marroncle	*DAPNIA/SPhN, CEA, Saclay*
Cristina Martinez-Perez	*Universidad Complutense, Madrid*
Jacques Martino	*SUBATECH, IN2P3, Nantes*
Samvel Mayilyan	*Yerevan Physics Institute*
Malek Mazouz	*Faculté des Sciences de Monastir, Tunisia*
Kathy McCormick	*Pacific Northwest National Laboratory*
Dustin McNulty	*University of Massachusetts, Amherst*
David Meekins	*Jefferson Laboratory*
Luis Mercado	*University of Massachusetts, Amherst*
Zein-Eddine Meziani	*Temple University*
Robert Michaels	*Jefferson Laboratory*
Bernard Michel	*Laboratoire de Physique Corpusculaire, Clermont-Ferrand*
Wilson Miller	*University of Virginia*
Joseph Mitchell	*Renaissance Technology*
Bryan Moffit	*Massachusetts Institute of Technology*
Peter Monaghan	*Massachusetts Institute of Technology*
Jean Mougey	*Laboratoire de Physique Subatomique et de Cosmologie, Grenoble*
Pierre Moussiegt	*Laboratoire de Physique Subatomique et de Cosmologie, Grenoble*
Carlos Muñoz Camacho	*Laboratoire de Physique Corpusculaire, Clermont-Ferrand*
Sirish Nanda	*Jefferson Laboratory*
Alan Nathan	*University of Illinois at Urbana-Champaign*
Vladimir Nelyubin	*University of Virginia*
Damien Neyret	*DAPNIA/SPhN, CEA, Saclay*
Dima Nikolenko	*Budker Institute of Nuclear Physics*
Blaine Norum	*University of Virginia*
Yoomin Oh	*Seoul National University, Korea*
Michael Olson	*St. Norbert College*
Mike Paolone	*University of South Carolina*
Zisis Papandreou	*University of Regina*
Diana Parno	*Carnegie Mellon University*
Kent Paschke	*University of Virginia*
Jen-Chieh Peng	*University of Illinois at Urbana-Champaign*
Lubomir Pentchev	*College of William and Mary*
Charles Perdrisat	*College of William and Mary*
Gerassimos G. Petratos	*Kent State University*
Artush Petrosyan	*Yerevan Physics Institute*
Eli Piasetzky	*Tel Aviv University*
Stephane Platchkov	*DAPNIA/SPhN, CEA, Saclay*
Roman Pomatsalyuk	*Kharkov Institute of Physics and Technology*
Ishay Pomerantz	*Tel Aviv University*
Luis Prieto	*Universidad Complutense, Madrid*
Dan Protopopescu	*University of Glasgow*

Andrew Pucket	*Massachusetts Institute of Technology*
Vina Punjabi	*Norfolk State University*
Thierry Pussieux	*DAPNIA/SPhN, CEA, Saclay*
Issam Qattan	*Indiana University*
Xin Qian	*Duke University*
Yi Qiang	*Massachusetts Institute of Technology*
Brian Quinn	*Carnegie Mellon University*
Igor Rachek	*Budker Institute of Nuclear Physics*
Abdurahim Rakhman	*Syracuse University*
Cesar Fernandez Raminez	*Universidad Complutense, Madrid*
Ronald Ransome	*Rutgers, The State University of New Jersey*
Brian Raue	*Florida International University*
Jörg Reinhold	*Florida International University*
Bodo Reitz	*Allegheny General Hospital, Pittsburgh*
Seamus Riordan	*Carnegie Mellon University*
Yves Roblin	*Jefferson Laboratory*
Javier Rodriguez Vignote	*Laboratoire de Physique Subatomique et de Cosmologie, Grenoble*
Mike Roedelbronn	*University of Illinois at Urbana-Champaign*
Guy Ron	*Tel Aviv University*
Oscar Rondon	*University of Virginia*
Guenther Rosner	*University of Glasgow*
Marat Rvachev	*Bank of America, New York*
Franck Sabatié	*DAPNIA/SPhN, CEA, Saclay*
Arun Saha	*Jefferson Laboratory*
Teijiro Saito	*Tohoku University*
Adam J. Sarty	*Saint Mary's University*
Brad Sawatsky	*Temple University*
Ralph Segel	*Northwestern University*
Andrei Semenov	*Kent State University*
Albert Shahinyan	*Yerevan Physics Institute*
Ran Sheyor	*Tel Aviv University*
Simon Sirca	*University of Ljubljana*
Karl Slifer	*University of Virginia*
Timothy Smith	*University of New Hampshire*
Patricia Solvignon	*Argonne National Laboratory*
Pavel Sorokin	*Kharkov State University*
Paul Souder	*Syracuse University*
Nikos Sparveris	*Massachusetts Institute of Technology*
Steffen Strauch	*University of South Carolina*
Ramesh Subedi	*Kent State University*
Riad Suleiman	*Jefferson Laboratory*
Vince Sulkosky	*Jefferson Laboratory*
Jeff Templon	*NIKHEF*
Tatsuo Terasawa	*Tohoku University*
Neil Thompson	*University of Glasgow*
H. Tsubota	*Tohoku University*
Jose Udias Moinelo	*Universidad Complutense, Madrid*
Hiroaki Ueno	*Yamagata University*

Paul Ulmer	*Renaissance Technology*
Guido Urciuoli	*INFN/Sezione Sanità*
Antonin Vacheret	*DAPNIA/SPhN, CEA, Saclay*
Luc Van de Hoorebeke	*Ghent State University*
Robert Van de Vyver	*Ghent State University*
Pascal Vernin	*DAPNIA/SPhN, CEA, Saclay*
Javier Vignote	*Laboratoire de Physique Subatomique et de Cosmologie, Grenoble*
Branislav Vlahovic	*North Carolina Central University*
Hakob Voskanyan	*Yerevan Physics Institute*
Eric Voutier	*Laboratoire de Physique Subatomique et de Cosmologie, Grenoble*
Richard Walter	*Duke University*
Kebin Wang	*University of Virginia*
Youcai Wang	*University of Illinois at Urbana-Champaign*
John Watson	*Kent State University*
Dan Watts	*University of Glasgow*
Larry Weinstein	*Old Dominion University*
Richard Wilson	*Harvard University*
Bogdan Wojtsekhowski	*Jefferson Laboratory*
Xinhu Yan	*University of Science and Technology of China (USTC)*
Huan Yao	*Temple University*
Yunxiu Ye	*University of Science and Technology of China (USTC)*
Xiaohui Zhan	*Massachusetts Institute of Technology*
Yi Zhang	*Lanzhou University*
Xiaochao Zheng	*University of Virginia*
Shuhua Zhou	*China Institute of Atomic Energy*
Lingyan Zhu	*University of Illinois at Urbana-Champaign*
Xiaofeng Zhu	*Duke University*

6 Publications

B. Anderson *et al., Extraction of the Neutron Magnetic Form Factor from Quasi-elastic* $^{3}\vec{H}e(\vec{e},e')$ *at* Q^2 *= 0.1 - 0.6 GeV*^{2}, Phys. Rev. C**75**, 034003 (2007)

Yi Qiang *et al., A Search for* Σ_5^0*,* N_5^0 *and* Θ^{++} *Pentaquark States*, Phys. Rev. C**75**, 055208 (2007)

J. Kelly *et al., Recoil Polarization Measurement for Neutral Pion Electroproduction at* $Q^2 =$ *1 GeV*^{2} *near the Delta Resonance*, Phys. Rev. C**75**, 025201 (2007)

A. Acha *et al., Precision Measurements of the Nucleon Strange Form Factors at* $Q^2 \sim$ *0.1 GeV*^{2}, Phys. Rev. Lett. **98**, 032301 (2007)

A. Danagoulian *et al., Compton-scattering Cross Section on the Proton at High Momentum Transfer*, Phys. Rev. Lett. **98**, 152001 (2007)

X. Jiang *et al., Recoil-Proton Polarization in High-Energy Deuteron Photodisintegration with Circularly Polarized Photons*, Phys. Rev. Lett. **98**, 182302 (2007)

M. Iodice *et al., High-Resolution Spectroscopy of* $^{12}B_\Lambda$ *by Electroproduction*, Phys. Rev. Lett. **99**, 052501 (2007), arXiv:0705.3332 [nucl-ex]

R. Shneor *et al., Investigation of proton-proton short-range correlations via the* $^{12}C(e,e'pp)$ *reaction*, Phys. Rev. Lett. **99**, 072501 (2007), nucl-ex/0703023

G. Ron *et al., The Proton Elastic Form Factor Ratio* $\mu_p G_E^p/G_M^p$ *at Low Momentum Transfer*, Phys. Rev. Lett. **99**, 202002 (2007), arXiv:0706.0128 [nucl-ex]

M. Mazouz *et al., Deeply Virtual Compton Scattering off the Neutron*, Phys. Rev. Lett. **99**, 242501 (2007), arXiv:0709.04501[nucl-ex]

A. Shahinyan *et al., The Electromagnetic Calorimeter in JLab Real Compton Scattering Experiment*, arXiv:0704.1830 [physics.ins-det]

7 Theses

i. "*Precision Measurement of the Proton Neutral Weak Form Factors at* $Q^2 = 0.1\ GeV^2$"
Lisa Kaufman, University of Massachusetts, Feb. 2007.

ii. "*Elastic Scattering of Longitudinally Polarized Electrons from* ^{4}He"
Bryan Moffit, College of William and Mary, May 2007.

iii. "*Search for Pentaquark Partners* Θ^{++}, Σ° *and* N° *in* $H(e, e'K(\pi))X$ *Reactions at Jefferson Lab Hall A*"
Yi Qian, Massachusetts Institute of Technology, May 2007.

iv. "*Neutron Arm Study and Calibration for the* G_E^n *Experiment at Thomas Jefferson National Laboratory*"
Timothy Ngo, California State University at LA, July 2007.

v. "*Studying Short-Range Correlations with the* ^{12}C *Reaction*"
Ramesh Subedi, Kent State University, Dec. 2007.

vi. "*The Spin Structure of* ^{3}He *and the Neutron at Low* Q^2*: A Measurement of the Generalized GDH Integrand*"
Vince Sulkosky, College of William and Mary, Dec. 2007.